Project *Aurora*

Team 24 Project Technical Report to the 2026 IREC

Cesar Briones Aranda[1], Van Ninh Vu[2], Minh Duc Nguyen[3], Christopher Michael Fernandez[4], Chiara Alessandra Deangelis[5], Cooper Kenney[6], Sama Hosam Ahmed Moussa Ahmed[7], Khoi Ton[8], Alan Nuesa Guyster[9], Samuel L Johnson[10], Zachary A. Tephford[11], Conner Nathan Schilaty[12], Enzo Martin Galeana[13], Sage Angelina Bundjund[14], Kadin Miller[15], Matthew Joseph West[16], Logan Burchfield[17], Jessie Nwokoye[18], Matthew David Raulerson II[19], Aden Rice[20], Amanda Michelle Chesney[21], Le Trung Kien Nguyen[22], Vo Minh Phu Chau[23], Venkata Naga Chetan Dasari[24], Jhen Huang[25], Pavan Moturi[26]

University of South Florida, Tampa, FL, 33620, United States of America

The University of South Florida's Society of Aeronautics Rocketry presents the Project *Aurora* vehicle competing in the 10,000 feet COTS category at the 2026 International Rocketry Engineering Competition. *Aurora* measures 6.17 inches in diameter, 100 inches in length, and weighs 64.05 lbs. The vehicle is powered by an M-class solid motor with a total impulse of 10,481.5 N-s and a burn time of 6.2 seconds, expecting an uncontrolled apogee of 11,943 feet. A custom autonomous airbrake system will be deployed to actively control the vehicle's drag coefficient and achieve a precise apogee of 10,000 feet. Telemetry will serve as a backup recovery system with its own SRAD GPS, IMU, and altimeter to cross-reference data with the COTS systems and livestream during launch. The payload will jettison and land separately from *Aurora*. It is an Earth Vegetation Evaluator (EVE) that scans for plants, classifies species, and measures health.

[1] Chief Engineer, cesar.briones.aranda@gmail.com
[2] Aerostructures Lead, airlighning@gmail.com
[3] Airbrakes Mechanical Lead, duchsgs1310@gmail.com
[4] Airbrakes EECS Lead, chfernandez05@gmail.com
[5] Payload EECS Lead, chiara.a.deangelis.18@gmail.com
[6] Payload Mechanical Lead, cooperkenney34@gmail.com
[7] Recovery and Flight Dynamics Lead, samamoussa5@gmail.com
[8] Safety Lead, khoittm2004@gmail.com
[9] Telemetry Lead, alanguyster1@gmail.com
[10] Payload EECS JE, johnson.samue12005@gmail.com
[11] Aerostructures JE, zat103005@gmail.com
[12] Secretary, cnschilaty@gmail.com
[13] Aerostructures JE, enzogaleana03@gmail.com
[14] Chief of Marketing, sageb3034@gmail.com
[15] Payload EECS JE, cerketbreaker@gmail.com
[16] Payload EECS JE, matthewjwest53@gmail.com
[17] Payload Mech JE, logantburchfield@gmail.com
[18] Payload Mech JE, jnwokoye834@gmail.com
[19] Telemetry JE, matthewraulerson7@gmail.com
[20] Telemetry JE, adenrice06@gmail.com
[21]Recovery and Flight Dynamics JE, mandimchesney@gmail.com
[22] Airbrakes Mechanical JE, nguyenletrungkien2006@gmail.com
[23] Airbrakes Mechanical JE, chauvominhphu0406@gmail.com
[24] Telemetry Member, flamingblackhole@gmail.com
[25]Payload EECS Member, jay35710@gmail.com
[26] Program Manager, pav9362005@gmail.com

I. Noclemature **4**
II. Introduction **4**
A. Overview 4
B. Stakeholders and Contributors 4
C. Team Structure and Management 5
III. System Architecture Overview **6**
A. Aerostructures 6
1. Objectives and Mission Statement 6
2. Propulsion 6
3. Nose Cone 7
4. Ballast 7
5. Mid Section 7
6. Booster Section 8
7. Fins 8
8. Modular Fin Assembly 9
9. Railguides 10
B. Recovery and Flight Dynamics 10
1. Objective and Mission Statement 10
2. Harness Type 11
3. Main Parachute Assembly 11
4. Drogue Parachute Assembly 11
5. Deployment Charges 11
6. Avionics Bay 11
C. Airbrakes 12
1. Objectives and Mission Statement 12
2. Mechanical Design 12
3. Construction and Materials 13
3. Flight Dynamics and Aerodynamic Modeling 13
4. Hardware 14
5. Software 14
D. Payload 15
1. Overview and Mission Statement 15
2. Deployment Method 15
3. Retention Mechanism 15
4. CubeSat Structure 15
5. Experimental Rover 16
6. Steering Mechanism 16
7. Electronics 17
8. State Machine 17
9. Plant Classification Model 17
10. Normalized Difference Vegetation Index 18

11. Dual Camera System..... 18
E. Telemetry..... 19
1. Overview..... 19
2. Telemetry Bay..... 20
3. Ground Station..... 20
3. Live Video Downlink..... 21
4. Flight Avionics..... 22
IV. Mission Concept of Operations Overview..... 22
A. Airbrakes..... 22
B. Payload..... 23
C. Recovery..... 23
D. Telemetry transmission..... 23
V. Conclusions and Lessons Learned..... 23
A. General..... 23
VI. Acknowledgements..... 25
VII. Technical Report Appendices..... 26
Appendix A: System Weights, Measures, and Performance Data..... 26
Appendix B: Project Test Reports..... 29
A. Recovery System Testing..... 29
1. Recovery System [DTEG 6.13]..... 30
2. Ground Test Demonstration [DTEG 6.13.4]..... 30
3. Flight Test Demonstration [DTEG 6.13.5]..... 30
4. Dual Redundancy of Recovery Electronics [R&R 2.6.2.10.a]..... 31
5. Stored-Energy Devices – Energetic Device Safing and Arming [DTEG 6.14]..... 31
6. Arming Devices [DTEG 6.15]..... 31
7. Arming Device Verification [DTEG 6.16]..... 32
B. SRAD Telemetry GPS Testing..... 32
1. First Battery Longevity Test..... 32
2. Second Battery Longevity Test..... 32
3. First Range Test..... 33
4. Second Range Test..... 34
5. Third Range Test..... 34
C. Payload Recovery System Testing..... 35
Appendix C: Hazard Analysis..... 37
Appendix D: Risk Assessment..... 39
Appendix E: Checklists..... 42
Appendix F: Engineering Drawings..... 47
Appendix G: Triangulation Methods..... 70

I. Nomenclature

F_d = Force of drag
C_d = Coefficient of drag
h_{cutoff} = Altitude after motor cutoff
v_{cutoff} = Velocity after motor cutoff
t = Time after motor cutoff
g = Gravity
Ma = Mach number
Re = Reynolds number
m = Mass

II. Introduction

A. Overview

The Society of Aeronautics and Rocketry (SOAR) is a student-led, nonprofit organization founded in 2013 by a dedicated group of undergraduate students in the College of Engineering at the University of South Florida (USF). SOAR's IREC Team engages in extracurricular activities that focus on research and development in rocketry and aerospace. With the intent of showcasing the team's excellence, SOAR is participating with the *Aurora* vehicle in the 2026 International Rocket Engineering Competition (IREC) hosted by the Experimental Sounding Rocket Association (ESRA) under the 10,000 ft apogee (10K) altitude category, powered by a Commercially-Off-The-Shelf (COTS) propulsion system utilizing solid propellant. Notable features of *Aurora* include its active airbrakes system, payload, and the Student Research and Development (SRAD) Telemetry GPS. The payload consists of a CubeSat structure and a rover entitled the Earth Vegetation Evaluator (EVE). This is the team's first year competing in the IREC and has the following objectives for the competition.

1. A nominal flight without anomalies. This includes drogue parachute deployment at apogee and main parachute deployment at the designated altitude in the COTS Flight Altimeters.
2. Deployment of the payload with the main parachute deployment and landing.
3. Separation of EVE from the CubeSat structure upon landing.
4. EVE Rover operation conducts a grid pattern scan, classifies, and measures the health of plants.
5. The airbrakes system successfully deploys flaps to strategically lower the apogee of *Aurora* to 10,000 ft.
6. SRAD Telemetry, GPS, and the Live Video Downlink System maintain transmission of in-flight Telemetry and in-flight live video to team-operated ground receivers throughout the duration of *Aurora*'s flight.
7. Minimal to no damage to *Aurora* or the payload

B. Stakeholders and Contributors

Aurora's success is supported by many stakeholders, ranging from student members to company sponsors. The primary stakeholders are the 100+ USF students who contributed to *Aurora* throughout the project's lifetime. Other stakeholders include SOAR's Executive Board, which allocates resources for the SOAR IREC Team. Faculty stakeholders include SOAR's Faculty Advisor, Dr. Nicholas Baksh, and other faculty leadership in the USF College of Engineering. Stakeholders outside of USF primarily consist of the team's Flyer of Record, Jonathan Fitzer, Team Mentor Jimmy Yawn, and the company sponsors of SOAR. For the 2025-26 academic year, the sponsors are Mike Crew, Joe Register, Epsilon3, Lonzo Law, Kenesto, Ansys, Five Star, Jim's Body Shop, and Monster Beverage Corp. They have contributed approximately $22,000 USD in monetary sponsorship and access to technology & resources valued at $20,000 USD.

C. Team Structure and Management

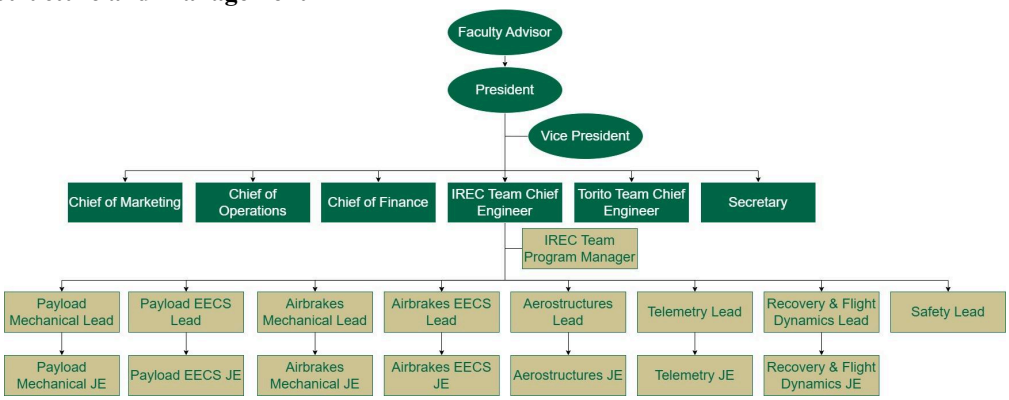


Figure 1. Team Organization

The SOAR Executive Board consists of the President, Vice President, Chief of Finance, Chief of Marketing, Chief of Operations, and Secretary. This E-Board is responsible for overseeing the IREC Team and Torito Team operations as well as organizational finances, sponsorships, and member engagement. The Chief Engineer is in charge of their respective team and has final authority on design decisions. Their responsibilities center around resolving technical conflicts, aiding Team Leads, ensuring project requirements are met through testing, and supervising subsystem integration. The Program Manager is responsible for the project timeline & ensuring resources are utilized on time. Both the Chief Engineer & Program Manager foster communication among all team members and share updates with stakeholders. The Junior Engineer (JE) role grants members more design & execution responsibility than regular subsystem members, and allows members to take a more active role in the development of the system. It additionally serves as an experiential training program for future Team Lead candidates. All Team Leads are assigned sections throughout the project technical report, and JE's were encouraged to assist them.



Figure 2. Team Timeline

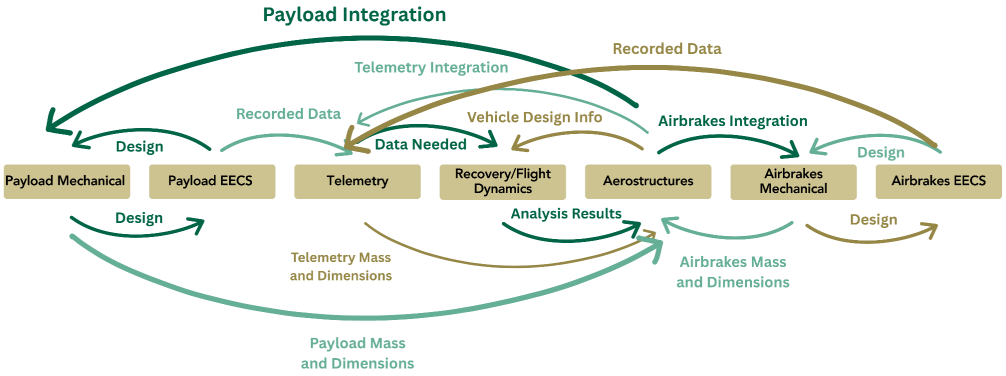


Figure 3. Team Dynamics

III. System Architecture Overview

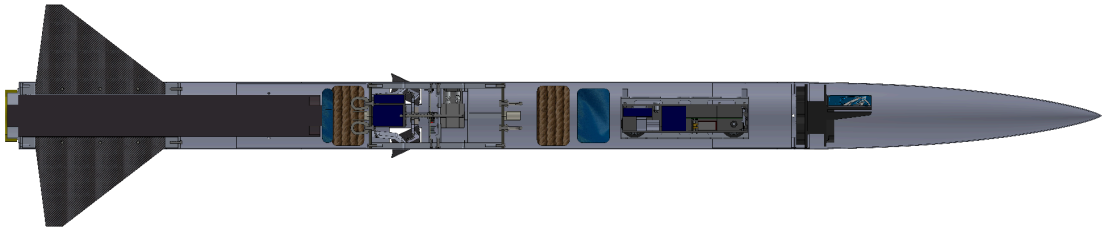


Figure 4. *Aurora* Section View

A. Aerostructures

1. *Objectives and Mission Statement*

The aerostructures subsystem is responsible for both the inner and outer structures of the launch vehicle, building the infrastructure for other subsystems, and facilitating a safe flight for the payload. The objectives of the aerostructures subsystem are as follows:

- The vehicle shall reach an altitude higher than 10,000 ft.
- The team shall facilitate the integration of other subsystems into the flight vehicle.
- The team shall ensure the structural integrity of the vehicle against liftoff and recovery loads.

To achieve these objectives, the team has utilized a combination of COTS and SRAD components. For this project, both the airframe and coupler tubes were bought from commercial sources. These were then customized by cutting them to length, drilling, and cutting slots as needed. Other subassemblies, such as the bolted fin assembly, were machined from aluminum stock.

2. *Propulsion*

The chosen method of propulsion for the launch vehicle is a COTS AeroTech M1939W-PS White Lightning solid rocket motor. This motor was selected due to its availability through various vendors and its high initial thrust and impulse. Specifically, the selected motor has an impulse of 10,481.5 N-s, which would sufficiently provide the thrust needed to reach a maximum altitude of approximately 12,000 feet. The use of this motor conforms with the team's plan to have a higher impulse margin and to modulate the energy state of the vehicle through an active airbrake system to reach the target apogee. The thrust curve and propellant over time are shown below.

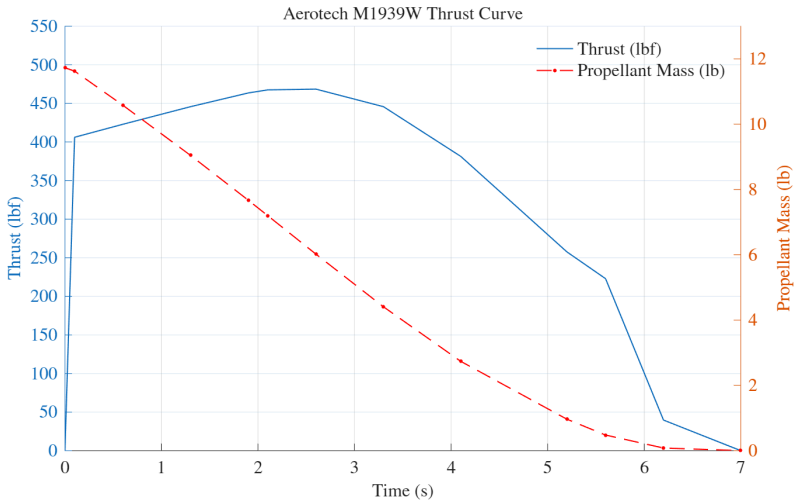


Figure 5. M1939W - PS Information

3. *Nose Cone*

The chosen nose cone is a fiberglass COTS nose cone from Wildman Rocketry. This component is bolted with 4 ¼-20 nuts and bolts to a 9-in coupler. Figure 6 shows the nose cone and coupler, along with the jigs used to drill the holes accurately. Additionally, the nose cone features an aluminum tip.

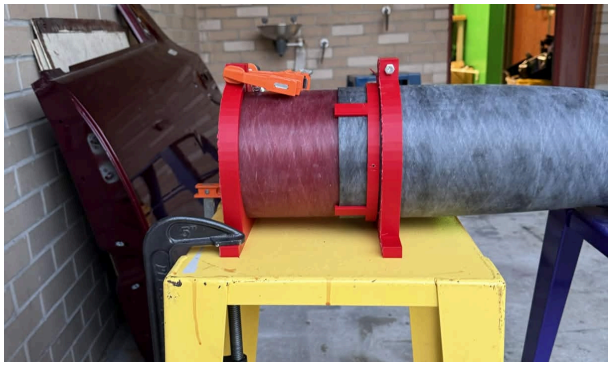
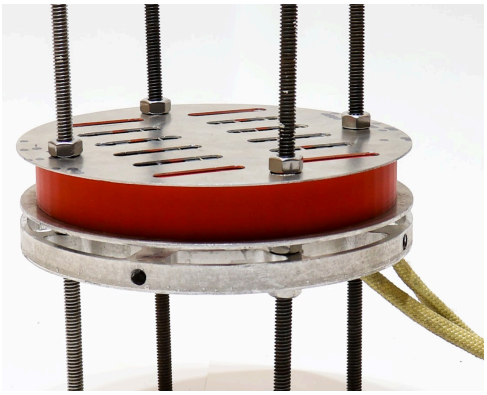


Figure 6. Jig for holes in the nose cone

4. *Ballast*

Figure 7 shows the ballast ring. This component holds the stackable ballast sled, the nose cone, and the coupler together. There are four radial holes with threads to bolt the nose cone and coupler to the ring. There are also four vertical holes for four threaded rods, which hold the ballast sled.

Figure 7 also shows the ballast sled. The sled is 3D printed from PLA and has eight slots, each slot holds three 1-oz iron ballast, which total to 24 ballast or 1.5 lbs. The four holes allow the sleds to slide into the threaded rods and be bolted to the ballast ring. There are also two aluminum plates on the top and bottom of the ballast sled to prevent the ballast from damaging the sled due to launch acceleration.



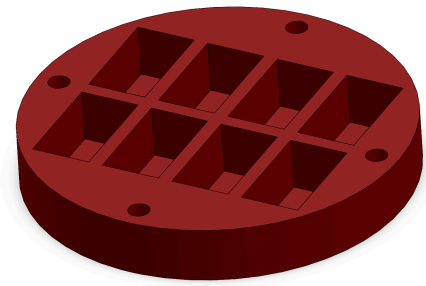


Figure 7. Ballast Assembly and Ballast Sled

5. *Mid Section*

The mid-section sits right below the upper section and consists of an airframe, the airbrake system, altimeters, and the camera bay. The dimensions of these components are specified in a later section. The mid-section is connected to the upper section and booster section by four shear pins on each side. The shear pins are expected to break upon recovery to deploy the payload, drogue, and main parachutes.

The airframe was cut to a length of 44 inches from a stock fiberglass tube. Next, four ⅛ in holes were drilled on each side, three inches away from the edge of the frame. These holes were positioned with a jig that constrains the distance from the holes to the edge and the distance between each hole, shown in Appendix A.

Figure 8 shows four airbrake flap cutouts, four holes to bolt the airframe to the stringers, and 5 key switch holes. The four stringer holes were drilled with a jig that positions those holes relative to the shear pin holes below. The four flap cutouts were traced with a jig and cut out with a rotary tool.

6. *Booster Section*

The booster section houses the vehicle's fins, the modular fin assembly, and the M1939 motor. The booster's body tube is bolted to a 12-in long coupler with four ¼-20 stainless steel hex screws.

On the lower side of the booster are four 14-in-long, 0.25-in-wide slots for four fins to slide in. To manufacture those slots, the airframe was fixed on the team's CNC router platform by placing a heavy aluminum cylinder inside. After that, the slots were machined with the CNC router. A 3D-printed jig was used to accurately mark the slot position with a Sharpie, and then the end mill was aligned with those slots.

The booster is connected to the modular fin assembly through seven 4/40 Phillips screws, four screwed into the top plate and three into the bottom plate of the modular fin assembly. There are only three screws on the bottom plate since a rail button is bolted to an L-bracket in the remaining quadrant, which is then bolted to the bottom plate. The specific top and bottom plate positions and dimensions are detailed in section 8. Modular Fin Assembly.



Figure 8. Outer Structures

7. *Fins*

Fins serve as aerodynamic control surfaces at the end of the vehicle. Aerodynamic stability is provided through four trapezoidal fins. Detailed dimensions of the fins are provided in Table 1. The height of the fins was optimized to provide a static stability margin caliber of 2.45, with the optimization shown in Figure 9. Various fin shapes were considered, such as elliptical and tapered swept, but ultimately the trapezoidal shape was chosen. Elliptical fins theoretically produce the least drag, but introduce increased difficulty in the manufacturing process. Further, tapered swept fins are suitable for high-speed flight, but are more prone to fin flutter, a high-frequency vibration that may happen to fins flying at higher velocities. Tapered swept fins that extend beyond the end of the vehicle are also prone to damage during transportation and recovery. Due to the reasons above, trapezoidal fins were chosen, as this shape provides a balance between low drag at high velocity, manufacturability, and structural reliability.

All fins were machined on a ShapeOKO HDM CNC Router from ⅛ inch carbon fiber sheet stock. After machining, the rough edges were sanded off with sandpaper and appropriate PPE.

Table 1. Fin Dimensions

Fin Parameter	Value (in)
Root chord	12
Tip chord	1.6
Height	7.2
Thickness	0.125

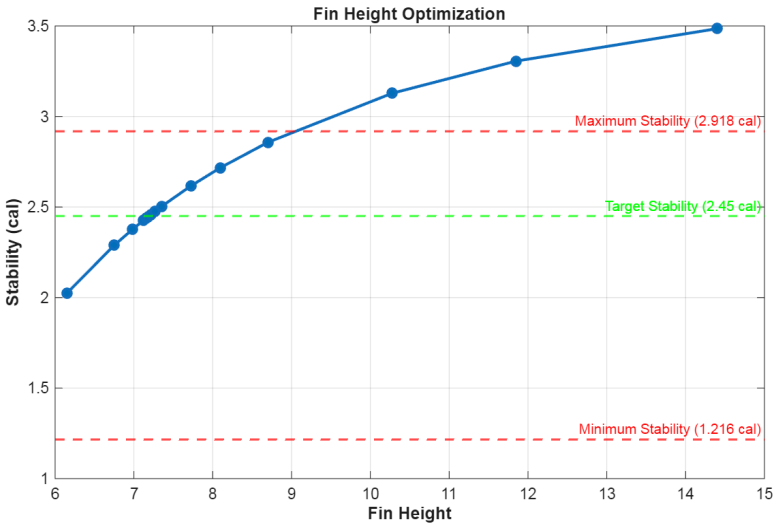


Figure 9. Fin Height Optimization

8. *Modular Fin Assembly*

The modular fin assembly is the inner structure that holds the fins and the motor to the booster airframe. This assembly replaces the legacy epoxy design utilized in the team's previous vehicle designs. This consisted of epoxying the fins and fin tabs to the booster and the motor tube. This design, although simple, is impossible to replace if the fins were to break on the field or if design modifications needed to be made to the fins. In the interest of improved modularity & repairs, the team opted for a modular fin design for *Aurora*.

Multiple different designs were considered before the current designs of fin clamps were chosen. One alternative design that stood out was aluminum brackets, which are two L-shaped brackets on each side of a fin to hold the fin to the booster. This design, however, was not possible to manufacture under the constraints of the team's 3-axis CNC router. Table 2 shows a trade study with all four competing designs. Based on this study, the fin clamp was ultimately chosen.

The manufacturing of the structure starts with the top and bottom plates. The two plates have a diameter of 6 in and were machined with the team's ShapeOKO HDM CNC router from 8x8x0.4in aluminum stock. Next, the beams were cut to 16 in from 0.5x1x24in stock aluminum beams, and the slots were machined with a ⅛ in end mill. The holes on the two ends of the beams were first drilled with a drill press, then tapped to the thread size of ¼-20. The three horizontal holes were drilled with a mill, and the fins were machined from a ⅛ in carbon fiber sheet.

The structure is assembled by first sliding the fins through the beam's slot and bolting them through the three holes. Next, each beam is bolted to the bottom plate. Afterwards, the assembly is flipped upright, and the top plate is bolted to all four beams.

Table 2. Modular Fin Assembly Design Trade Study

	Price	Manufacturability	Drag	Weight	Strength	Final score	Ranking
Weighing	7	9.5	7	8	8		
Fin clamps	9	9	10	7	9	346.5	1
Aluminum brackets	6	3	2	1	10	172.5	2
Fin slots	3	3	5	5	5	164.5	3
Seatbelt tabs	2	2	9	5	3	160	4



Figure 10. Modular Fin Assembly

9. *Railguides*

The team is using two aerodynamic railguides in the booster and mid-section. They are connected to the airframe via a bolt that threads into an internal structure. On the bottom side, given that the airframe is weakened, it bolts directly to the bolted fin assembly.

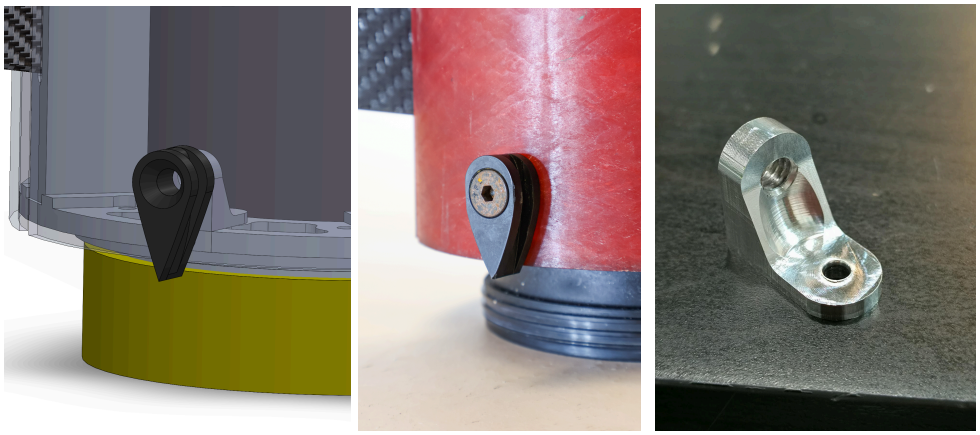


Figure 11. Railguide in Booster Section CAD / Picture / Railguide Support

B. Recovery and Flight Dynamics

1. *Objective and Mission Statement*

To ensure a safe, reliable, and controlled descent of both the vehicle and payload, *Aurora* utilizes a dual-deployment recovery system with triple-redundant avionics. The success criteria for this subsystem are as follows:

- The recovery system can reliably deploy the drogue parachute at apogee and the main parachute at around 1,000 ft AGL in both expected and unexpected conditions.
- The system maintains stable descent rates to reduce drift and ensure a safe landing for both the vehicle and payload.
- The recovery system is built to handle launch forces, deployment events, and landing without failing.
- The avionics system uses multiple independent altimeters to provide redundancy, ensuring deployment even if one system fails.
- The system supports accurate recovery after landing using GPS tracking and backup location methods.

The recovery system is fully compliant with IREC safety requirements, utilizing redundant deployment electronics, independently powered systems, and validated deployment charges. All recovery events are triggered using barometric altimeters and are independent of the SRAD Telemetry GPS, ensuring reliable operation under all flight conditions.

2. *Harness Type*

The harness used for all connection points is the Alpine Hatch knot. It creates a loop within the shock cord, allowing a quick link to be connected. In some points, like in the Principal Bay, two loops are used instead of one.



Figure 12. Double Alpine Hitch knot

3. *Main Parachute Assembly*

The main parachute is deployed at approximately 1,000 ft AGL to reduce descent velocity and ensure a safe landing. The system is designed to achieve a descent rate of approximately 18 ft/s, which minimizes landing impact forces on the vehicle. The parachute is packed using Nomex protection to prevent damage from deployment charges and is connected to the main harness through reinforced attachment points. This arrangement ensures reliable inflation and stable descent under expected flight conditions.

4. *Drogue Parachute Assembly*

The drogue parachute is deployed at apogee to stabilize the vehicle and initiate a controlled high-speed descent. This limits horizontal drift while maintaining vehicle orientation. The drogue system is designed to lower the descent rate to approximately 110 ft/s by the time it gets to the main deployment altitude, ensuring compliance with competition requirements while maintaining stability. The drogue parachute is connected to the forward section using a Kevlar harness and is properly sized to balance stability and drift reduction during descent.

5. *Deployment Charges*

The deployment charges store the energetics required for parachute deployment. *Aurora* contains three pairs of deployment charges: three for main parachute deployment and three for drogue parachute deployment. Each pair is connected to an independent MissileWorks RRC3+ altimeter, for a total of three RRC3+ units. The primary RRC3+ is connected to two charge wells through e-matches: one containing 6 g of black powder for the main parachute and one containing 5.5 g for the drogue parachute. The secondary and tertiary RRC3+ altimeters are each connected to their own independent pair of charge wells, with each redundant charge containing an additional 0.5 g of black powder to improve deployment reliability.

6. *Avionics Bay*

The avionics bay has the flight-critical electronics that are responsible for recovery deployment, including three independent RRC3+ altimeters. Each altimeter is powered by its own battery and connected to its own e-match, ensuring full redundancy. The primary altimeter deploys the drogue parachute at apogee and the main parachute at approximately 1,000 ft AGL. The secondary and tertiary altimeters provide redundancy by triggering drogue deployment at apogee +1s and +2s, respectively, while maintaining the same main deployment altitude. The avionics bay is designed to isolate electronics from mechanical loads and environmental factors while maintaining reliable electrical connections throughout flight. All components are secured to withstand launch vibrations and recovery forces.

C. Airbrakes

1. *Objectives and Mission Statement*

To minimize error between the vehicle's apogee and the target apogee of 10,000 ft, *Aurora* utilizes an airbrakes subsystem. The success criteria for this subsystem are as follows:

- The airbrakes module can automatically measure, calibrate, and actuate the control surfaces according to the launch environment, using an in-house algorithm to control apogee.
- The airbrakes module can be integrated and survive launch conditions without maintenance (excluding battery changes and minor modifications).
- The airbrakes module demonstrates its ability to help the launch vehicle reach the target apogee.

The airbrakes module is fully compliant with DTEG 7.0 by not deploying until the motor burns completely and the vehicle reaches its critical altitude. The airbrakes deploy symmetrically around the lead screw with the sole purpose of aerodynamic braking, remaining in yaw neutral position in case of failure, deploying only after motor cutoff, and only after the launch vehicle has passed 6561.68 ft AGL.

2. *Mechanical Design*

The airbrakes system consists of four simultaneously actuated control surfaces, referred to as flaps, and is symmetrically located around the main axis of the vehicle. Each flap is a curved rectangular panel conformal to the vehicle's outer body surface and airframe radius with a cylindrical radius of 6 in (matching the airframe radius). The flap has dimensions of 2.5 in chordwise by 3 in spanwise. When actuated, the flaps will open from 0° with respect to the airframe to a measured of 48°.

The core airbrake actuation mechanism consists of an inverted slider-crank system. From a single input, a lead screw drives a travel nut downward and symmetrically drives four flap linkages. The lead screw is actuated by a stepper motor, converting rotary input into controlled linear motion.

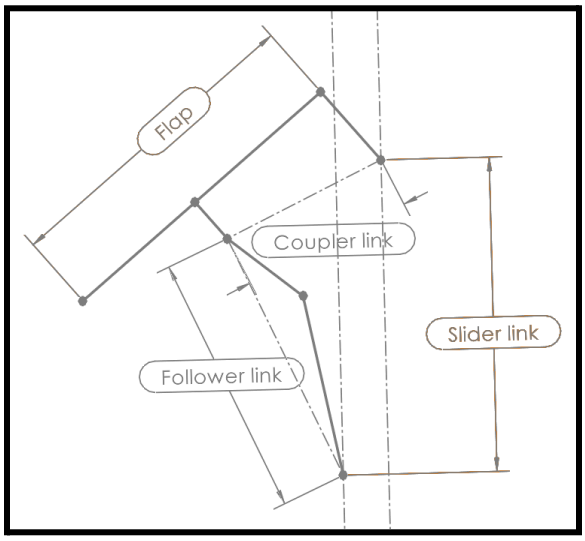


Figure 13. Skeleton graph of airbrakes mechanism

The trade-offs between the flap's angular velocity, required holding torque, and actuator size were carefully considered. For the current configuration, a NEMA 23 frame size stepper motor is used, providing approximately 200 in-oz of torque at up to 200 RPM under no-load conditions. Even after finalizing the design, these parameters can be tuned by selecting different lead screw pitches, which directly affect the linear travel per revolution and thus, the resulting mechanical advantage.

This design choice was selected due to its simplicity and modularity, allowing the flaps to be changed easily by cutting new flaps and enlarging the opening to increase drag if necessary. It is also convenient to calculate the relevant kinematic parameters of this mechanism, as the system can be modeled as a derivative of a four-bar mechanism.

3. *Construction and Materials*

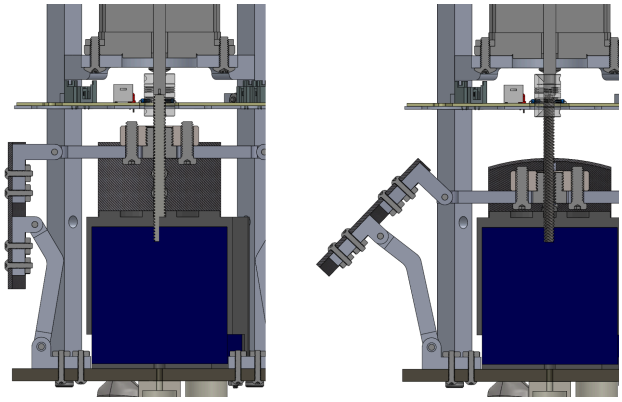


Figure 15. Airbrakes open at 0° and 48°

Airbrakes are housed inside the airframe by two carbon fiber bulkheads and supported vertically using four aluminum bars, referred to as stringers. All aforementioned components and links (arm, lever, mount) are machined in-house using Aluminum 6061. The airbrakes assembly is built vertically, starting from the lower bulkhead, which separates the midsection from the booster. The batteries for both the airbrakes PCB and the motor are housed directly above the lower bulkhead. Above the batteries is the lever/slider linkage, which is guided and constrained by a lead screw. Above this section sits the PCB compartment, supported by an aluminum weak plate. The actuation system, consisting of the stepper motor, is mounted above the lead screw and supported by a stronger aluminum plate. At the top of the stack is the avionics bay (avi-bay).

3. *Flight Dynamics and Aerodynamic Modeling*

The governing equations for the altitude and velocity of the launch vehicle are derived from Newton's laws, with the assumption that the launch vehicle moves only in the z-direction:

$$h = h_{cutoff} + v_{cutoff}t - \frac{1}{2}gt^2 - \int_0^t (\int_0^t \frac{F_d}{m} dt) dt$$

$$0 = v_{cutoff} - gt - \int_0^t \frac{F_d}{m} dt$$

The system of equations can be solved using the numerical method Runge-Kutta using the computer on board.

In order to determine F_d, a CFD study is carried out to estimate the drag coefficient and drag force at different flight stages. A maximum velocity of Mach 0.85 C_d is estimated as a function of Reynolds number (Re) and Mach number (Ma). ANSYS Fluent simulations of the launch vehicle at different airbrake opening positions and various combinations of Re, Ma, and Geometry are conducted, with the results summarized in Figure 14. This data is used to tune the controller and will be verified against launch data.

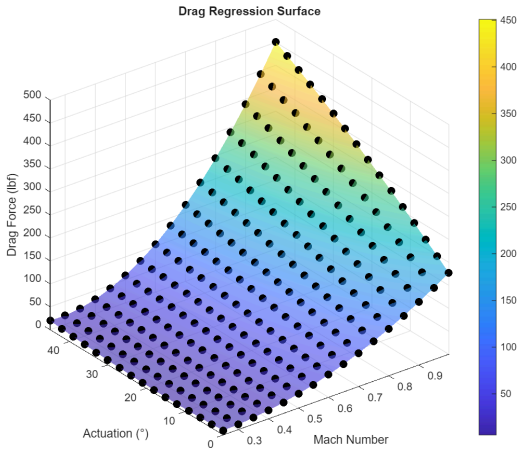


Figure 14. Drag Force over Mach number and actuation

4. *Hardware*

The PCB for the airbrakes system, as seen in Figure 15, was designed to integrate all sensors and controllers needed to meet the requirements for the control software. The components were selected based on reliability found by previous experience or after rigorous iterative testing.

The custom four-layer PCB, designed in EasyEDA, uses a dedicated stack-up of Signal-Power-Ground-Signal. This configuration was chosen to provide low-impedance return paths and electromagnetic interference shielding. At the core of the PCB is a Raspberry Pi Zero 2 W, selected for its high throughput and pinout, including an I2C bus. On the I2C bus are the BMP580 for altitude, pressure, and deriving velocity, and the BNO085 IMU for acceleration and orientation data. To control the NEMA 23 stepper motor, a TMC2209 was selected as a driver to accurately actuate the airbrakes to the desired angle. Power to the board is sourced from two Lithium Ion batteries, one 7.4V and the other 24V. The 7.4V battery is stepped down to 5V through a buck converter to power the Raspberry Pi and logic circuits. The 24V battery is dedicated to powering the stepper motor and is only connected to the motor driver. All components external to the PCB, such as the batteries, motor, and mechanical key switch, are connected through Molex Mini-lock connectors. The PCB also consists of LEDs and piezoelectric buzzers for system diagnostics. A future addition to the hardware is an external temperature sensor to obtain a more accurate reading for air temperature outside of the vehicle.

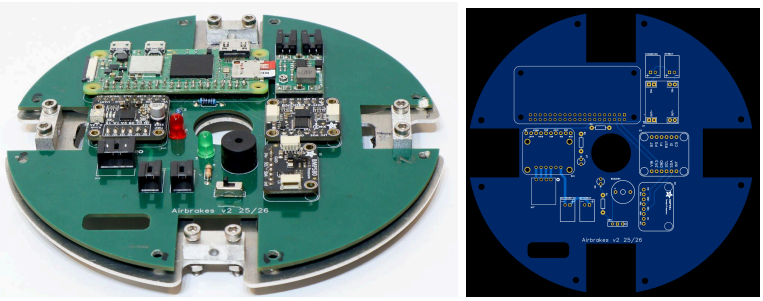


Figure 15. Airbrakes PCB

5. *Software*

The major parts of the airbrakes software are the state machine with six defined states (ready, launched, active, full stop, descent, landed) and a PID controller. The main program collects data from each sensor to determine which state the vehicle is in. Starting at the ready state, the program waits until reading an acceleration reading from the IMU that exceeds the set launch threshold. While in the ‘active’ state, all sensor data is processed by a Fourth Order Runge-Kutta algorithm, using drag force tables from CFD simulations, to calculate the predicted apogee. The predicted apogee is used in the PID controller to determine the error between the predicted and target apogees to calculate the airbrake angle, which will provide the desired amount of drag. In the case that the vehicle passes the

target apogee of 10,000 ft, the system enters the 'full stop' state, where the airbrakes fully actuate to stop the vehicle. If a system abort occurs or the attitude of the vehicle exceeds 30°, the airbrakes will return to a neutral state to comply with DTEG Section 7.3.1. In the 'descent' state, the airbrakes fully retract to prevent damage upon landing. To handle noisy data during flight, a Kalman filter is implemented in the main loop to use more accurate data in calculations.

D. Payload

1. *Overview and Mission Statement*

Aurora will carry a functional, deployable payload that consists of two parts: the CubeSat structure and the experimental rover, EVE. The CubeSat structure is an aluminum box that acts as an adapter, housing EVE, which is held in place by a retention mechanism. This combined assembly will be located in the mid-section of the vehicle's airframe. This ensures that the entire payload conforms to the Payload Cube Unit physical standard, which was encouraged for teams to adopt. For the mission statement, the payload shall perform the following mission objectives to be considered a success:

- The rover will stay fixed to the CubeSat throughout ascent.
- The payload will deploy with the main parachute.
- The payload will land as one piece in the correct orientation.
- The retention system will release the rover from the CubeSat.
- The rover will begin scanning for plant life.

2. *Deployment Method*

The payload will reside directly above the main parachute, packed with fire-resistant cellulose insulation (dog barf), which will ensure a repeatable, simplistic deployment of the system. The black powder charges are located below the main parachute, ensuring that upon ignition, the main parachute will push the payload out of the mid-section, allowing it to fall under its own weight. Once deployed from the midsection, the payload parachute will inflate and cause a snatch force that will be distributed among four separate connection points, located at each corner of the CubeSat. The decision to fix the parachute to the corners was made to guarantee proper load distribution, as well as to ensure fixed pitch and roll axes to force an optimal landing orientation.



Figure 16. Payload Independent Descent

3. *Retention Mechanism*

The rack and pinion is the retention system to secure EVE to the CubeSat throughout the flight up until landing. Upon landing, it will retract and allow EVE to depart from the CubeSat and begin its tasks. It is designed to ensure that EVE will not separate prematurely from the CubeSat during flight due to vibrations, payload jettison, or while under a chute. Additionally, it has been tested to withstand the impact force while still maintaining the ability to retract, ensuring that EVE does not become stuck inside the CubeSat after landing.

4. *CubeSat Structure*

The primary goal of the CubeSat structure is to protect and carry EVE safely to the ground after jettisoning while simultaneously providing a mounting point for the parachute. The CubeSat is milled from a piece of extruded square tubing made of 6061-T6 aluminum to help reduce weight. Since the part is experiencing the brunt of the impact force, FEA was performed in Ansys to ensure the part will not deform more than 0.12 in inward, which would restrict the deployment of EVE. The assumptions for the analysis were a fixed impact velocity of 15.68 ft/s calculated from a

payload weight estimated at 7 lbs under a 52 in parachute, and a fixed support steel plate to represent the ground. To overengineer and ensure the survival of the structure, the impact was simulated on steel with the goal of a factor of safety above one, therefore providing high certainty that the structure would not severely deform during a soil/sand impact, resulting in a minimum factor of safety of 1.0396.

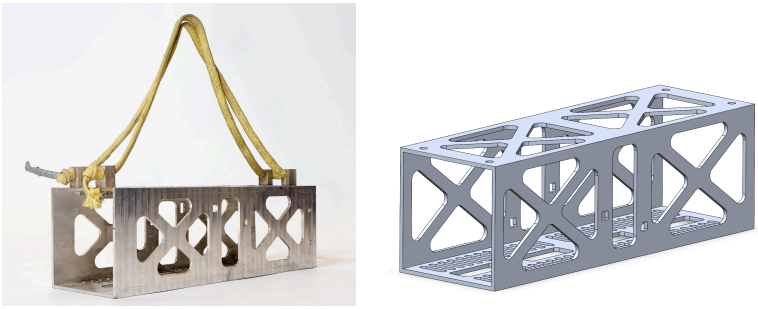


Figure 17. Cubesat structure

5. *Experimental Rover*

EVE is integrated within a 3U CubeSat structure. Upon successful deployment and landing, EVE will use the state machine and various sensors to detect a landing state. Once landing is detected, the rack and pinion retention system will retract, allowing EVE to exit from the CubeSat through the use of two independent 12V high-torque motors located in EVE's rear. Once clear of the CubeSat, EVE will begin its mission to explore the terrain and seek out plant life using computer vision and infrared analysis to identify and measure the health of nearby plants. EVE will perform a grid scanning pattern to ensure comprehensive data collection while maximizing terrain coverage.

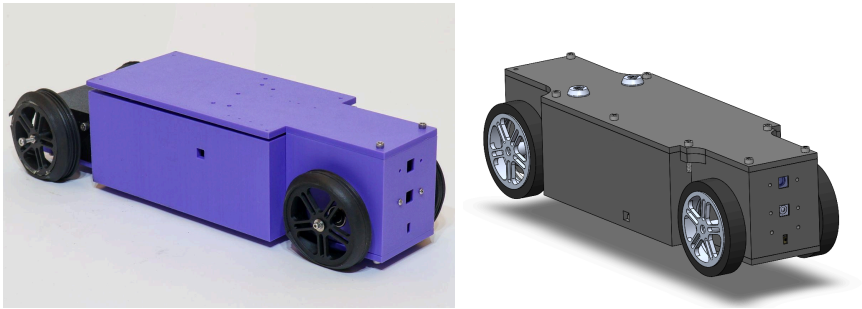


Figure 18. Rover Structure

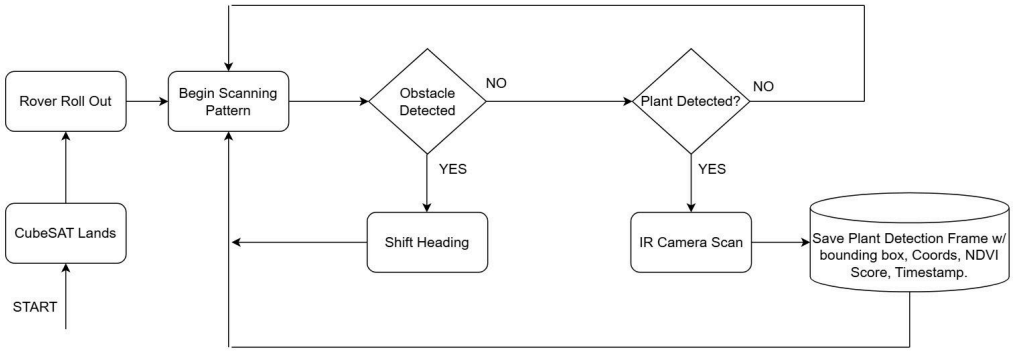


Figure 19. Rover Main Control Loop

6. *Steering Mechanism*

EVE's steering mechanism is responsible for controlling its direction and allowing it to move effectively across the uneven terrain surrounding the landing site. A steering rack system similar to that of automobiles was implemented to provide the ability to adjust the wheel direction as much as required. This design provides accurate

and smooth turning, which is needed for obstacle avoidance and to ensure that EVE will be able to effectively find its way to a plant identified for analysis.

7. *Electronics*

The team used a Raspberry Pi Zero 2W for EVE's computer. It collects acceleration data from the Adafruit BNO085 Inertial Measurement Unit (IMU) sensor and collects altitude and pressure data from the Adafruit BMP580 Barometric sensor. The computer sends control signals directly to two worm gear motors. EVE has a dual-camera system using the Arducam Multi Camera Adapter. This allows EVE to switch between a Raspberry Pi AI Camera for visual object detection and a Raspberry Pi NoIR Camera Module 3 with an infrared filter to identify and collect data on different plant species. The Adafruit Time of Flight sensor is used for obstacle detection, allowing EVE to sense incoming hazards and modify its route accordingly. These electronics are housed on a custom two-board PCB stack to maximize available space. It incorporates a 12V battery and the MP1584 DC-DC step-down converter for power supply to the motors and electronics. The 12V battery and DC-DC converter share ground planes to encourage accurate signal transmission between the motors and the Raspberry Pi.

8. *State Machine*

EVE's state machine is used to track the phase of flight and influence its behavior accordingly. The most important phase is landing, as it triggers a transition into driving mode. The state machine is crucial to the proper functioning of EVE. An error in the landing state transition could cause premature deployment of EVE or prevent it from functioning at all. These states are tracked using the IMU and the barometer. Specifically, acceleration, altitude, and vertical velocity data are all used to transition between states.

Several methods are used to improve the reliability of the state machine by requiring that transition conditions be maintained over multiple timesteps. This approach helps prevent a short burst of anomalous readings from causing premature transitions in EVE. Additionally, the data is smoothed using an exponential moving average (EMA), which prevents invalid readings from disrupting the state transition logic. Finally, during testing, an instance of power loss was observed, leading to the implementation of a power recovery feature that restores the state machine to its previous state.

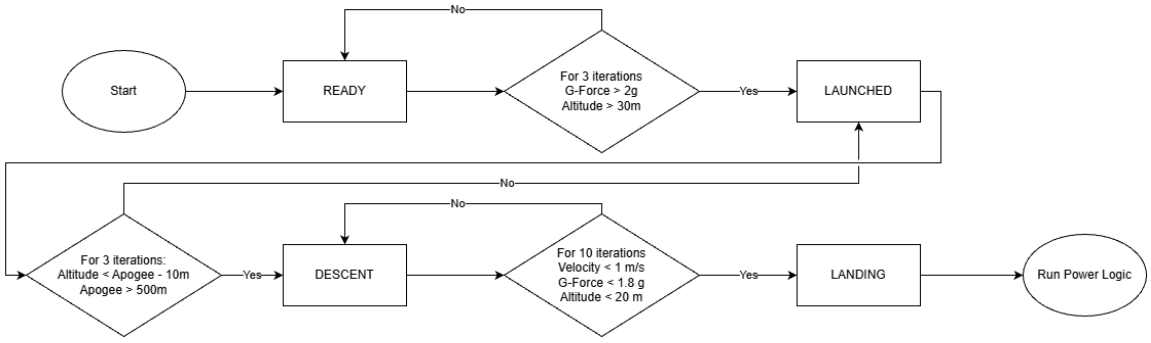


Figure 20. Rover State Machine logic

To validate the proper functioning of the state machine, an array of tests was performed. Most frequent testing came from hand tests, where the transition thresholds were lowered to allow all states to be reached by moving EVE in the air. This form of testing provided a quick way to verify the functionality of features. To complement this form of testing, a simulation test mode was introduced to allow the EVE's main programs to run directly on a computer, supplying simulated data based on past launches. The final form came from performing an actual launch with EVE, providing the most accurate conditions that it would face during flight. Throughout all these tests, the current state, time, and sensor data were saved to a CSV file for later analysis and use.

9. *Plant Classification Model*

EVE uses a You Only Look Once (YOLO) convolutional neural network to detect and classify plants. The model was trained on data made from a custom virtual environment made in Unreal Engine, mimicking the expected terrain and plant life of the launch site in Midland, Texas. Training was done using Ultralytics libraries in conjunction with PyTorch, powered by SOAR's in-house cluster of 2 RTX 3090 GPUs utilizing NVIDIA's CUDA framework. The

Raspberry Pi AI Camera runs the classification model directly on its NPU coprocessor. The frames sent to the main Raspberry Pi board include both pixel borders and classification of detected objects.



Figure 21. Yolo Model Testing Results, Bounding Boxes around Plants

10. *Normalized Difference Vegetation Index*

After a plant has been detected by EVE, it will measure the health of the plant. A technique to analyze green vegetation is to measure the difference between infrared and red light. This measurement is the Normalized Difference Vegetation Index (NDVI), which is used to assess a plant's health, density, and growth. Red light is absorbed by plants, and healthy plants strongly reflect infrared light. The formula outputs a value that ranges from -1 to 1. A value greater than 0.5 indicates high, dense, and healthy vegetation, such as crops. Values between 0.1 and 0.5 suggest low, sparse vegetation, like shrubs. A value below 0.1 signifies the absence of plant life, representing non-vegetative elements. A filter with the NoIR camera takes a picture of the plant. The blue channel is used to observe the infrared light, as all green and blue wavelengths are filtered physically. This is used in conjunction with an unfiltered red channel to calculate the NDVI of a specific plant.

11. *Infrared Filtering*

The Raspberry Pi NoIR Camera does not isolate the NIR light it takes in. Instead, those wavelengths are detected within its blue channel of the RGB Bayer filter. To isolate this NIR data to calculate NDVI, the team is using the Edmund Optics 550 nm Longpass Filter, which blocks wavelengths shorter than 550 lets longer wavelengths pass. That means most blue light (~400–500 nm) and much of the green light below ~550 nm are removed, while red and near-infrared light pass through. This yields two clean channels of red light and NIR light, which are utilized for the NDVI calculation.

12. *Dual Camera System*

EVE utilizes a vertically mounted, dual-camera system to classify plants and determine their health using NDVI. Specifically, the visible light AI Camera is used for plant detection and classification by using its onboard Neural Processing Unit, and the infrared-enabled NoIR Camera will be used to perform NDVI calculations. The dual-camera system's workflow is to classify a plant using the AI Camera's YOLO classification model, then to linearly approximate the distance to the specific plant using four frames of video. The approximate distance and the physical offset of the cameras are then used to calculate the offset in pixels of the object between the two cameras. This offset is used to shift the classified pixels to the frame of reference of the NoIR Camera for NDVI calculation.

The shifting of pixels between camera frames was developed to use the model's classification boundary in NDVI calculations. This involved treating the size of an object in the video as a function of distance, approximated through linear interpolation and inverted to find the distance to the plant. The pixel offset was calculated using a standard disparity equation. To evaluate this method's accuracy, a simulation was created using object position, size, camera focal length, and rover speed to project the object onto the camera's coordinate grid. This resulted in a percent error of about 10-13% from the actual distance, varying with distance and speed.

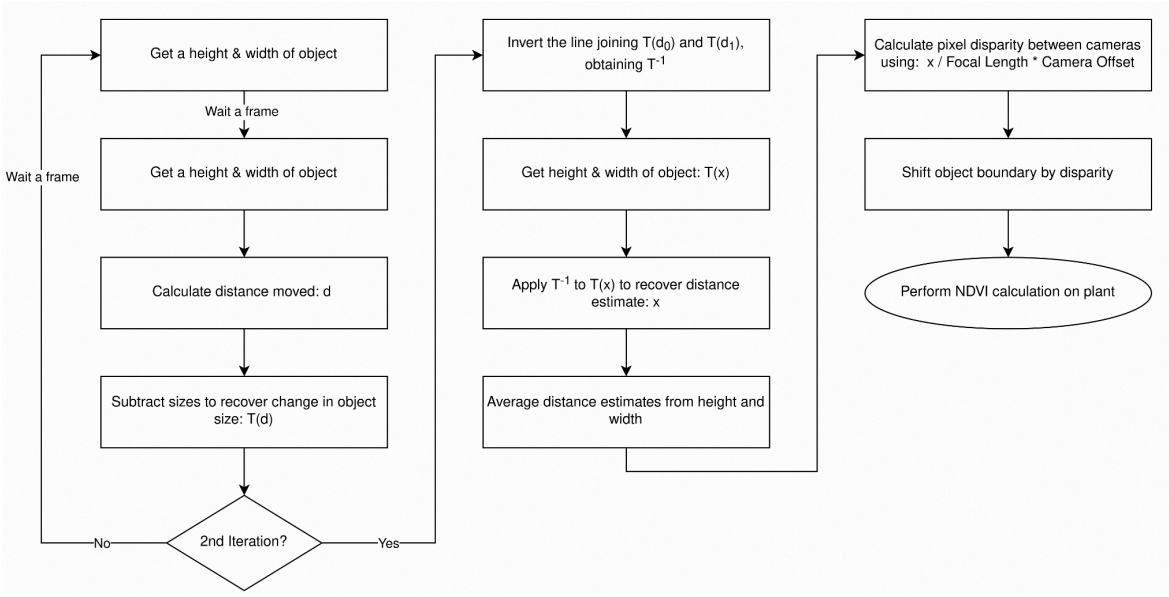


Figure 22. Payload Plant Detection State Machine

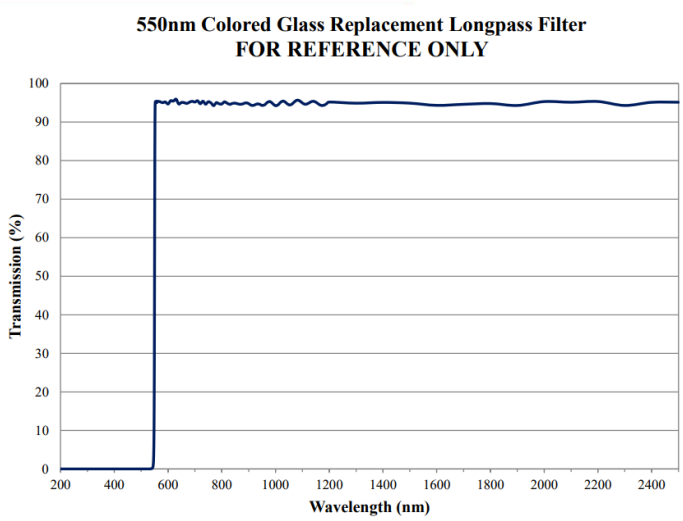


Figure 23. Edmund Optics 550 nm Longpass Filter Transmission vs. Wavelength

E. SRAD Telemetry GPS

1. *Overview*

The SRAD Telemetry GPS subsystem is composed of the Telemetry Bay PCB located on *Aurora* and the team-operated Ground Station. The Telemetry Bay PCB transmits filtered motion, height, and GPS data to the Ground Station, composed of a computer and an external receiver circuit. Both the receiver circuit and the Telemetry bay are built on PCBs with a Signal-Ground-Ground-Signal stack-up for high-speed digital-signal processing. The combination uses RFM96W transceivers that operate on the 70 cm band through LoRa modulation techniques to communicate. The bandwidth and spreading factor used are 60 kHz at a spreading factor of 9. The main purpose of the subsystem is to serve as a backup recovery system to the COTS systems, offer additional data to cross-reference for post launch analysis, and provide a live data feed throughout the flight. The SRAD Telemetry GPS subsystem shall perform the following mission objectives to be considered a success:

- Collect and filter data from the IMU, GPS, and altimeter data using a Kalman Filter.
- Maintain two-way communication during flight with the team-operated Ground Station.
- The Ground Station can receive and display data in the custom GUI.
- The Ground Station antenna can autonomously track *Aurora*'s trajectory during flight.

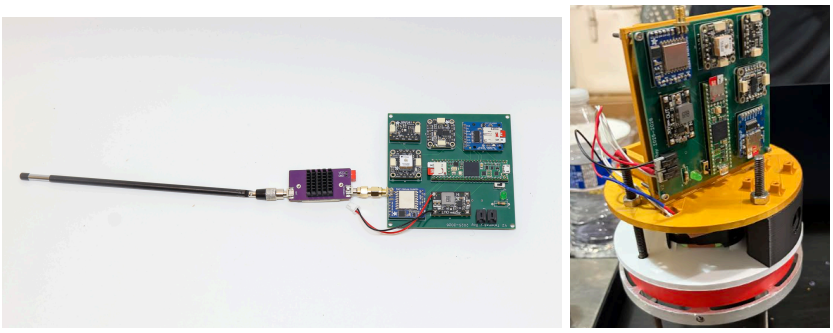


Figure 24. Telemetry Bay w/RF Amplifier & Telemetry Bay Mounted on Sled

2. *Telemetry Bay PCB*

It utilizes the RFM96W transceiver, Adafruit BNO085 IMU, Adafruit BMP581 barometer, Teensy 4.1 MCU, DFR0831 DC-DC buck converter, Adafruit MiniGPS PA1010D, Adafruit MicroSD card reader, DykoRadio 70 cm band bidirectional RF amplifier, and the 75 MHz to 1 GHz ANT500 tunable antenna. It is powered by a 14.8V 4000 mAh 4S1P lithium-ion battery. A bidirectional amplifier was chosen so that the bay can handle commands from the Ground Station. The antenna itself is omnidirectional horizontally with a vertical angle of around 60°. When the RFM96W sends a data packet, it is assigned a unique number to denote the type of data it contains (e.g., GPS, IMU).

The SRAD Telemetry GPS starts at the Ground Station, where it sends the command to the Telemetry Bay PCB. Before the on command, the Bay remains in standby mode once turned on via the mechanical key switch. Once activated, the Bay sends out the team number, KR4JIA callsign, and a "beginning transmissions" message. From there, the Kalman Filter process takes altimeter, GPS, and IMU data, which will be utilized for the simple state machine to determine where the vehicle is throughout the flight. This data is stored in a corresponding CSV file on two microSD cards in the Bay and sent to the Ground Station. The transmission scheme between the bay and the Ground Station follows a basic TCP structure using confirmation ACK packets to track data loss.

3. Ground Station

The Ground Station consists of a computer connected via a USB cable to an external PCB composed of the XIAO ESP32S3 MCU, RFM96W transceiver, 3.5 DBi 70 cm band whip antenna, and a MicroSD card reader. The Ground Station has three commands: turn on, reboot, and set frequency. By default, both the Telemetry and Ground Station are set to 430 MHz. If the frequency needs to be changed, the Ground Station can send a command that will change the Telemetry Bay PCB frequency. The frequency command is sent, the bay receives it and sends confirmation, the bay and Ground Station change to the updated frequency, and the bay sends confirmation. If the first confirmation is not received by the Ground Station, it will not change frequency. For the "turn-on" command, the Telemetry Bay PCB transmissions are off by default, so the bay is constantly checking for the on command. This command should be used as a last resort, as the Telemetry Bay PCB has a built-in watchdog from the Teensy to reboot itself in the event of a system failure.



Figure 25. Current Ground Station Setup

The Ground Station's Graphical User Interface (GUI) is used to view telemetry reception and upload commands to the bay. It reads the serial output from the Ground Station PCB, parses the wrapped lines into datasets for the collected data, and displays them in live plots using the library PyQT6, numeric stat cards, and a scrolling NMEA log. The application also consists of a leaflet map overlay, fed by an embedded HTTP tile server sourced with tiles from OpenStreetMap's database, and plots the vehicle's GPS position and ground track as a path. The commands the user is able to send through the embedded terminal emulator are as follows: on/off, ping, reboot, frequency change, and raw text, which allow interactivity to the otherwise isolated Telemetry Bay PCB bay. The RSSI and packet count indicators also give an instant quality rating. All the plotting happens at 10 Hz, and the architecture of the program allows it to be modular and have a connection to any serial port at various baud rates.

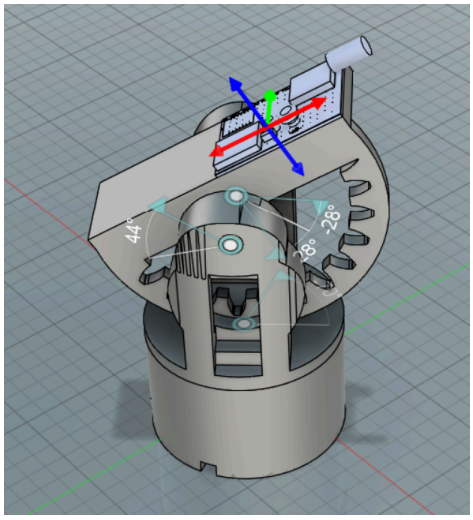


Figure 26. Antenna Orientation Design

Due to the vertical directionality of the antennas used on the Ground Station and Telemetry Bay PCB, orienting the Ground Station antenna has become important. Currently, a mount that the PCB will be attached to is being manufactured. It will be actuated by 2 Miuzei 21G Mini Digital Servos - 1 for rotating the horizontal axis and the other for the vertical axis that will be powered by another external 14.8V battery and DFR combination. Orientation can be calculated by making predictions on where the signal will go using the received filtered altitude, acceleration, and velocity data. In the event the orientation is wrong, the alternative would include removing the PCB from the mount and orienting it manually by hand. Orientation can be determined to be wrong by a lack of incoming data, random jittering, incoming data being off, or a clear orientation mismatch if the vehicle is visible.

3. *Live Video Downlink*

The live video downlink system is designed to provide a live feed during the flight while simultaneously recording onboard footage for post-flight analysis. The onboard camera transmits a live video feed and records

high-resolution footage to a micro SD card, ensuring data retention in the event of signal loss. The camera is directly connected to a flight controller, which utilizes BetaFlight On-Screen Display (OSD) software to overlay the team's HAM call sign and identification onto the video feed in compliance with FCC regulations. This ensures that all transmitted video is properly labeled throughout the duration of the flight. The processed video signal is then routed from the flight controller to a video transmitter (VTX), which broadcasts the signal to a ground-based video receiver (VRX). The Ground Station receives the live feed and relays it through the ESRA-provided livestream connection point for real-time display and evaluation. This system provides both real-time situational awareness during flight and a reliable backup recording, ensuring that mission footage is preserved under both nominal and off-nominal conditions.

4. *Flight Avionics*

The flight avionics system is responsible for triggering all recovery events based on altitude. The vehicle uses three independent MissileWorks RRC3+ altimeters operating in barometric mode. The primary altimeter is programmed to deploy the drogue parachute at apogee and the main parachute at approximately 1,000 ft AGL. The secondary and tertiary altimeters provide redundancy by triggering drogue deployment at apogee +1s and +2s, respectively, while maintaining the same main deployment altitude of 1,000 ft AGL. These deployment points were selected to ensure a stable descent and safe landing. To improve reliability, the altimeters are configured in a triple-redundant system, each with its own power source and e-match. This ensures that recovery events can still occur in the event of partial system failure. Before flight, all avionics are tested to verify proper functionality and deployment timing.

IV. Mission Concept of Operations Overview

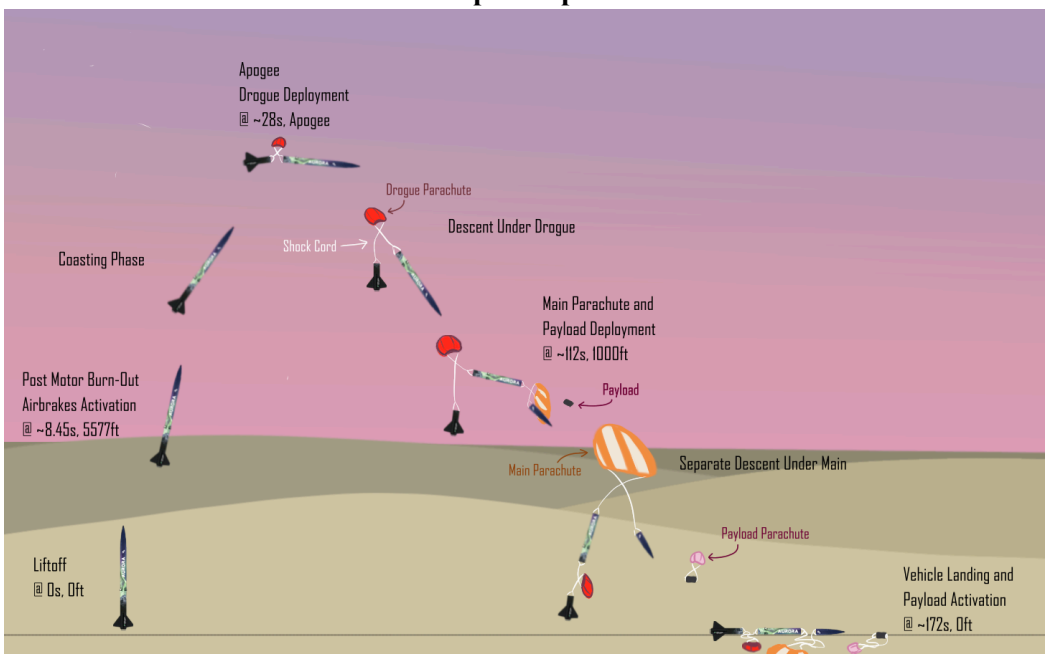


Figure 27. Mission Concept of Operations (CONOPS) showing key flight phases

A. Airbrakes

The airbrakes are deployed during the post-burnout coast phase to regulate the vehicle's ascent and ensure the target apogee is not exceeded. Following motor burnout (~6.2s), the airbrake system starts to activate at approximately 6,500 ft AGL, where dynamic pressure remains sufficient for effective aerodynamic control. The primary objective of the airbrake system is to minimize apogee variation due to environmental variability, particularly wind conditions. By modulating drag during ascent, the system reduces overshoot and improves landing predictability, which is critical for maintaining recovery within the designated launch area. The deployment logic is informed by pre-flight simulations, which evaluate altitude sensitivity to drag changes. This ensures that airbrake actuation produces measurable trajectory corrections without introducing instability.

B. Payload

The payload is deployed during the main recovery event at approximately 1,000 ft AGL. At this altitude, aerodynamic forces are sufficiently low to allow safe and stable separation while still providing adequate time for independent payload descent. Payload deployment is mechanically triggered simultaneously with main parachute deployment. Upon separation, the payload descends under its own parachute system, designed to achieve a controlled descent rate that balances landing safety with drift minimization. This deployment strategy ensures:

- Reduced risk of mid-air entanglement with the main vehicle
- Independent recovery capability using the COTS GPS
- Controlled landing conditions for both systems

C. Recovery

The recovery system utilizes a dual-deployment architecture to balance descent rate control and drift minimization. At apogee (~28 s), a drogue parachute is deployed to stabilize the vehicle and initiate a controlled high-speed descent. This phase minimizes horizontal drift while maintaining vehicle orientation. At approximately 1,000 ft AGL (~112 s), the main parachute is deployed, significantly reducing descent velocity to ensure a safe landing. This event also triggers payload separation. The recovery system is designed with triple-redundancy and reliability as primary considerations. Three independent RRC3+ altimeters are used to ensure deployment events occur even in the event of partial system failure. Ejection charges are sized and tested to ensure consistent deployment under expected flight conditions. Descent rates for both drogue and main configurations were determined through simulation and validated against design constraints to ensure:

- Structural integrity during deployment
- Acceptable landing velocities
- Minimal drift under expected wind conditions

Upon landing, vehicle and payload recovery are supported by real-time GPS tracking using the Altus Metrum TeleGPS system, with position data received on the ground through a TeleBT receiver. This system provides continuous location updates during descent and after landing, allowing for rapid locating of the vehicle. While the SRAD Telemetry GPS is used for in-flight data transmission, the TeleGPS system serves as the primary tracking method for post-flight recovery.

D. SRAD Telemetry GPS Transmission

After *Aurora* lands after flight, the telemetry data from the Telemetry Bay PCB would denote ~0 velocity and close to ground altitude. From here, the latest GPS coordinate will be cross-referenced with the COTS GPS coordinates to determine the exact location of the recovery vehicle. If the Ground Station fails to receive data during flight and recovery fails, then switch the Ground Station antenna to a Yagi to determine the approximate direction of the vehicle. If that fails, refer to triangulation in Appendix G.

V. Conclusions and Lessons Learned

A. General

The team has faced many challenges while designing and building the vehicle for the IREC 2026 competition. SOAR has had previous experience through the NASA Student Launch (NSL), which greatly helped with prior design knowledge and organization. For the first time, the team was able to push through and complete all the previous milestones.

B. Aerostructures

The primary takeaway during the development and manufacturing of the aerostructures subsystem was designed for manufacturability and proper GD&T control. For example, during the manufacturing of the fin assembly, two longitudinal holes on the beam must be drilled with the drill press. However, the beam turned out to be longer than the vertical capacity of the drill press. Therefore, a component must be designed to align with available machinery or include a plan for specialized equipment from the outset.

Moreover, while precise machinery such as the CNC router was heavily used to manufacture components with high tolerance, a large number of parts were still manufactured by hand tools such as a hand drill or rotary tool due to complex geometry. Certain features, such as airframe holes or airbrake cutouts, must be done by hand drill or rotary tool and guided by 3D-printed PLA jigs. However, 3D-printed PLA jigs have low tolerance and low stiffness, which

in turn often lead to the jig flexing during the cutting or drilling, reducing manufacturing accuracy. To resolve this problem, the team seeks to transition to high-performance filaments, such as carbon fiber-reinforced PETG or resin, to prevent deformations under operation.

C. Airbrakes

One of the biggest lessons learned was the importance of designing any system using first-principles engineering to predict system performance. For instance, the angular velocity and dynamics of each airbrake flap can be calculated using variables such as motor performance and lead screw characteristics. The dimensions of the flap can be determined using the governing equations of the airbrake system and CFD simulations. Putting these equations side by side helps predict airbrake performance and balance requirements, leading to better engineering decisions. GD&T should also be properly planned during the design phase to ensure manufacturability, assembly, and proper fit. Properly planning these two aspects can result in a much better design. On other topics, rapid prototyping, iterative design, and clear communication are key to building a good subsystem.

Another big lesson learned came from testing the actuation speed of the airbrakes. The airbrakes were designed using the maximum rpm value found from the stepper motor's datasheet; however, due to a lack of research, the team failed to realize that the maximum RPM could only be achieved with twice the input voltage than was being supplied. This situation taught the team that before finalizing a design, all specifications of each part should be confirmed either through datasheets or directly from the manufacturer, instead of making assumptions about functionality and therefore adding to the time and cost of system design.

D. Payload

The integration of the scientific payload was a complex and iterative process. One of the main lessons learned was the necessity for repeated validation of the design and manufacturing processes. The team had to conduct both FEA and physical testing to ensure integrity during launch and landing conditions. The biggest part of the iterative phase was electronic integration and designing parts to be manufactured with correct tolerances. While working with different materials, such as printed plastics, aluminum, brass, etc., the team had to learn tolerancing between parts to ensure proper integration. While designing with specific size constraints, the team also went through a fastener selection phase. During this time, the team discussed a size standard for all fasteners in the payload system to reduce failure points.

E. SRAD Telemetry GPS

Throughout the creation of the SRAD Telemetry GPS, many different challenges arose from experimenting with different challenges arose from experimenting with maximizing GPS. To start out, the first iteration challenges using the DRA-818V and APRS. The main issues with this transceiver stemmed from the APRS protocol and from the difficulty designing attenuating circuits to lower the discrete power output of 500 mW. To solve this, the transceiver was switched out for the RFM96W, which had a lower power specification (100 mW). Before determining the need for an RF amplifier and orientation manipulation through signal tracking, many range tests were conducted. Each range test kept resulting in different ranges based on the surrounding areas' Electromagnetic Interference (EMI). Throughout the range tests, research was conducted to determine how to improve the range without strictly changing the antennas or power, which involved optimization of the spreading factor and signal bandwidth as programmed on the RFM96W (done through trial and error from looking at RSSI). The full operational range of the bay was realized following the mitigation of EMI, achieved by isolating the site from high-power buildings and power lines.

Issues regarding range revealed the need to increase the RF power limit from the RFM from 100 mW to 200 mW using an RF amplifier and manipulating the antenna orientation. The other issue during range tests was transport, which was critical when one range test failed before arriving at the site due to a short, causing an entire iteration of the Telemetry system to be lost. The solution to this was the use of static bags to contain the parts during transport.

Other than the basic logistical problems, much experimentation was done to challenge the technical ability of the Telemetry Team. Since this is SOAR's first year competing in IREC, there was pressure to create a new Telemetry system not present during NSL competitions. First, SMD designs were attempted from scratch as opposed to using breakout board components, as well as creating custom circuits, such as a custom bi-directional RF amplifier and attenuator. Even before the DTEG changes no longer allowed frequency hopping, the team was in the process of automating the frequency change command. Despite not fully implementing many of these DIY ideas, the lesson learned here was to take things one step at a time. The team may not have fully been able to customize the bay for

this competition year, but the lessons learned from working with the equivalent breakout boards (the RF amplifier, for example) helped foster a better understanding of how such circuits work and will inspire future custom systems.

VI. Acknowledgements

The team is grateful to ESRA for organizing the competition, Jonathan Fitzer and Jimmy Jawn as team mentors, and the University of South Florida for providing the resources for the team's development. The team is grateful to the sponsors who provided monetary support and software access: Mike Crew, Joe Register, Epsilon3, Lonzo Law, Kenesto, Ansys, Five Star Pizza, Jim's Body Shop, and Monster Beverage Corp.

VII. Technical Report Appendices

Appendix A: System Weights, Measures, and Performance Data

1. Basic Vehicle Information

Table 3. Basic Vehicle Information

Description	Value	Unit
Number of stages	1	N/A
Length	100	in
Airframe diameter	6.17	in
Number of fins	4	N/A
Fin semi-span	7.2	in
Fin tip chord	1.6	in
Fin root chord	12	in
Fin thickness	0.125	in
Weight on launch rail	64.05	lb
Propellant weight	12.5	lb
Empty motor case/structure weight	7.35	lb
Payload weight	8.59	lb
Liftoff weight	64.05	lb
Center of pressure	80.721	in
Center of gravity	65.584	in
Launch rail length	204	in

2. Propulsion Information

Table 4. Propulsion Information

Information	Value	Unit
Motor type	Solid	N/A
COTS or SRAD	COTS	N/A
COTS manufacturer and designation	AeroTech M1939W-PS	N/A
Motor letter classification	M	N/A
Average thrust	1,939	N
Total impulse	10,481.5	Ns
Motor burn time	6.2	s

3. Predicted Flight Data

Table 5. Predicted Flight Data

Description	Value	Unit
Liftoff thrust-weight ratio (X:1)	4.51	N/A
Rail departure velocity	84.6	ft/s
Minimum static margin	2.45	cal
Maximum acceleration	7.23	G
Maximum velocity	954	ft/s
Fin flutter velocity	1,762	ft/s
Target apogee	10,000	ft
Predicted apogee	11,943	ft

4. Flight Profile Graph

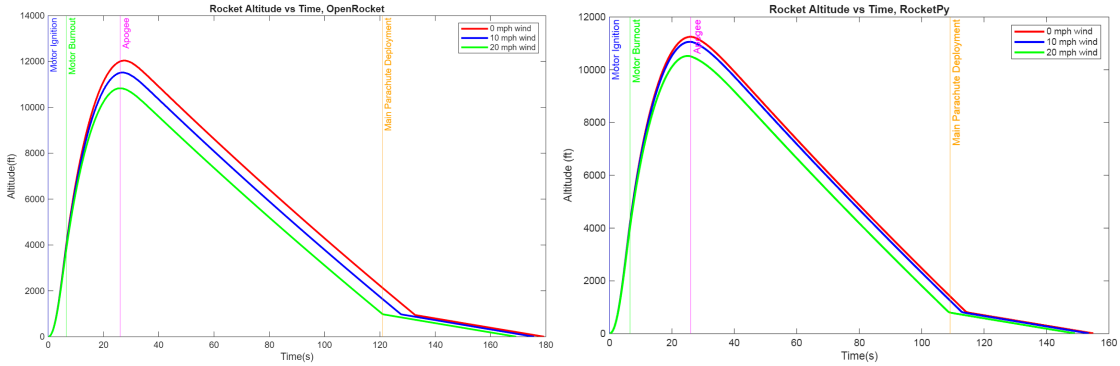


Figure 28. Altitude by Time, OpenRocket (left) vs RocketPy (right)

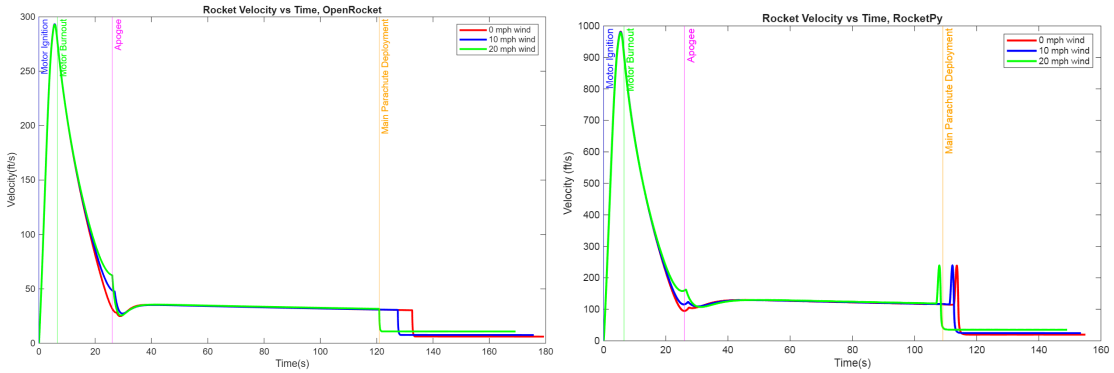


Figure 29. Velocity by Time, OpenRocket (left) vs RocketPy (right)

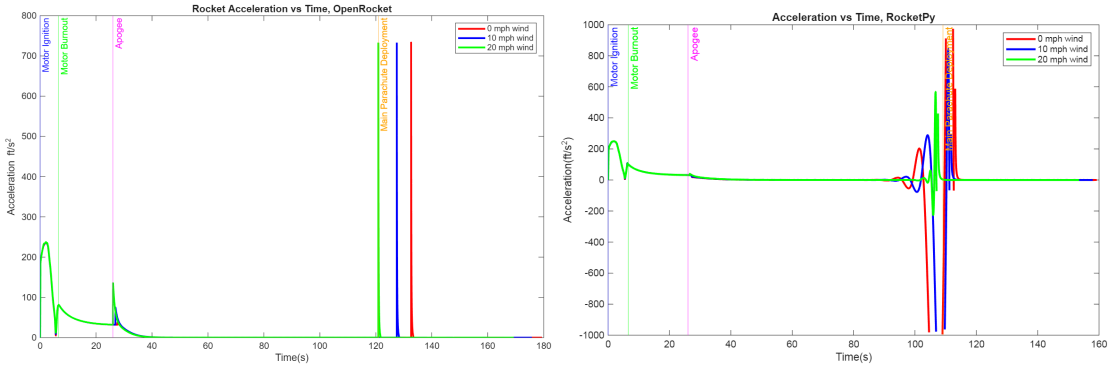


Figure 30. Acceleration by Time, OpenRocket (left) vs RocketPy (right)

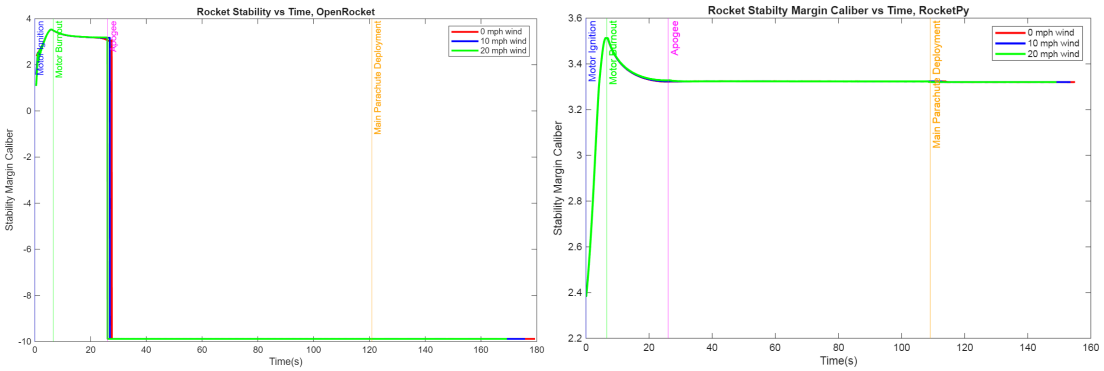


Figure 31. Stability Margin Caliber by Time, OpenRocket (left) vs RocketPy (right)

5. Recovery Information

Table 6. Altimeters Used

Altimeter Used	
Category	**Description**
COTS	MissileWorks RRC3+ altimeter (primary)
Redundant	Two additional MissileWorks RRC3+ altimeters are configured as secondary and tertiary units.

Table 7. Drogue Parachute Information

Drogue Parachute Information		
Description	**Value**	**Unit**
Primary Deployment Charge (Black Powder)	5.5	g
Backup Deployment Charges (Black Powder)	6	g

Backup Deployment Charges (Black Powder)	6.5	g
Deployment Altitude	Apogee	N/A
Descent Rate	108.6	ft/s

Table 8. Main Parachute Information

Main Parachute Information		
Description	**Value**	**Unit**
Primary Deployment Charge (Black Powder)	6	g
Backup Deployment Charges (Black Powder)	6.5	g
Backup Deployment Charges (Black Powder)	7	g
Deployment Altitude	1,000	ft (AGL)
Descent Rate	18.7	ft/s

4. Parachute shock cords

Kevlar shock cords are used for both drogue and main recovery systems, each with a length of 25 ft and a load rating of 6,000 lbf.

5. Mechanical links

Shock cords are connected to the booster's upper plate and the nose cone's ballast ring with an Alpine Butterfly knot. The cords are connected to the Nomex and parachutes through an Alpine Butterfly knot and quicklinks. The cords are connected to the top and bottom of the principal bay through a Double Alpine Butter,knot and two quick links, and an eye nut on each side.

6. Payload

Table 9. Payload

Description	**Value**	**Unit**
CubeSat Structure Weight	1.77	lb
Minimum Structure Factor of Safety	1.0396	N/A
Structure LxWxH	11.81 x 3.86 x 3.86	in
Maximum Descent Velocity	16.07	ft/s
Impact Velocity	15.682	ft/s
Rover Weight	3	lb
Rover LxWxH	11.54 x 3.37 x 2.62	in
Battery Payload	0.66	lb
Cameras	0.09	lb
Cubesat fasteners	0.97	lb

Motors	0.73	lb
Parachute	0.30	lb
Rover Axle	0.02	lb
Rover Bearings	0.01	lb
Rack and Pinion	0.19	lb
Rover Risers	0.01	lb
Rover Structures	0.30	lb
PCB/Electronics	0.10	lb
Wheels	0.12	lb

Appendix B: Project Test Reports

A. Recovery System Testing

1. Recovery System

The recovery system utilizes a dual-deployment architecture with triple-redundant avionics to ensure reliable descent and safe landing. Drogue deployment occurs at apogee to stabilize the vehicle and minimize drift, followed by main parachute deployment at approximately 1,000 ft AGL to reduce descent velocity before landing. The system is designed to ensure complete separation of rocket sections, proper parachute deployment, and stable descent under both nominal and off-nominal conditions. All testing was conducted in accordance with local safety regulations and best practices for handling energetic devices.

2. Ground Test Demonstration

Ground testing was conducted to validate the effectiveness of black powder deployment charges in separating airframe sections and ejecting parachutes. The first test evaluated both main and drogue charge wells using 0.18 oz of black powder. The upper section successfully deployed, fully shearing pins and ejecting the payload and main parachute. However, the booster section failed to separate, preventing drogue deployment. This failure was attributed to insufficient internal pressure caused by airframe gaps. To address this, the team sealed gaps in the booster section and increased the drogue charge mass to 0.23 oz. A second test was conducted using the updated configuration, resulting in successful pin shearing, full separation of the booster and mid sections, and complete drogue parachute deployment. Sensor electronics were functionally included in testing through simulated deployment conditions using altimeter-based activation systems. These tests confirm that the selected charge masses generate sufficient pressure for reliable deployment and validate recovery system functionality.

3. *First Black Powder Test*

Objective: *Validate that the black powder charges generate enough internal pressure to shear all pins to successfully separate into sections and ensure recovery system deployment.*

Testing Variables: Black powder mass for main and drogue charge wells

Success Criteria: The nose cone and booster must separate from the mid section, without damage to parts, and parachutes must be completely ejected from the airframe.

Reasoning: The test ensures that e-matches will send an electrical signal to the charge wells. This signal will ignite the black powder, creating enough pressure to break the shear pins, separating the sections, and deploy the drogue and main parachute, allowing proper recovery.

Method

1. Take two small containers, measure 0.18oz of black powder into each.
2. Take the fully assembled airbrakes and distinguish the e-matches, one for the booster charge well and the other for the upper charge well.
3. Place one end of the booster e-match into the middle charge well on the bottom bulkhead.
4. Funnel 0.18oz of black powder into the charge well, encapsulating the e-match.
5. Fill the remaining space of the charge well with dog barf and cover with electrical tape.
6. Repeat steps 3-5, using the upper e-match, remaining black powder, and upper bulkhead.
7. Create multiple knots on both the upper and booster shock cords.
8. Fold the parachutes and wrap them in Nomex cloth.
9. Using quicklinks, secure the wrapped parachutes to the shock cords and the shock cords to the bulkheads.
10. Assemble all sections of the airframe by connecting the mid airframe to the couplers with shear pins.
11. Secure the integrated vehicle to the test stand.
12. Attach two ends of the booster e-match to a switch, then attach a 9-volt battery to the other end of the switch.
13. Once all participants are 5 yards clear from the testing space, activate the switch to detonate the black powder.
14. After detonation has occurred and the area is deemed safe, repeat steps 12-13 with the upper e-match.

Results: The upper section fully deployed, with all pins shearing completely, allowing the cubesat and main parachute to eject completely from the airframe. The booster section did not separate upon black powder detonation. This restricted the drogue from ejecting from the airframe. The team believes that the booster section did not properly deploy due to a lack of pressure as a result of gaps in the booster airframe.

Mitigation: To cover the gaps in the airframe, the team put the fins into the booster section and used tape to cover the area surrounding the motor retainer. Additionally, the amount of black powder will be increased to 0.23oz for drogue charge wells.

Conclusion: The upper section's success allows it to remain the same. However, another black powder test needs to be conducted on the booster section with the changes implemented.

4. ***Second Black Powder Test***

Objective: Validate that the booster section's black powder charge will generate enough internal pressure to shear all pins successfully, separating the booster and mid airframes to ensure recovery system deployment.

Testing Variables: Black powder mass, drogue charge wells, and airframe gaps

Success Criteria: The booster must separate from the mid section, without damage to parts, and the drogue parachute must be completely ejected from the airframe.

Reasoning: The test ensures that e-matches will send an electrical signal to the charge wells. This signal will ignite the black powder, creating enough pressure to break the shear pins, separating the sections and deploying the drogue parachute, allowing proper recovery.

Method:

1. Take a small container and measure 0.23oz of black powder.
2. Take the fully assembled airbrakes and place the bottom e-match into the middle charge well on the bottom bulkhead.
3. Funnel 0.23oz of black powder into the charge well, encapsulating the e-match.
4. Fill the remaining space of the charge well with dog barf and cover with electrical tape.
5. Create multiple knots on both the upper and booster shock cords.
6. Fold the parachutes and wrap them in Nomex cloth.
7. Using quicklinks, secure the wrapped parachutes to the shock cords and the shock cords to the bulkheads.
8. Assemble all sections of the airframe by connecting the mid airframe to the couplers with shear pins.
9. Secure the integrated vehicle to the test stand.
10. Attach two ends of the booster e-match to a switch, then attach a 9-volt battery to the other end of the switch.
11. Once all participants are 5 yards clear from the testing space, activate the switch to detonate the black powder.

Results: The black powder successfully sheared booster pins, separating the booster section and fully deploying the drogue parachute.

Mitigation: Since both sections were successfully separated, the test is complete, and no more changes are needed.

5. Flight Test Demonstration



Figure 32. Recovery Sequence During Flight : (a) Main parachute deployment, (b) Post-flight landing configuration in field conditions.

A full-system flight test was conducted to validate the recovery system under real flight conditions, including deployment sequencing, separation reliability, and parachute performance. During flight, drogue deployment occurred successfully at apogee, resulting in proper stabilization of the vehicle and controlled descent. However, the main parachute deployment was observed to be delayed relative to the programmed altitude. Despite this delay, the recovery system was ultimately deployed, and the vehicle descended safely. This behavior is consistent with previously observed timing inconsistencies during ground-based altimeter testing. Based on these results, further testing and configuration adjustments are being conducted to improve deployment timing accuracy and ensure consistent performance across all altimeter units. The flight test provided critical validation of system integration and confirmed that the recovery system is capable of functioning under real flight conditions, while also identifying areas for refinement before competition.

6. Dual Redundancy of Recovery Electronics



Figure 33. Triple-Redundant Recovery Avionics System: (a) Battery Mounting Plate showing three independent power supplies, (b) Integrated Avionics Bay with three RRC3+ altimeters

The recovery system utilizes a triple-redundant avionics architecture using three independent MissileWorks RRC3+ altimeters. Each altimeter operates with its own dedicated power source, arming switch, e-match, and deployment charges, ensuring full independence between systems. The primary altimeter deploys the drogue parachute at apogee and the main parachute at approximately 1,000 ft AGL. The secondary and tertiary altimeters provide redundancy by initiating drogue deployment at apogee +1 s and +2 s, respectively, while maintaining the same main deployment altitude. Each altimeter is connected to its own pair of charge wells, eliminating single points of failure and ensuring recovery events occur even in the event of partial system failure.

7. Stored-Energy Devices – Energetic Device Safing and Arming

Black powder deployment charges are treated as stored-energy devices and are handled with strict safety procedures. The recovery system is designed such that all energetic devices are considered “made safe” during handling, requiring two independent actions—arming the altimeter and triggering deployment—before energy release can occur. E-matches remain disconnected from powered avionics until final arming procedures are initiated. Energetic devices remain in a safe configuration until the vehicle is placed on the launch pad, at which point they are armed under controlled conditions. All charges are sealed and protected to prevent accidental ignition due to

environmental factors or static discharge. These procedures ensure safe handling, transport, and operation of all energetic devices.

8. Arming Devices

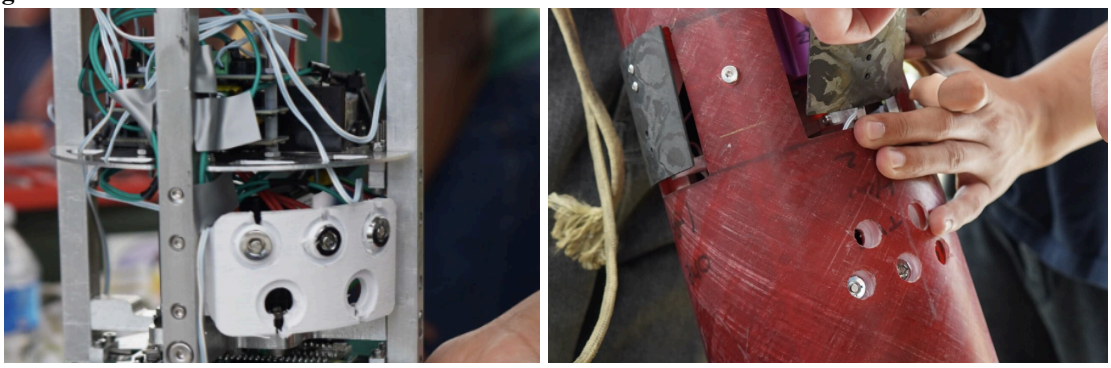


Figure 34. Avionics Bay with a Mechanical Key Switch Arming System

Each altimeter is armed using an independent external mechanical switch, allowing each recovery system to be activated separately. This ensures that no single switch failure can disable the entire recovery system. All arming switches are externally accessible and positioned such that they can be safely operated without placing personnel in hazardous proximity to the vehicle. The design allows safe actuation while wearing the required personal protective equipment and ensures compliance with all accessibility requirements.

9. Arming Device Verification

All arming devices are verified before flight through continuity checks and system diagnostics. Each altimeter is powered individually, and audible indicators are used to confirm proper activation. Continuity testing ensures that each e-match is properly connected and capable of receiving a deployment signal. Arming verification is designed to be performed at a safe distance and under high-noise conditions, ensuring reliable confirmation of system readiness in field environments.

B. SRAD Propulsion System Testing

"THIS PAGE IS INTENTIONALLY LEFT BLANK"

C. SRAD Pressure Vessel Testing

"THIS PAGE IS INTENTIONALLY LEFT BLANK"

D. SRAD Telemetry GPS Testing

1. First Battery Longevity Test

Objective: *Ensure the SRAD Telemetry GPS operates for at least 8 hours continuously with the battery provided.*

Testing Variables: The length of time of consistent transmission and reception.

Success Criteria: The Telemetry Bay PCB transmits continuously for at least 8 hours. The Ground Station receives all the data accurately over time.

Reasoning: This test ensures that the SRAD Telemetry GPS lasts long enough not to die while on standby waiting for the go-ahead to launch.

Method:

1. Assemble the Telemetry Bay PCB and Ground Station.
2. Run Arduino IDE to monitor serial.
3. Distance the Bay away from the receiving antenna by 1 meter.
4. Record the time everything was powered on.
5. Go to bed, wake up, unpower everything (if it is still on based on the light indicator on systems), and record the time.
6. Check the microSD cards on both the Ground Station and the Telemetry bay for data loss and the timestamp.
7. Compare the latest time stamp with the time difference between the power-on and power-off.

Results: Partial success, the Bay only lasted 7.5 hours before stalling, but was still on for 11 hours. Voltage dropped by 1V from 14.5 V to 13.5 V. The data sent closely matches the data received (# of entries varied only by 241 over 7.5 hours of uptime).

Mitigation: Implement a watchdog to automatically reset the system if the system stalls.

Conclusion: The team needs to conduct another battery test.

2. Second Battery Longevity Test

Objective: *Ensure the SRAD Telemetry GPS operates for at least 8 hours continuously with the battery provided.*

Testing Variables: The length of time of consistent transmission and reception.

Success Criteria: The Telemetry Bay PCB transmits continuously for at least 8 hours. The Ground Station receives all the data accurately over time.

Reasoning: This test ensures that the SRAD Telemetry GPS lasts long enough not to die while on standby waiting for the go-ahead to launch.

Method:

1. Assemble the Telemetry Bay and Ground Station.
2. Run Arduino IDE to monitor serial.
3. Distance the transmitter away from the receiving antenna by 1 meter.
4. Record the time everything was powered on.
5. Go to bed, wake up, unpower everything (if it is still on based on the light indicator on systems), and record the time.
6. Check the microSD cards on both the Ground Station and the Telemetry Bay PCB for data loss and the timestamp.
7. Compare the latest time stamp with the time difference between the power-on and power-off.

Results: success, bay lasted 11 hours before dying, relative to a 12-hour time cycle. Voltage dropped by 1.4 V from 13.5 V to 12.1 V.

Mitigation: N/A

Conclusion: The battery is adequate for powering the Telemetry Bay PCB and does not need further testing.

3. First Range Test

Objective: *The objective of this test is to ensure efficient transmission over a range of 10,000 feet reliably.*

Testing Variables: Distance before data cuts out completely.

Success Criteria: 10% or less data packet loss and consistent transmission reception at a distance of 10,500 ft between the Telemetry Bay PCB and Ground Station.

Reasoning: This test ensures that the Telemetry system communicates reliably during competition launch.

Method:

1. Gather materials and begin setup in the Engineering II Building on the University of South Florida Tampa Campus.
2. Assemble and configure the Telemetry Bay PCB and Ground Station according to the schematics in the team's EasyEDA workspace.
3. Flash both systems with the latest firmware from the team's GitHub repository.
4. Position the Telemetry Bay PCB at the fixed transmitter location.
5. Starting at 500 ft from the transmitter, as determined using Google Maps pins, have the Ground Station operator walk in a straight line away from the Telemetry Bay PCB.
6. At each 500 ft interval, record a 5-minute dataset using the Excel Test Log template. For each interval, document:
    - Transmission rate, in packets per minute, using serial monitor timestamps
    - Qualitative packet loss, based on the number of data points recorded in the Telemetry Bay PCB logs
    - Estimated distance and location from Google Maps
    - Any relevant observations on system behavior
7. Save each dataset as a unique CSV file labeled with the corresponding test distance.
8. Repeat the measurement process at 500 ft increments until either:
    - The test distance reaches 10,500 ft, or
    - The transmission rate becomes inconsistent or drops to zero
9. After testing, review each CSV file for accuracy and verify that the number of recorded data points matches the expected 5-minute count. Based on the January 22 firmware, the expected count is 1,500 data points per 5-minute interval.
10. If reliable communication is not maintained before 10,500 ft, investigate RF range improvements that do not increase transmit power, such as antenna design, antenna placement, ground-plane configuration, polarization alignment, and receiver placement. Repeat the test using revised antenna configurations as needed.
11. The test is considered successful if the ratio of received to expected data points is approximately 90% at 10,500 ft.

Results: Failure, bay only lasted 1,500 ft before dying.

Mitigation: Change the testing area because of significant EMI from the research infrastructure on the university campus.

Conclusion: Another range test needs to be conducted at a location with minimal EMI.

4. Second Range Test
Objective: *The objective of this test is to ensure efficient transmission over a range of 10,000 feet reliably.*

Testing Variables: Distance before data cuts out completely, and the antenna combination between the Ground Station and the Telemetry bay.

Success Criteria: 10% or less data packet loss and consistent transmission reception at a distance of 10,500 ft between Telemetry and Ground Station.

Reasoning: This test ensures that the Telemetry system communicates reliably during competition launch.

Method:
1. Gather materials and begin setup in a safe location near N 40th St, Tampa, FL 33605, United States.
2. Assemble and configure the Telemetry Bay PCB and Ground Station according to the schematics in the team's EasyEDA workspace.
3. Flash both systems with the latest firmware from the team's GitHub repository.
4. Position the Telemetry Bay PCB at the fixed transmitter location.
5. Starting at 500 ft from the transmitter, as determined using Google Maps pins, have the Ground Station operator walk in a straight line away from the Telemetry Bay PCB.
6. At each 500 ft interval, record a 5-minute dataset using the Excel Test Log template. For each interval, document:
    - Transmission rate, in packets per minute, using serial monitor timestamps
    - Qualitative packet loss, based on the number of data points recorded in the Telemetry Bay PCB logs
    - Estimated distance and location from Google Maps
    - Any relevant observations on system behavior
7. Save each dataset as a unique CSV file labeled with the corresponding test distance.
8. Repeat the measurement process at 500 ft increments until either:
    - The test distance reaches 10,500 ft, or
    - The transmission rate becomes inconsistent or drops to zero
9. After testing, review each CSV file for accuracy and verify that the number of recorded data points matches the expected 5-minute count. Based on the January 22 firmware, the expected count is 1,500 data points per 5-minute interval.
10. If reliable communication is not maintained before 10,500 ft, investigate RF range improvements that do not increase transmit power, such as antenna design, antenna placement, ground-plane configuration, polarization alignment, and receiver placement. Repeat the test using revised antenna configurations as needed.
11. The test is considered successful if the ratio of received to expected data points is approximately 90% at 10,500 ft.

Results: Failure, telemetry data packets were received until the 1-mile mark was reached, short of the target 10,500 ft range.

Mitigation: Change the testing area due to interference from power lines and urban buildings in the test location. Determine the optimal settings of the RFM96W bandwidth and spreading factor. Have the bay and Ground Station track data loss through sequence addition.

Conclusion: The team needs to conduct another range test.

5. Third Range Test
Objective: *The objective of this test is to ensure efficient transmission over a range of 10,000 feet reliably.*

Testing Variables: Distance before data cuts out completely, antenna combination between Ground Station and Telemetry bay, and RFM96W settings for bandwidth and spreading factor.

Success Criteria: 10% or less data packet loss and consistent transmission reception distance of 10,500 ft between Telemetry and Ground Station.

Reasoning: This test ensures that the Telemetry system communicates reliably during competition launch.

Method:

1. Gather materials and begin setup in a safe location near 80 Foot Rd, Florida 3380, United States of America.
2. Wire the Ground Station and Telemetry Bay hardware according to the approved schematics.
3. Connect each system to a laptop and upload the latest corresponding firmware to each device.
4. Keep both systems connected to their respective laptops throughout the test to enable serial monitoring and data logging.
5. Have the Ground Station operator carry the receiver, laptop, and Ground Station hardware away from the Telemetry Bay transmitter.
6. Record the following test data in the Excel template:
    - Transmission rate, determined from serial monitor timestamps
    - Packet loss, determined from missing or nonsequential packet sequence numbers
    - GPS-based distance from the Telemetry Bay transmitter
    - The distance at which telemetry becomes inconsistent or is lost
    - Relevant observations on system behavior
7. Save each test dataset as a unique CSV file labeled with the corresponding test distance or antenna/configuration used.
8. Update the telemetry configuration as needed, including spreading factor, bandwidth, and antenna selection.
9. Repeat the measurement process until either:
    - Reliable telemetry is demonstrated at 10,500 ft, or
    - The transmission rate becomes inconsistent or drops to zero
10. Review each CSV file for accuracy and calculate the maximum reliable transmission distance using the recorded GPS data.
11. The test is considered successful if approximately 90% of the expected data packets are received at 10,500 ft.

Results: Partial success, bay only lasted 1.5 mi before dying due to decline on a hill. Determined the best spreading factor was 9, and the bandwidth was 60 kHz.

Mitigation: Implement an RF amplifier to increase the RF power from 100 mW to 200 mW. Create an apparatus or protocol for orientating the Ground Station antenna by hand.

Conclusion: The team needs to conduct another range test or launch.

E. Payload Recovery System Testing

1. Ground Testing

Objective: *Rack and pinion mechanism retracts from the CubeSat, allowing the rover to drive out under its own power and perform predetermined duties.*

Testing Variables: Rack and pinion mechanism, state machine, and camera systems to detect vegetation

Success Criteria: Rover successfully departs from the CubeSat structure and performs scanning duties in a grid pattern. Successful data collection and storage/transmission of no less than 50% of applicable plant life detected.

Reasoning: This test is conducted to ensure no plastic deformation of any part occurs.

Method:

1. Ensure batteries are charged
2. Plug the battery into the PCB
3. Ensure PCB continuity
4. Check all systems before integration to ensure functionality
5. Integrate electronics into the rover
6. Enclose the assembly to prevent contaminants from entering that may affect the internal electronics.
7. Insert the rover into the CubeSat structure
8. Lift the payload and place it on the ground to simulate a landing state
9. Observe the rack and pinion retracting from the CubeSat back into the rover
10. Rover drives out under its own power
11. Rover conducts a predetermined scanning path

Results: Rover successfully deployed and completed all assigned tasks.

Mitigation: N/A

Conclusion: The team shall conduct this test repeatedly to ensure function.

2. Deployment Testing

Objective: *Test parachute inflation using different weights and parachute sizes to find the optimal size while saving the most space*

Testing Variables: The team will test with different weights ranging from 5-10lbs and parachute sizes ranging from 42”-96”.

Success Criteria: Successful inflation of the parachute and soft landing of the CubeSat on the desired side to allow rover deployment

Reasoning: If the team chooses a parachute that is too small for the given weight of payload, the CubeSat will impact at an undesired force and risk plastically deforming, restricting the rack and pinion from actuating, which will not allow the rover to be able to deploy. If the team chooses a parachute that is too big for the given weight of the payload, the CubeSat will not fit inside the mid-section of the vehicle and will risk covering the payload upon landing, not allowing the rover to be able to egress from the structure.

Method:

1. Assemble the rover
2. Ensure all systems are functional
3. Insert into CubeSat
4. Actuate the rack and pinion to secure the rover into the CubeSat
5. Tie the shock cord in a knot to make one loop connecting to all 4 corners of CubeSat
6. Attach the quick link to the shock cord
7. Attach the parachute swivel connector to the quick link
8. Fold the parachute using the flaking (pleating) method
9. Wrap the parachute in Nomex
10. Drive to the “Beard” parking garage
11. Take the elevator to the 8th floor
12. Ground team ensures a clear drop zone
13. Ground team gives the all clear
14. The drop team conducts the testing
15. The drop team returns to the ground to verify the results

Results: The team has deduced that the optimal parachute size for space saving and landing velocity using a 7lb payload will be a 52” parachute.

Mitigation: Conduct testing in a remote location to minimize the risk of collision with vehicles or people.

Conclusion: Drop testing was successful. Repeat testing to maximize the chance of success.

Appendix C: Hazard Analysis

Hazard Category	Specific Source / Hazard	Description of Hazard & Potential Consequences	Mitigation Approach (Process and/or Design)
Energetics (Propulsion)	COTS AeroTech M1939W-PS Motor	Explosion/casing failure causing blast or flying debris.	Process: Visually inspect grains/casing. Enforce a 200ft standoff behind a barrier at launch. Design: Secure firmly with SRAD aluminum fin support and centering rings.
Energetics (Recovery)	Black powder charges & e-matches	Premature detonation causes severe burns or failure, causing ballistic impact.	Process: Maintain 30-foot ground test standoff. Keep e-matches shunted until upright on the pad. Design: Increase charge to 0.19oz. Dual redundant avionics.
Handling & Transport	Black powder, e-matches, motors	Accidental ignition of the energetics during the 1,000+ mile transport from FL to TX.	Process: Store energetics in a designated, static-free, padded day box physically separated from vehicle electronics and heat sources.
Handling & Storage	Toxic chemicals, epoxies, resins	Exposure to VOCs can cause respiratory issues or skin sensitization during storage and application.	Process: Store in sealed, climate-controlled containers. Mandate nitrile gloves, safety glasses, and well-ventilated workspaces during application.
Flight Dynamics	Airframe, Fins, Airbrakes	Rocket deviates from the nominal flight path, contacting personnel/property at high speed.	Design: Aerodynamic modeling (OpenRocket) for static margin. Trapezoidal fins to minimize flutter. Software forces airbrakes to neutral if the altitude is > 30°.
Pad Operations	Launch Rail & 60 lb Vehicle Weight	Rocket falls from the launch rail during prelaunch assembly, causing crushing injury.	Process: Require a minimum of two trained personnel to lift and mount the vehicle. Verify rail guide structural integrity prior to transport.
Pad Operations	Igniter / Motor System	Hang fire (Rocket does not ignite on command); ignites when approached.	Process: Wait ESRA-mandated 60 seconds before approaching the pad. Disconnect launch control power and pocket safety key before approaching.

Pad Operations	Recovery Electronics / Altimeters	Recovery system deploys during assembly/prelaunch, causing blast trauma.	Process: Key switches for altimeters remain in the OFF position until all personnel are ready to clear the pad.
Electrical (Design)	14.8V, 24V, and 12V Li-ion batteries	Short circuit causing thermal runaway, fire, or total avionics loss.	Design: Thick, heavy-duty 3M self-fusing rubber tape (rated to 194°F) isolates contacts. Batteries secured tightly in 3D-printed PLA sleds.
Mechanical (Design)	Airbrakes NEMA 23 stepper motor	Inadvertent actuation of 200 in-oz torque linkages causing crushing/pinching.	Process: Keep the 24V battery disconnected during mechanical assembly. Establish clear verbal warnings. Design: Mechanical key switch to save the PCB.
Mechanical (Design)	EVE Rover dual 12V motors	Motors driving post-flight are causing pinch injuries during manual extraction.	Process: Verbally confirm power is cut before extraction.Design: Rover State Machine includes a physical manual override/kill switch.
Manufacturing	Carbon fiber & fiberglass	Inhalation of toxic dust or ocular damage during CNC routing/cutting.	Process: Mandate N95 respirators/safety glasses. Use wet sanding. Design: Heavy aluminum cylinder jig to secure the airframe during CNC slotting.
Manufacturing	Power tools and Soldering irons	Lacerations, punctures, thermal burns, or flux fume inhalation.	Process: Adhere to tool SOPs. Wear proper PPE (glasses, closed-toe shoes). Solder only in well-ventilated areas.
Testing Operations	CubeSat Drop Testing	A 6 lb payload dropped can cause injuries	Process: Strict exclusion zone with spotters. Design: Payload guided down a taut wire into a designated catch tarp.
Testing Operations	70cm band RF Amplifier	Localized tissue heating due to concentrated RF energy exposure.	Process: Never power on the transmitter while touching the antenna. Design: Use dummy loads for bench testing instead of broadcast antennas.

Appendix D: Risk Assessment

Hazard / Failure Mode	Possible Causes	Risk of Mishap and Rationale	Mitigation Approach (Design / Process)	Risk of Injury after Mitigation
Explosion or catastrophic failure of a solid rocket motor	Motor casing failure, nozzle blockage, or grain defect in the COTS AeroTech M1939W-PS White Lightning motor.	Medium: While COTS motors are highly reliable, this M-class motor generates over 500 lbf of peak thrust.	Strictly follow the manufacturer's assembly instructions. Secure the motor casing firmly, utilizing the SRAD aluminum fin support structure and centering rings. Enforce ESRA standard safe standoff distances (200 feet) behind a barrier during launch operations.	Low
The rocket deviates from the nominal flight path	Fin flutter, asymmetrical airbrake deployment, thrust misalignment, or high launch winds.	Medium: High-speed aerodynamic instability can cause the vehicle to veer toward personnel.	Utilize aerodynamic modeling (OpenRocket) to ensure proper static margin. Trapezoidal fins selected to minimize flutter. Airbrakes software is programmed to return flaps to neutral if the vehicle attitude exceeds 30°.	Low
Premature or failed deployment of black powder charges	Short circuit in avionics, static discharge to e-matches, or loss of internal pressure during ejection.	Medium / High: A ground test revealed that internal pressure leaked through airframe gaps, causing the drogue deployment to fail. Failure in flight results in a ballistic descent.	Increase black powder to 0.19 oz for drogue charge wells and seal airframe gaps. Use dual redundancy in recovery electronics. Maintain a 30-foot minimum standoff distance during ground testing.	Low
Main parachute deploys at or near apogee	Altimeter logic error, incorrect altitude settings, or premature structural failure of shear pins.	Medium: High-altitude main deployment will cause the vehicle to drift far outside the safe recovery zone.	Utilize dual independent altimeters with verified settings. Utilize SRAD Telemetry (GPS/IMU) as a backup tracking system to locate the vehicle if it drifts into highways or restricted zones.	Low
Rocket falls from the launch rail during prelaunch	Improper rail guide installation, high winds during mounting, or personnel slipping while lifting the vehicle.	Medium: Dropping the heavy vehicle can crush extremities and damage the airframe.	Require a minimum of two trained personnel to lift and slide the vehicle onto the rail. Verify rail guide structural integrity prior to transport.	Low
Hang fire (Rocket does not ignite on command)	Igniter failure, short in the launch control system, or poor igniter placement.	High: Igniter could smolder and ignite the M-class motor while personnel are approaching the pad.	Wait the ESRA-mandated minimum of 60 seconds (or standard LCO protocol) before approaching the pad. Disconnect the launch control power source completely and pocket the safety key before approaching the	Low

			vehicle.	
Recovery system deploys during assembly/prelaunch	Premature altimeter arming, static discharge to e-matches, or short circuits.	High: Black powder detonating while hands are inside the airframe causes severe burns and trauma.	Keep e-matches shunted until the vehicle is upright on the pad. Mechanical key switches for altimeters remain in the OFF position until all personnel are ready to clear the pad.	Low
Electrical short circuit or thermal runaway of high-capacity batteries	Improper charging, physical damage, or shorting across terminals of the 14.8V Telemetry, 24V airbrakes, or 12V payload batteries.	Medium: A previous iteration of the Telemetry bay experienced a short circuit during transport, destroying the system.	Transport all sensitive electronics and PCBs in anti-static bags. Secure batteries tightly within the 3D-printed PLA sleds and support structures to prevent shifting during flight. Thick, heavy-duty electrical insulation materials are used whenever possible to avoid all potential points of contact. For instance, self-fusing ethylene propylene 3M rubber backing rated up to 194°F was utilized.	Low
Crush or pinch injuries from active kinematic mechanisms	Unintended actuation of the NEMA 23 stepper motor (which generates up to 200 in-oz of torque), the airbrakes slider-crank system, or the EVE Rover's rack and pinion retention system.	Medium: High-torque motors actuating mechanical linkages can easily trap or injure fingers during assembly, testing, or arming.	Keep the 24V motor battery completely disconnected during mechanical assembly. Utilize the mechanical key switch to safeguard the airbrakes PCB. Establish clear verbal warnings before powering systems.	Low
Inhalation of hazardous particulates or physical injury during manufacturing	Machining 1/4 inch carbon fiber sheets for the fins on the CNC router, or cutting/drilling fiberglass airframes.	Medium: Carbon fiber and fiberglass dust pose severe respiratory and ocular hazards if PPE is not utilized.	Mandate N95 respirators or equivalent respirators and safety glasses for all fabrication. Sand rough edges of carbon fiber using appropriate dust mitigation (e.g., wet sanding). Use the heavy aluminum cylinder jig to safely secure the airframe during CNC slot machining.	Low
Injury to personnel or bystanders from falling objects during drop testing	Conducting physical drop tests of the EVE Payload (estimated 6 lbs)	High: Dropping a 6 lb aluminum CubeSat structure from seven stories poses a blunt-force hazard to anyone below.	Strictly guide the payload down a taut wire into a designated catch tarp. Maintain a strict exclusion zone at the base of the drop site with dedicated spotters to prevent access.	Low
Physical injuries from the use of power tools	Improper use of drills, saws, or other power tools during manufacturing or pad assembly.	Medium: Tools operate at high speeds and can cause severe lacerations or eye injuries if misused or if safety guards are	Mandate appropriate PPE (safety glasses, closed-toe shoes, no loose clothing). Strictly adhere to established Standard Operating Procedures (SOPs) and safety precautions for each tool.	Low

		bypassed.		
Thermal burns or fume inhalation during soldering	Contact with a hot soldering iron, splattering of solder, or inadequate ventilation while working on PCBs.	Medium: Soldering irons reach extreme temperatures, and vaporized flux fumes are respiratory irritants.	Mandate the use of safety glasses and operate only in well-ventilated areas or utilize fume extractors. Follow strict soldering SOPs, including proper iron resting and handling.	Low
Heat exhaustion or heat stroke during launch operations	Prolonged exposure to extremely high temperatures and intense sun during the June launch window in Midland, TX.	High: June temperatures in Midland routinely exceed 100°F, posing a severe and highly probable risk of heat-related illness during long shifts on the pad.	Enforce mandatory hydration schedules. Team leadership will maintain an ample, accessible stock of water and electrolyte-replenishing drinks. Utilize shaded rest areas and rotate crew members to prevent overexposure.	Low
Minor cuts, scrapes, or abrasions during vehicle assembly	Handling machined parts, unfinished fiberglass edges, or sharp metallic components during the integration of the vehicle.	High (Probability) / Low (Severity): Minor scratches are highly probable during complex mechanical assembly, though they rarely result in serious harm.	Maintain a fully stocked, on-site first aid kit containing hydrogen peroxide, isopropyl alcohol (IPA), bandages, and gauze for immediate, on-the-spot care.	Low
Radio Frequency (RF) exposure	Proximity to the Telemetry Bay's 70cm band bidirectional RF amplifier and antennas.	Low (Probability) / Medium (Severity): The added amplifier increases localized RF energy, which can cause tissue heating.	Never power on the Telemetry transmitter while personnel are directly touching the antenna. Utilize dummy loads for bench testing.	Low
Driver fatigue and vehicular accidents during transport	The long cross-country drive from the University of South Florida to Midland, TX.	High: Driving over 1,000 miles is physically exhausting and increases the risk of sleep-deprived accidents.	Enforce a strict driver rotation schedule (switch drivers every 4 hours). Require overnight rest stops.	Low
Pinch injuries from the EVE Rover egress mechanisms	Handling the payload post-flight while the rover's dual 12V high-torque motors attempt to drive out.	Medium: Personnel might try to free a stuck rover while the motors are actively driving.	Ensure the rover's state machine has a manual kill switch. Visually and verbally confirm power is cut before manual extraction.	Low
Accidental ignition of energetic materials during transport	Transporting black powder and e-matches from Florida to the launch site.	High: Static, friction, or extreme heat in vehicles could trigger energetics.	Store all explosives and flammable substances in a separate, designated, static-free, and padded fiberglass ammo box away from heat sources and vehicle electronics.	Low

Appendix E: Checklists

Upper Final Assembly Checklist					
Time Estimate	10 minutes	**Leads Responsible**	Ninh, Sama, Alan	Completion	☐
Description					
Assemble the *Aurora* Nosecone. Includes assembling & securing the Telemetry subsystem and COTS GPS equipment in the nosecone					
Materials & Tools					
Nosecone		24oz Ballast Bay		COTS GPS Battery	
Upper-Mid Coupler		Ballast Plates (Top & Bottom)		Nuts for Rods (8)	
Shear Pins (4)		Telemetry Bay (Top & Bottom)		Battery Straps (2)	
Screws 4-40 (4)		Telemetry PCB		Screws for PCB & GPS (8)	
Threaded Rods (4)		Telemetry Battery		Keyswitch Holder	
Ballast Ring		COTS GPS		Key switches (2)	
Procedures			**Notes**		
☐	Ensure PCB, GPS, and both batteries are secured via screws and straps.				
☐	The threaded rods go through everything, starting with the ballast ring.				
☐	The ballast bottom plate, ballast bay, and ballast top plate are placed in that order. Fill the ballast bay with weights before adding to the threaded rod stack.				
☐	Place the Telemetry top and bottom bays, ensuring the Telemetry battery wire goes through the hole in the top bay. The key switch holder goes with the bottom bay.		Batteries and key switches need to be wired properly as needed.		
☐	After all pieces are connected via threaded rods, secure the rods with nuts.				
☐	Place everything into the upper-mid coupler and nosecone. Secure ballast ring to nosecone with 4-40 screws.		Use 1 quarter 20 bolts.		

Booster Final Assembly Checklist					
Time Estimate	20 minutes	**Leads Responsible**	Ninh	**Completion**	☐
Description					
Assemble the Booster Section of *Aurora*. Including the bolted fin assembly and motor.					
Materials & Tools					
Booster Fuselage		Screws 1/4-20 (8)		Motor Retainer	
Mid-Booster Coupler		Rail Guide Support		Nuts & Bolts for Motor Retainer (12)	
Centering Rings (Top & Bottom)		Rail Guide Piece		Motor Grains (4) + 4 for 2 launches	
Beams (4)		Shear Pins (4)		Silicon Lubricant	
Fins (4)		Screws 4-40 (6)			
Hex Head Nuts & Bolts 1/4-20 (12 of each)		10240 Motor Casing (w/ forward and back closures + seal disc)			

Procedures		**Notes**
☐	Assemble Bolted Fins, slide fins into the beams, and secure them with bolts. Secure beams to both centering rings with screws. Also, secure rail guide support	Follow all markings for fin orientation and beam placement.
☐	Ensure the fuselage and coupler are securely connected with screws.	Follow the markings
☐	Slide the fin assembly into the fuselage, and secure it with screws through the fuselage holes.	Follow the markings
☐	Secure the motor retainer to the bottom centering ring with nuts and bolts.	Motor assembly before
☐	Load grains into the motor casing	
☐	Slide the motor through the centering rings.	

Airbrakes Final Assembly Checklist					
Time Estimate	30 minutes	**Leads Responsible**	Duc, Chris	**Completion**	☐
Description					
Assembling electronics, tightening motor coupler and screws, and adding Loctite.					
Materials & Tools					
Bulkhead (2)		Strong plate (2)		Hex key	
Stringer (4)		Weak plate (2)		Duct tape	
Stepper motor (1)		Lead screw (1)		Zip tie	
Battery (2)		Shaft coupler (1)		Screw driver	
PCB (1)		Fastener (5-40, 4-40, 10-24)		Tweezer	
Battery holder (1)		Flaps (4)			

	Procedures	**Notes**
☐	Install the shaft coupler on the motor, 0.25in-0.2in above the motor shaft.	
☐	Install the lead screw.	
☐	Install the motor on a strong plate, with a 0.15in socket screw.	0.15in socket screw
☐	Install the PCB on the weak plate using 4-40 screws and a spacer.	4-40 screws
☐	Install weak plates using 1in 4-40 screws.	1in 4-40 screws
☐	Install battery holder, battery, spacer, etc., on the bulkhead.	payload
☐	Flip the bulkhead upside-down, align the lead screw with the hole on the battery holder.	
☐	Tighten everything, making sure to include washers. Shoulder bolts on moving joints should be fastened with a lock nut.	4-40 lock nut
☐	Install flaps: Fasten the bottom, and then the top. Be sure to use the smaller screws on the bottom. It may be helpful to actuate the flaps into the deployed position. Be sure the mounts are fully covered by the flaps, too.	5-40 1/2 bolt
☐	Test for actuation	
☐	Remove flaps, and insert the remaining assembly into the airframe. Once inside, open the flaps.	REMOVE FLAPS BEFORE INSERTING IN AIRFRAME
☐	Secure the airbrakes to the airframe with 1/4-20 wide screws.	1/4-20 wide screws
☐	Reinstall flaps, then test for actuation once again.	

Payload Final Assembly Checklist					
Time Estimate	15 minutes	**Leads Responsible**	Cooper, Chiara	**Completion**	☐
Description					
Assemble the Rover in the CubeSat structure and secure the parachute to the CubeSat structure.					
Materials & Tools					
Cubesat structure		Rover Chassis parts		Parachute	
Quicklinks		2 PCB layers		2 Cameras	
ToF Sensor		12V Battery		Steering System	
Retention System		1 Key switch		Harness	
10 M3 bolts		6 M4 bolts		Nomex	

Procedures		**Notes**
☐	Add the retention and steering system to the chassis using 6 M3 bolts.	
☐	Place the battery and the 2-layer PCB in the rover using 4 M3 screws.	
☐	Plug in the two cameras, ToF, two motors, 2 servos, and battery wires to the PCB.	
☐	Attach the key switch to the chassis.	Friction fit
☐	Turn on the system and reset the servo in the retention system.	Reset the gear rack to align with the chassis.
☐	Configure launch ready program to run on startup, then turn off the system.	
☐	Attach the roof using 6 M4 bolts.	
☐	Place the rover in the CubeSat structure.	
☐	Tie the harness to the 4 eyebolts on the CubeSat structure and create a single knot.	
☐	Fold the parachute and wrap it with Nomex cloth.	
☐	Attach a quicklink to that knot and the parachute.	
☐	Before putting it in the vehicle, turn on the system and check that the servo is zero.	Zero angle is the gear rack aligned with the structure's exterior.

Final Vehicle Integration					
Time Estimate	45mins	**Leads Responsible**	Cesar	**Completion**	☐
Description					
Full Vehicle Integration. Upper, Booster, Airbrakes, and Payload need to be assembled before this.					
Materials & Tools					
Booster assembly		Principal Bay Assembly		Nomex and dogbarf	
Midsection		Avionics		Shear pin, fasteners	
Booster section		Drogue		Hex key, screwdrivers	
Nosecone		Main parachute		Payload assembly	
Coupler (2)		Harness		10 shear pins	

	Procedure)	**Notes**
☐	Prepare the assembled module in order: Nose cone, Telemetry, coupler, payload, midsection, principal bay (with black powder), coupler, assembled booster.	
☐	Secure coupler to the upper midsection	
☐	Z- Fold parachutes and wrap Nomex around parachutes. Attached quicklinks and harnesses to both parachutes.	
☐	Slide the principal bay from the bottom midsection. Secure the principal bay.	
☐	Secured main parachutes with harness inside the midsection, attached harness to nosecone bulkhead. Main parachutes should be constrained by principle bay.	
☐	Slide assembled payload from the top of the midsection, stuffed payload with dogbarf	
☐	Secured midsection with nose cone using shear pin	
☐	Attach drogue parachute to principle bay lower bulkhead. Secure the other end of the drogue parachute to the booster section.	
☐	Attach the other end of the drogue harness to the bottom of the principal bay.	
☐	Attach the midsection and booster section using the coupler. Fasten using 4 shear pins.	
☐	Inspect for damage and proper alignment.t	
☐	Conduct necessary tests	
☐	Attached e-match, open key switches	
☐	Secure launch vehicle on launch pad, final inspection	
☐	Attach the e-match to the fire control system. Clear pad	

Appendix F: Engineering Drawings

1. Full Vehicle

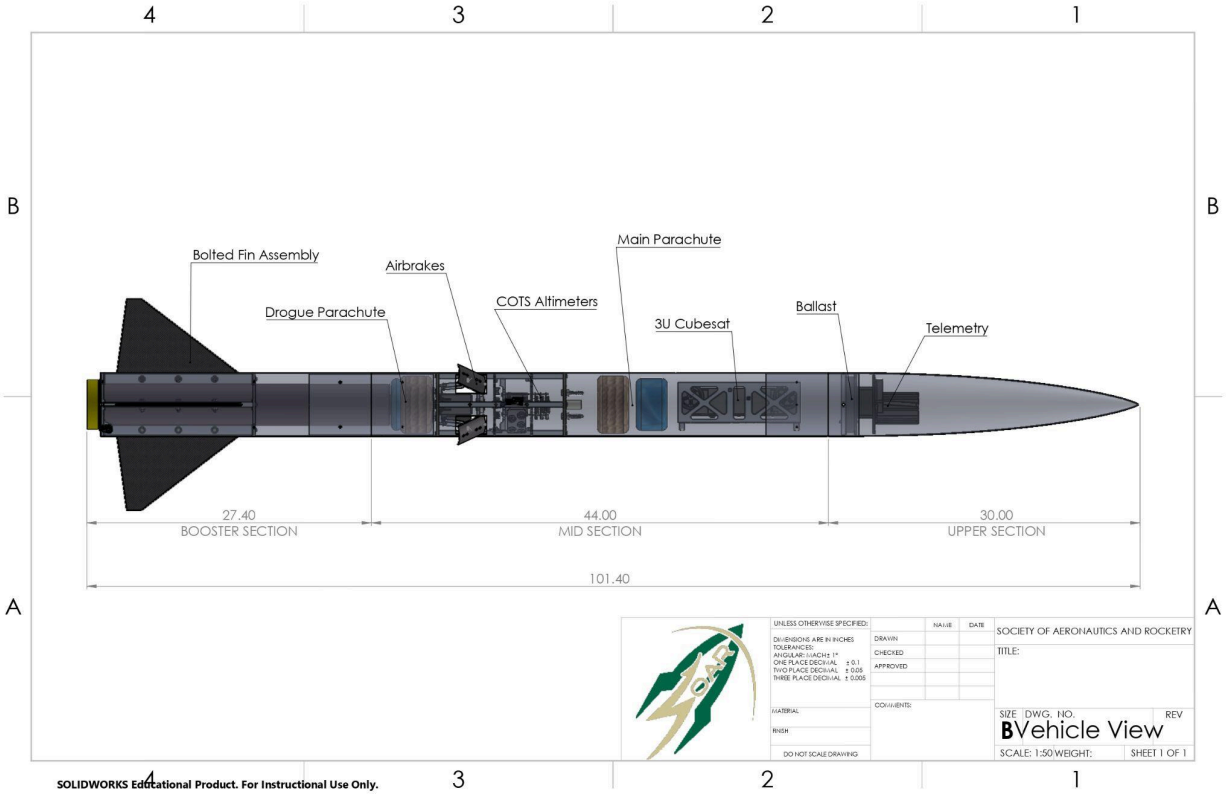


Figure 35. Full Vehicle Engineering Drawing

2. Aerostructures

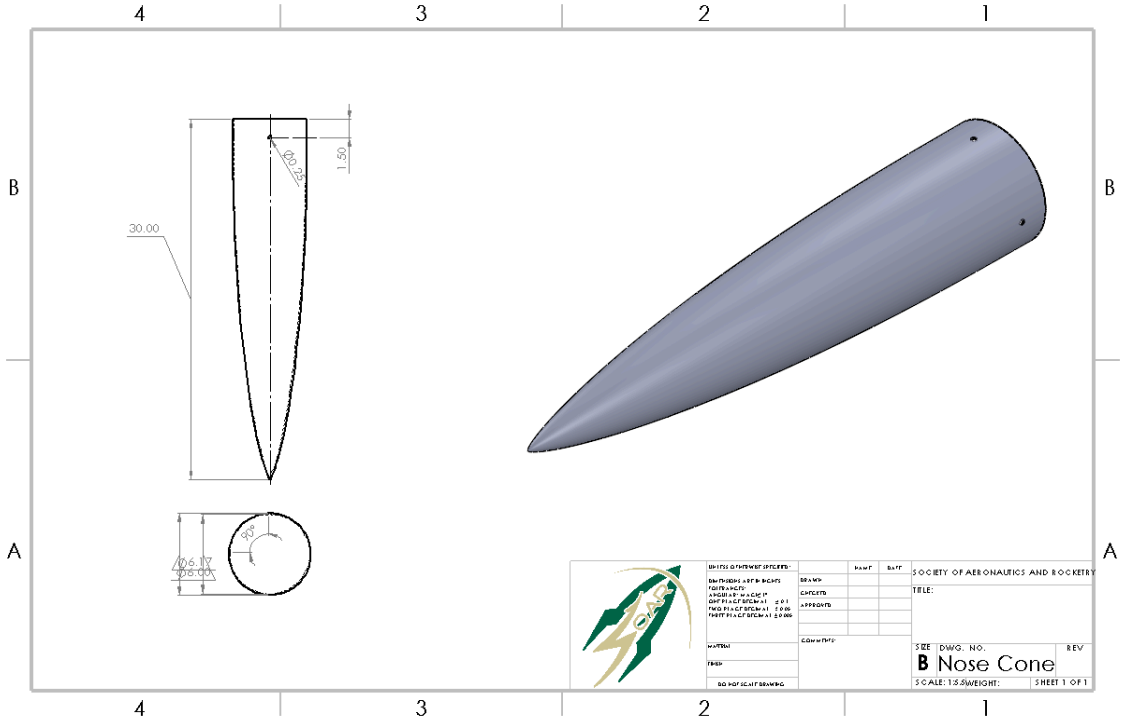


Figure 36. Nosecone

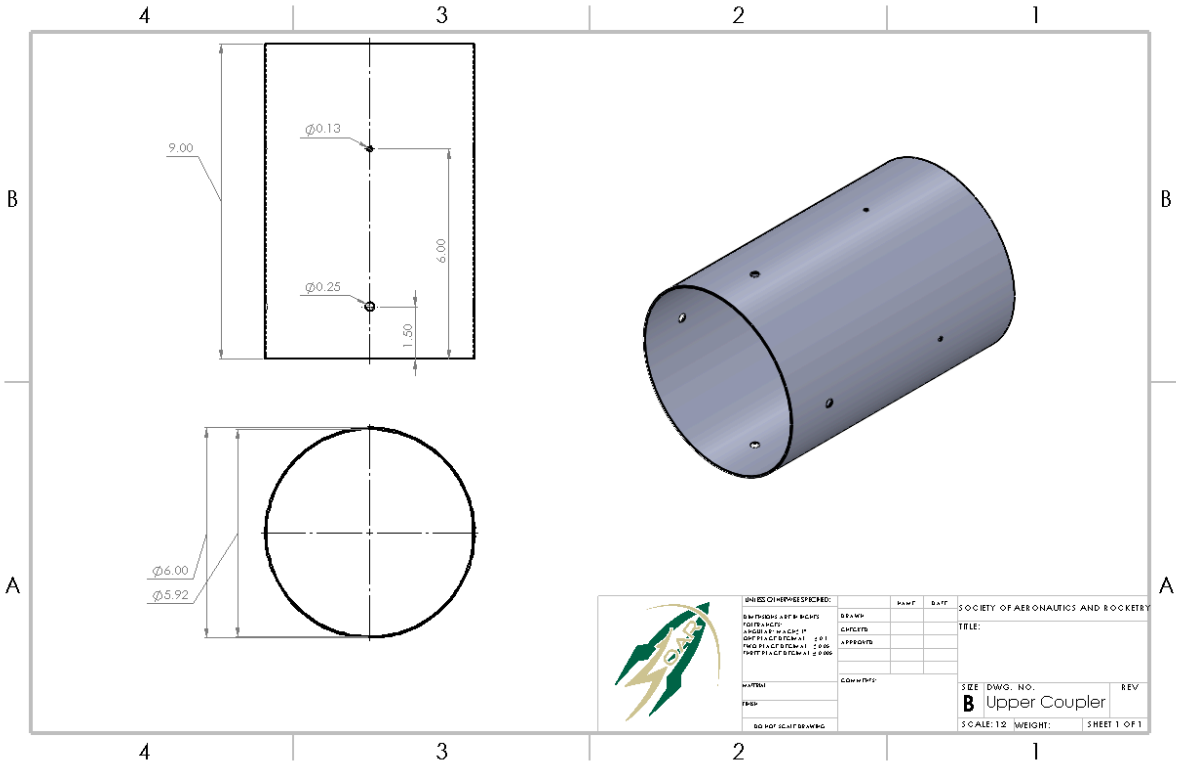


Figure 37. Upper Coupler

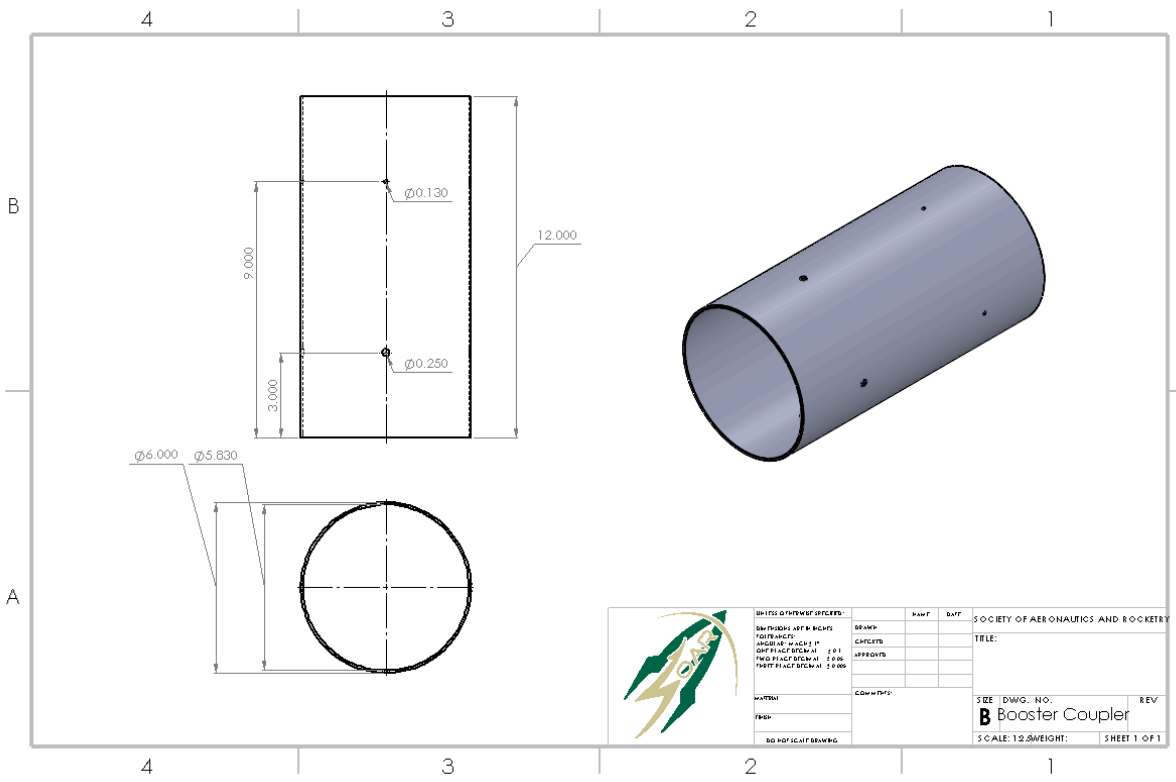


Figure 38. Booster Coupler

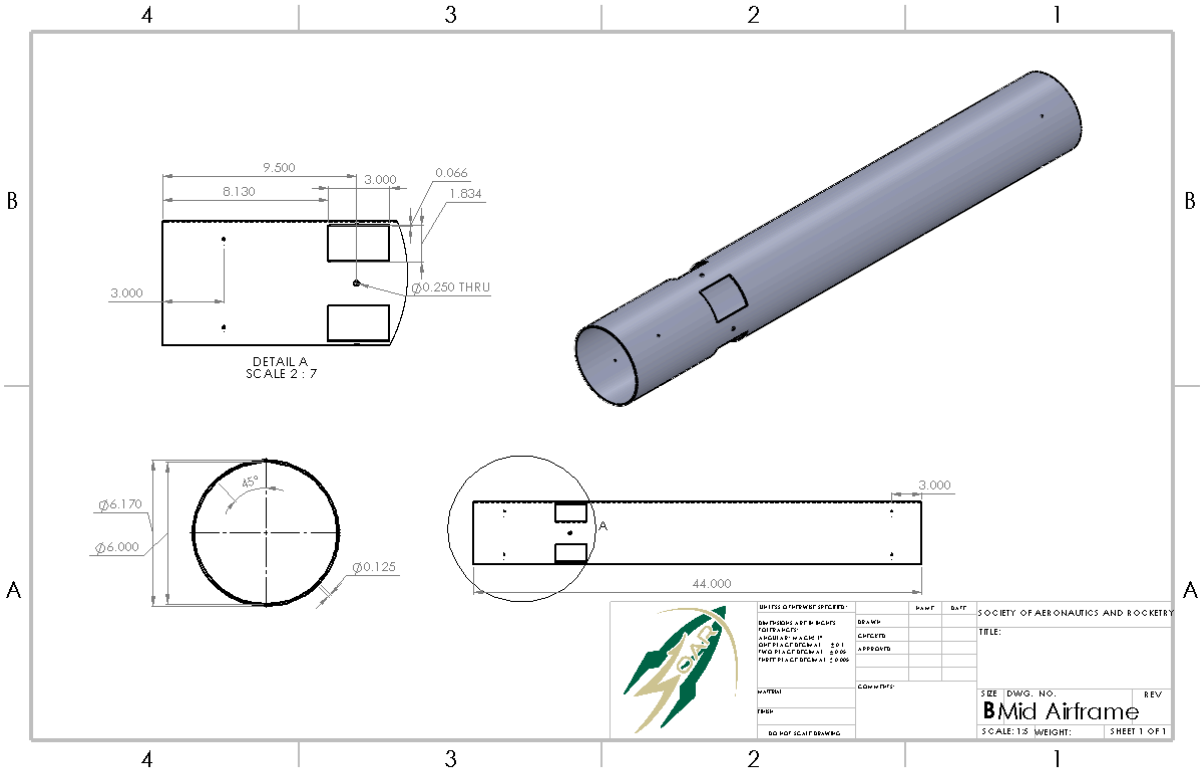


Figure 39. Mid Section Airframe

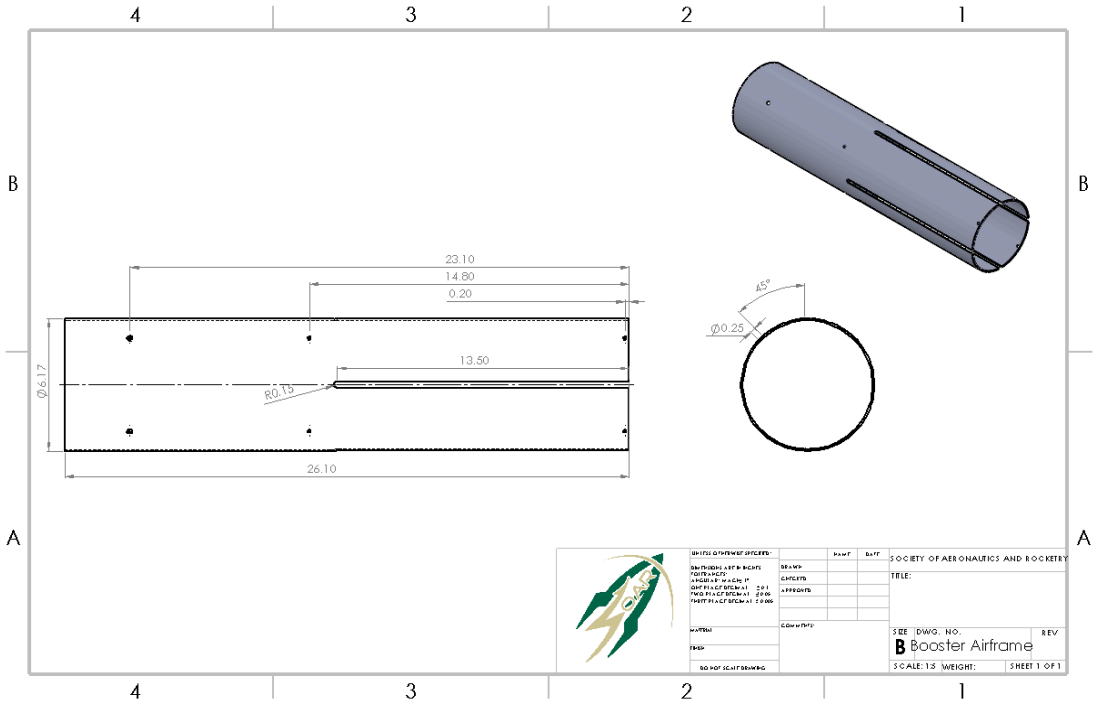


Figure 40. Booster Tub Engineering Drawing

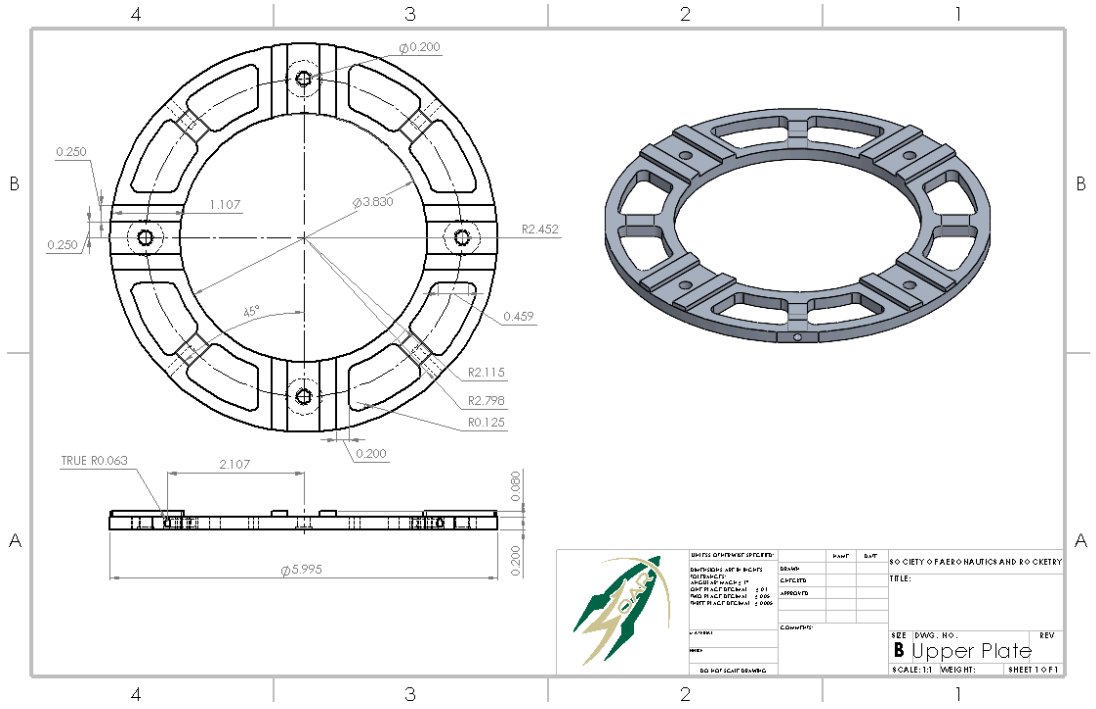


Figure 41. Upper Plate Engineering Drawing

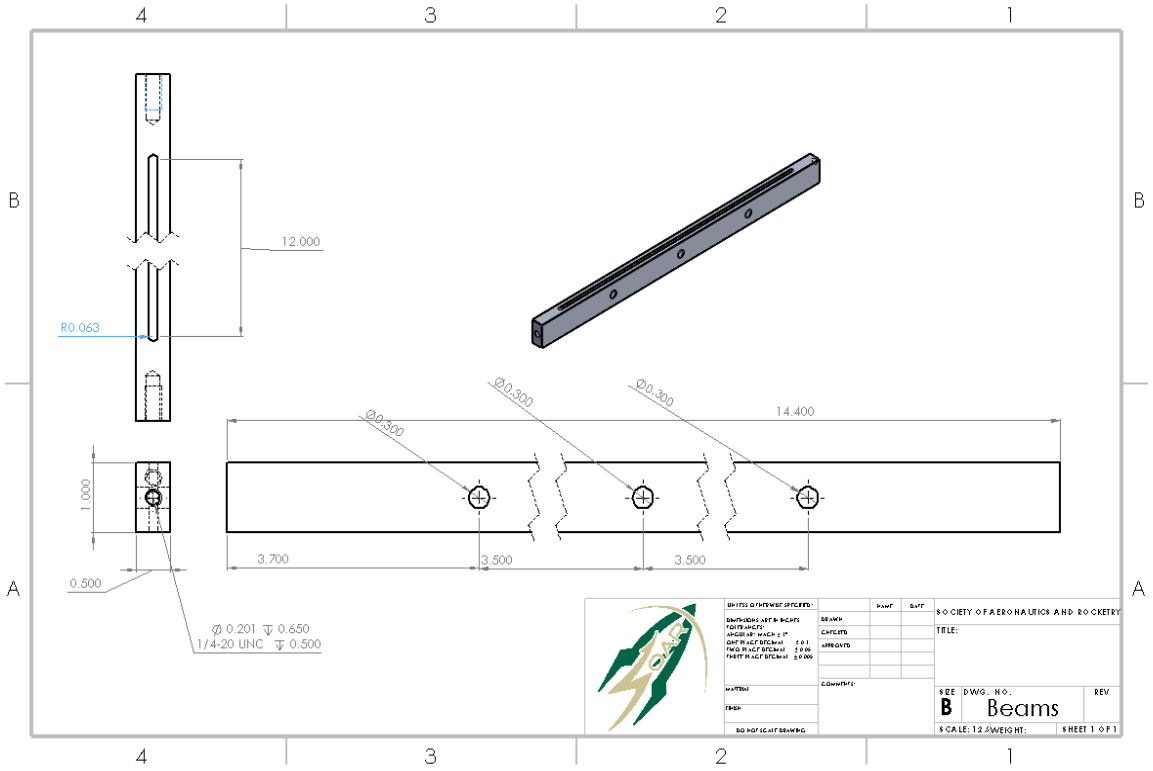


Figure 42. Beams

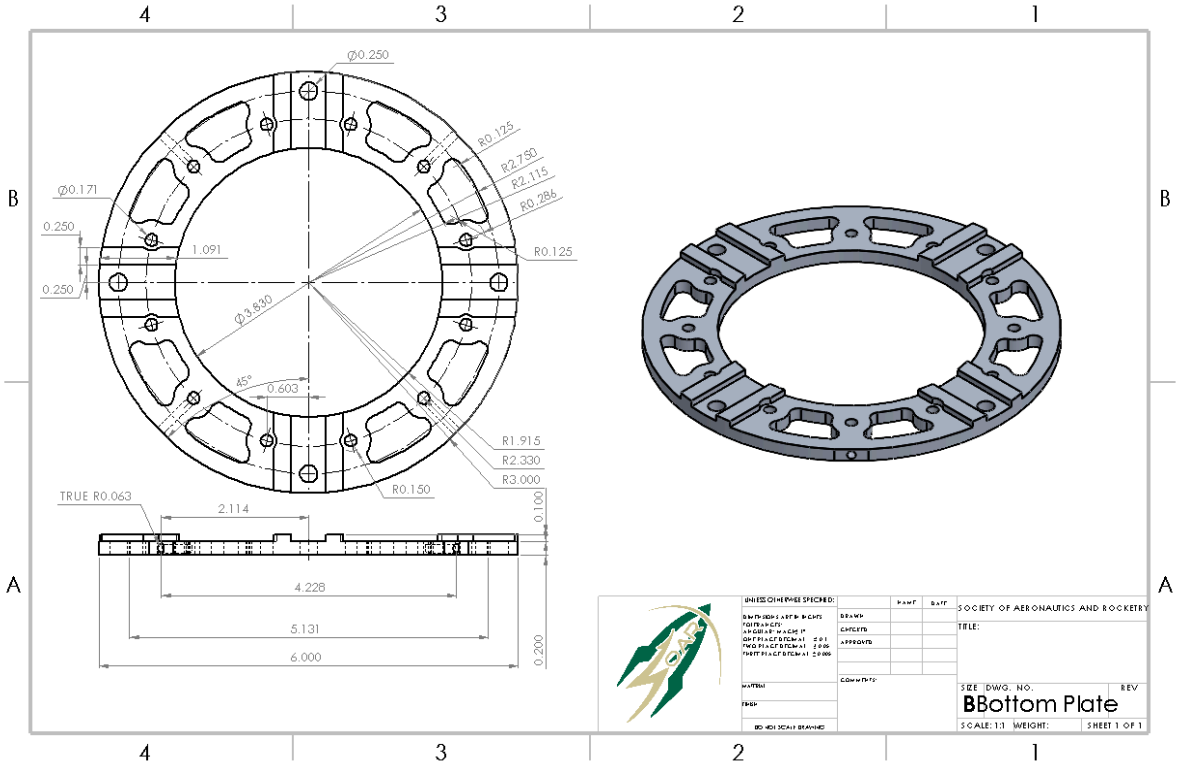


Figure 43. Bottom Plate

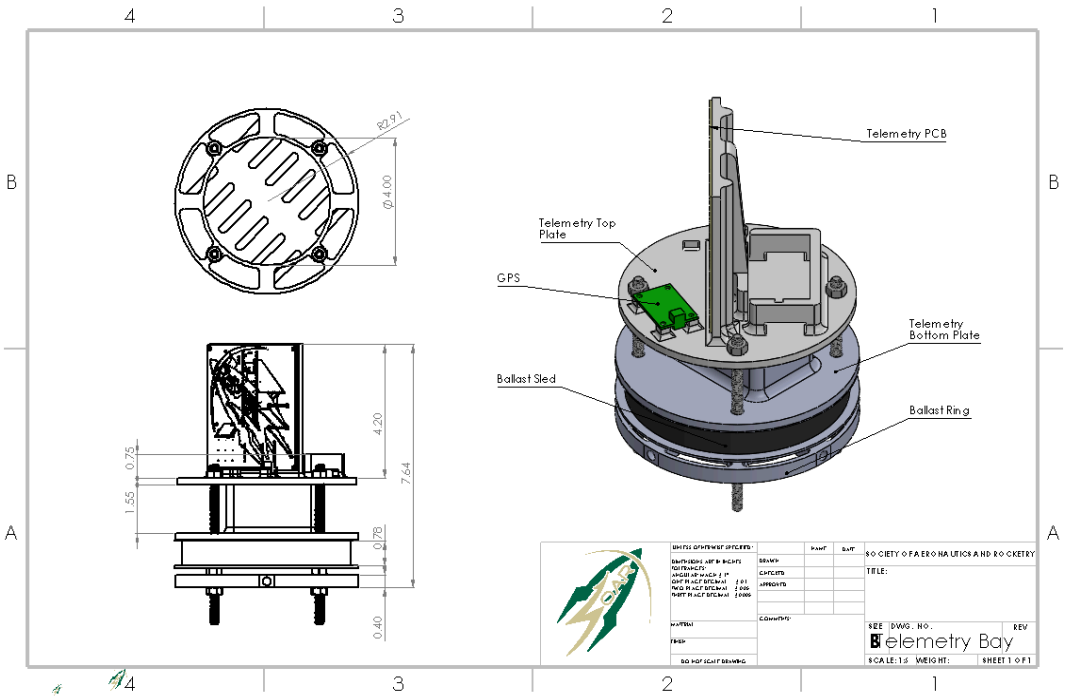


Figure 44. Telemetry Bay

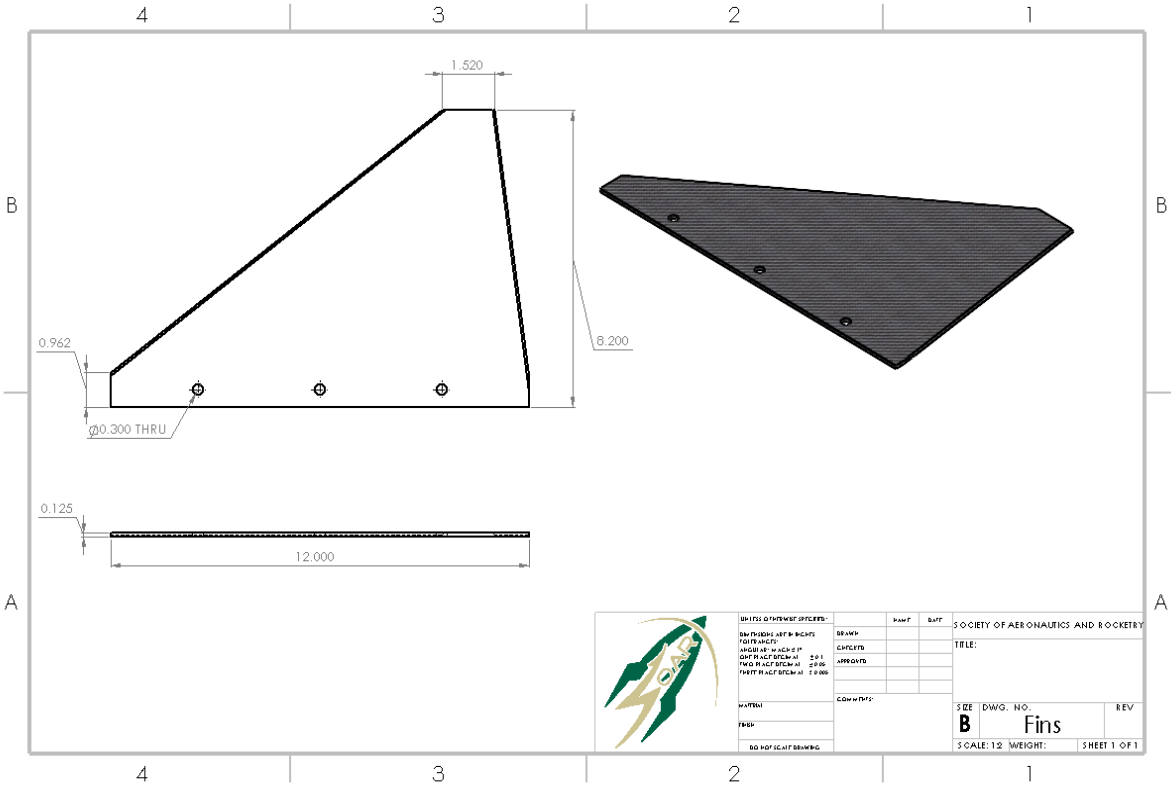


Figure 45. Fins

3. Payload

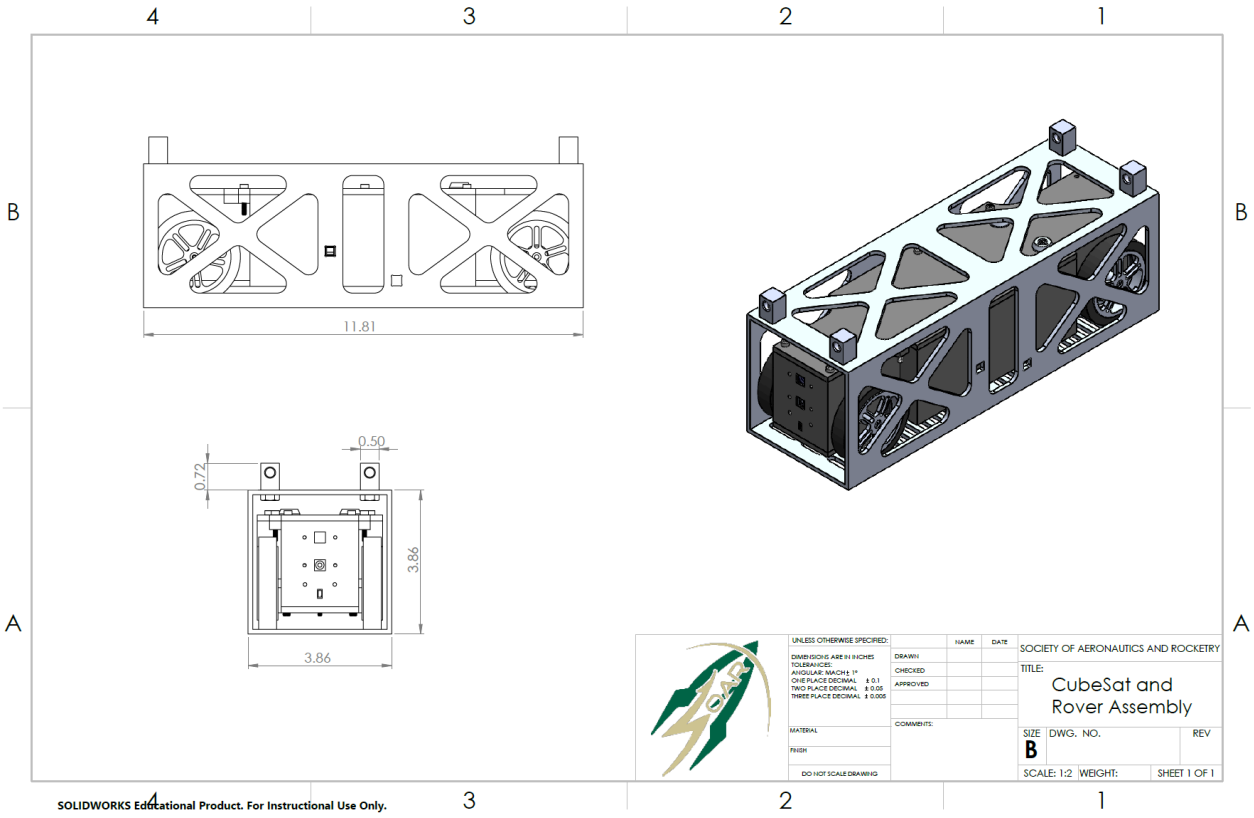


Figure 46. CubeSat and Rover Assembly

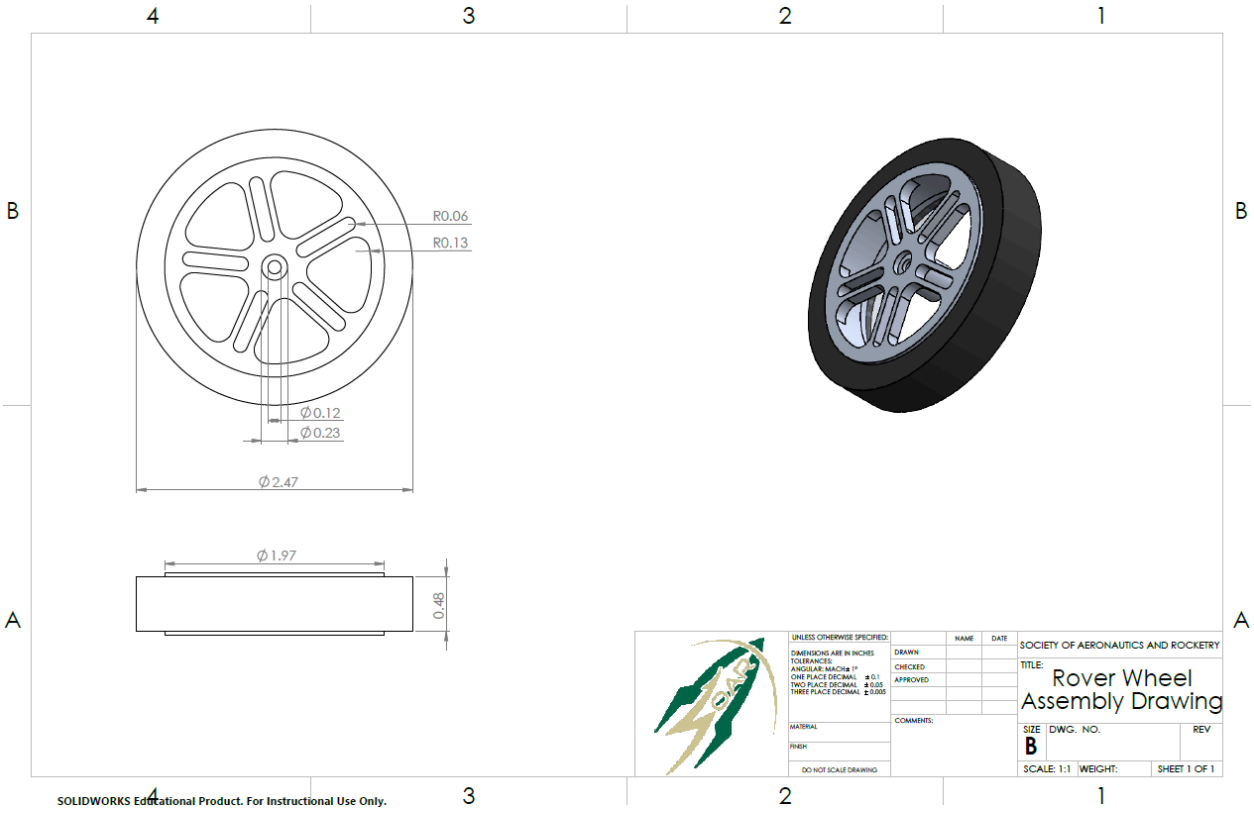


Figure 47. Rover Wheel Assembly

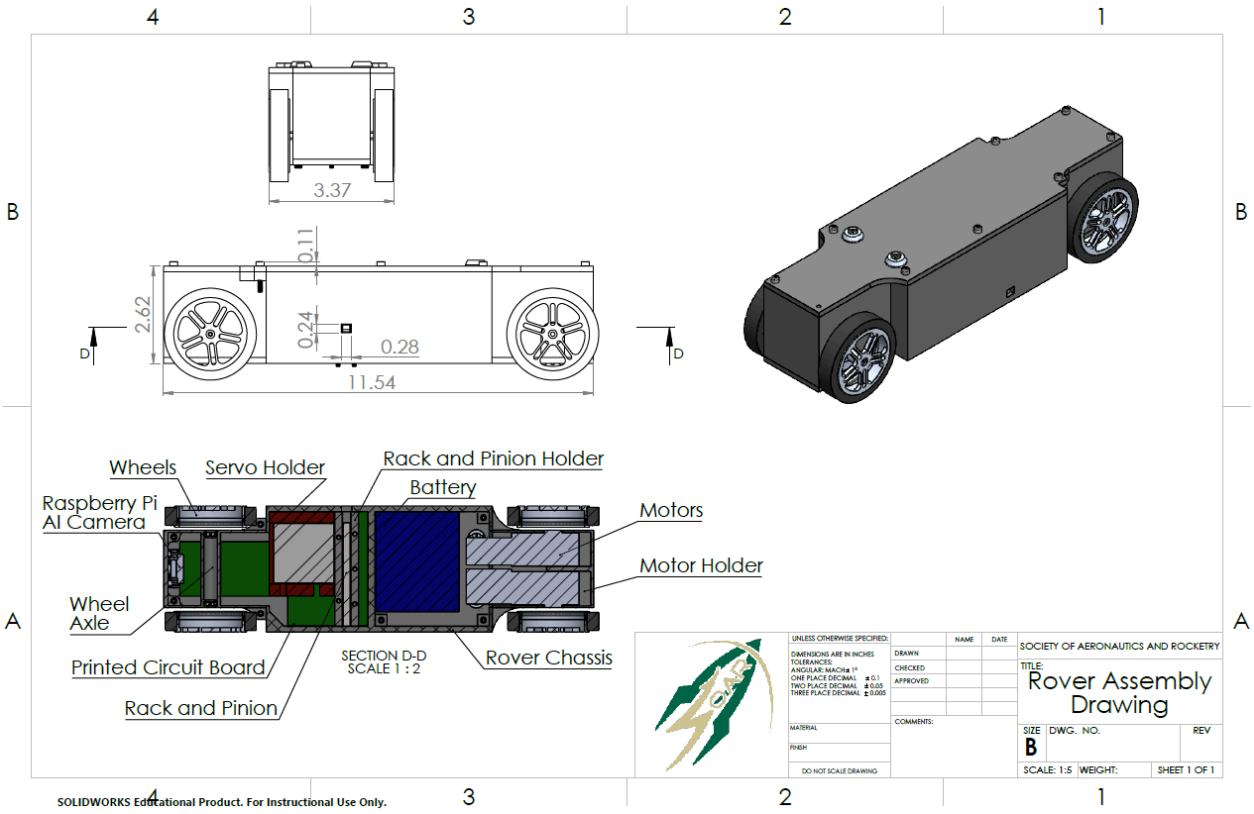


Figure 48. Rover Assembly

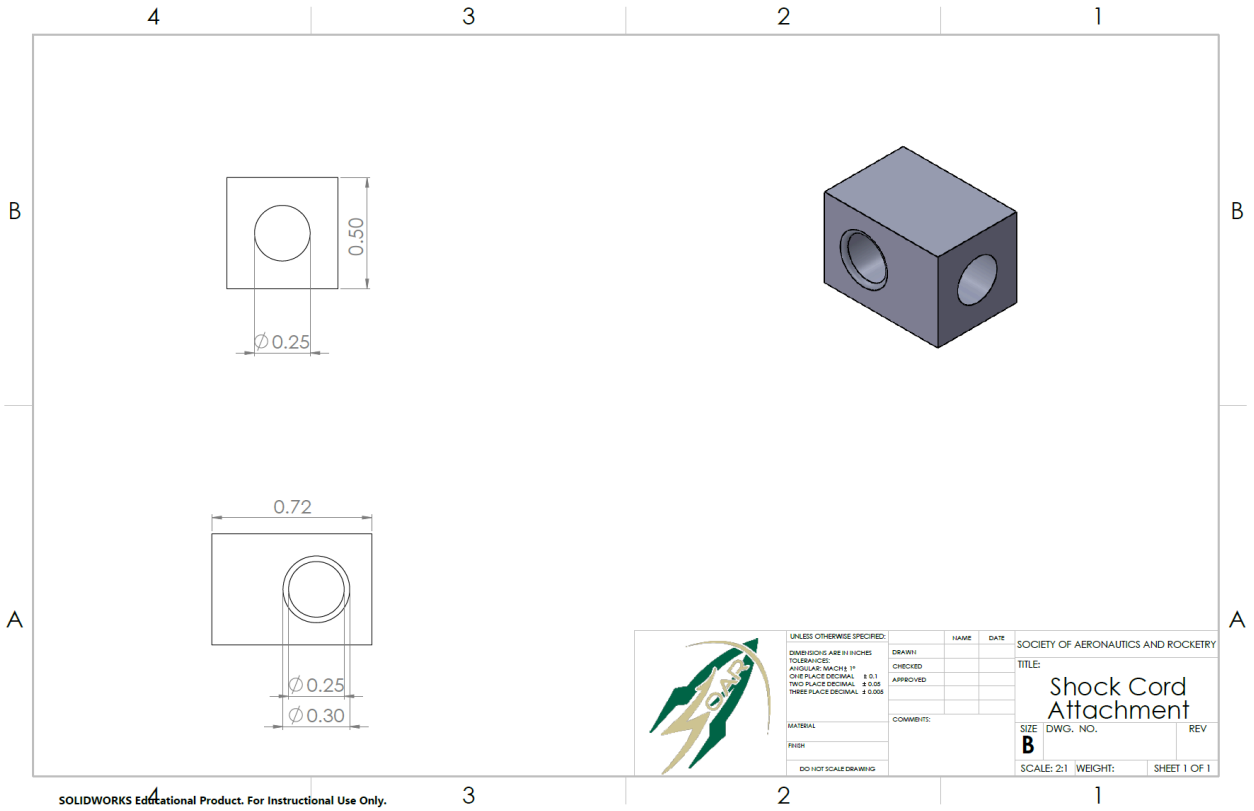


Figure 49. Shock Cord Attachment Engineering Drawing

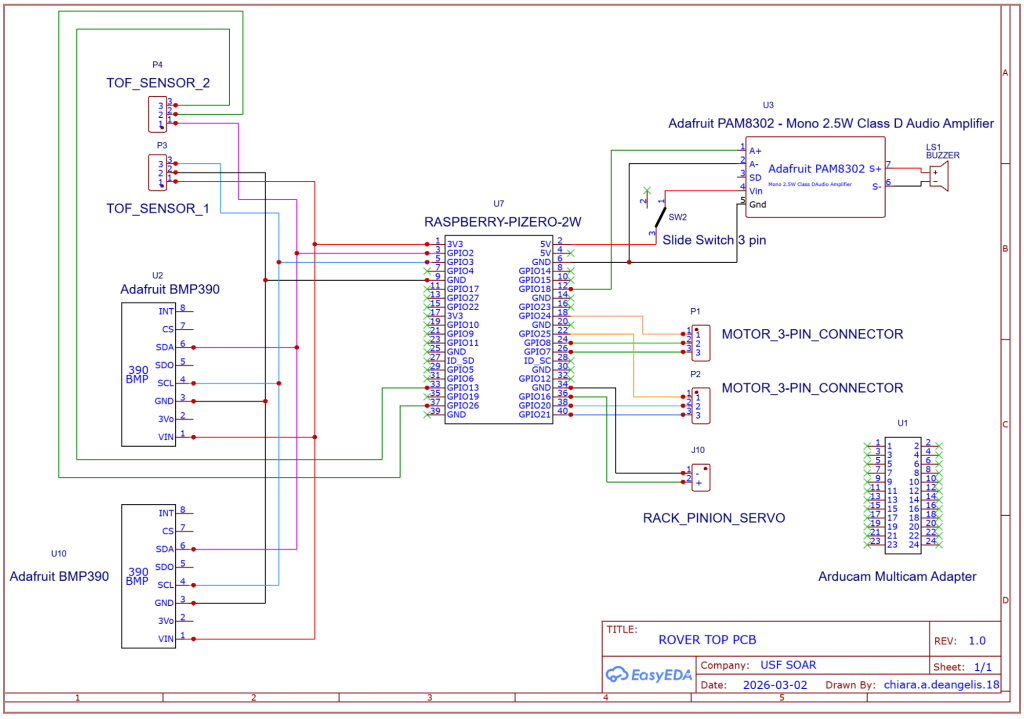


Figure 50. Payload Rover Top PCB

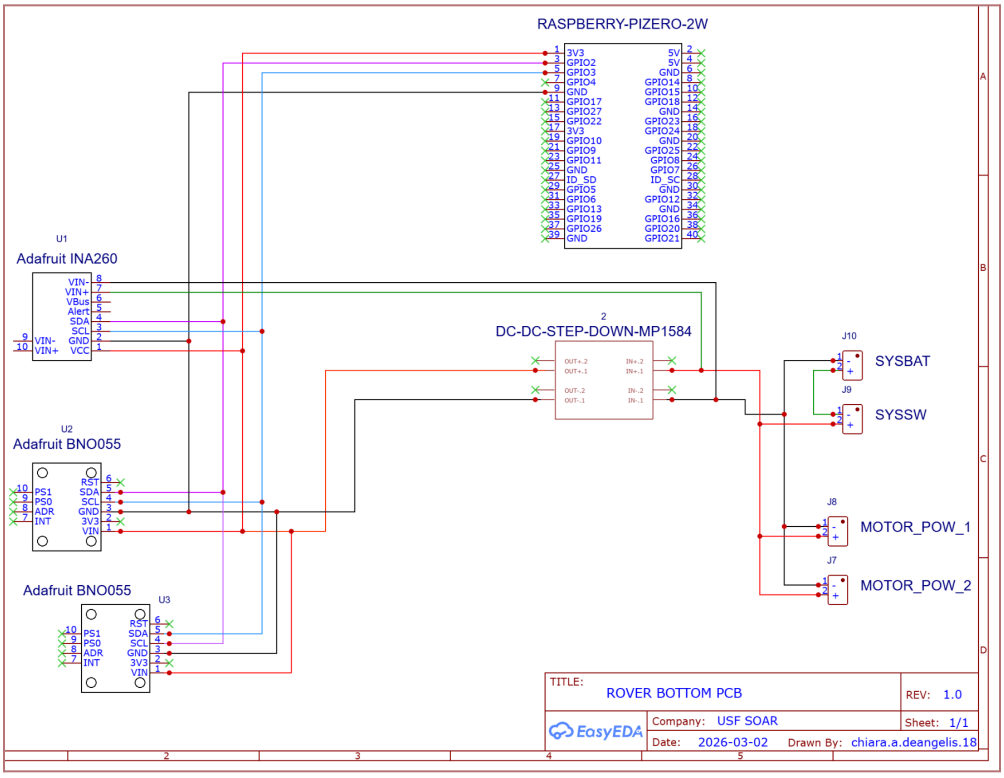


Figure 51. Payload Rover Bottom PCB

4. Airbrakes

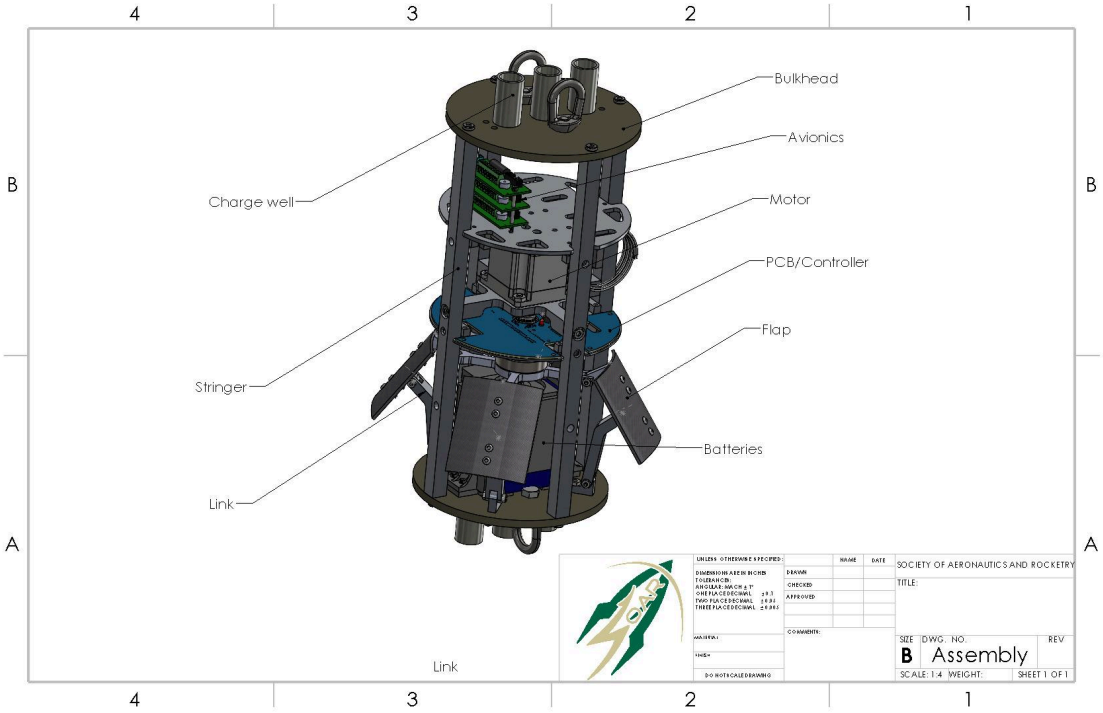


Figure 52. Airbrakes System Assembly Engineering Drawing

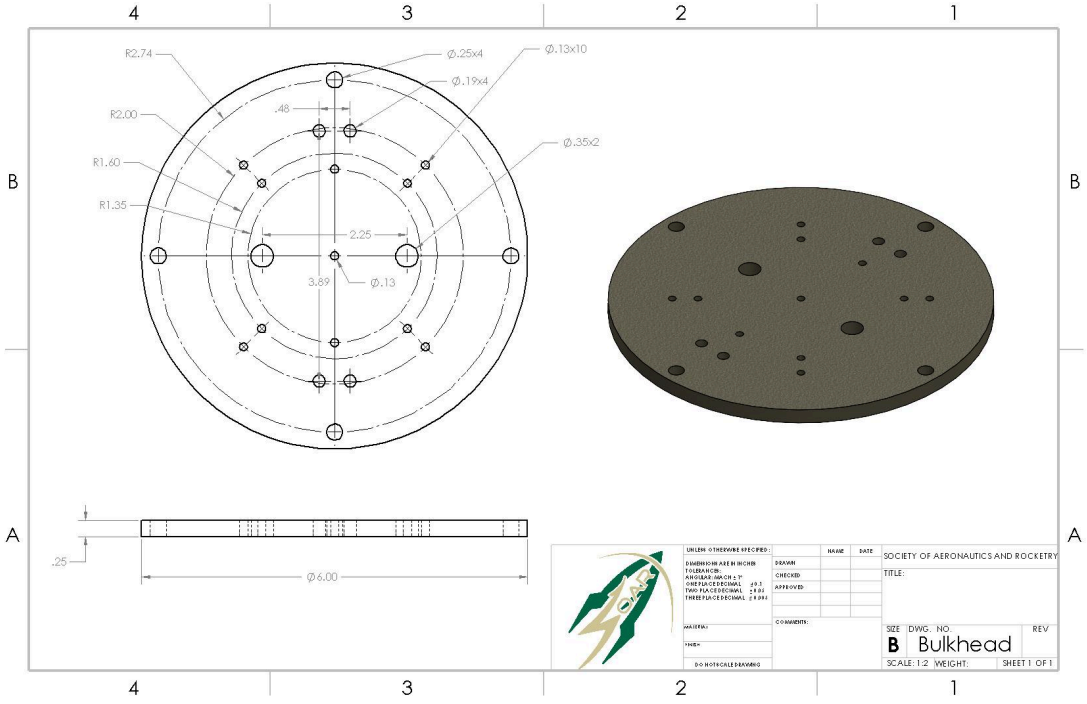


Figure 53. Bulkhead Engineering Drawing

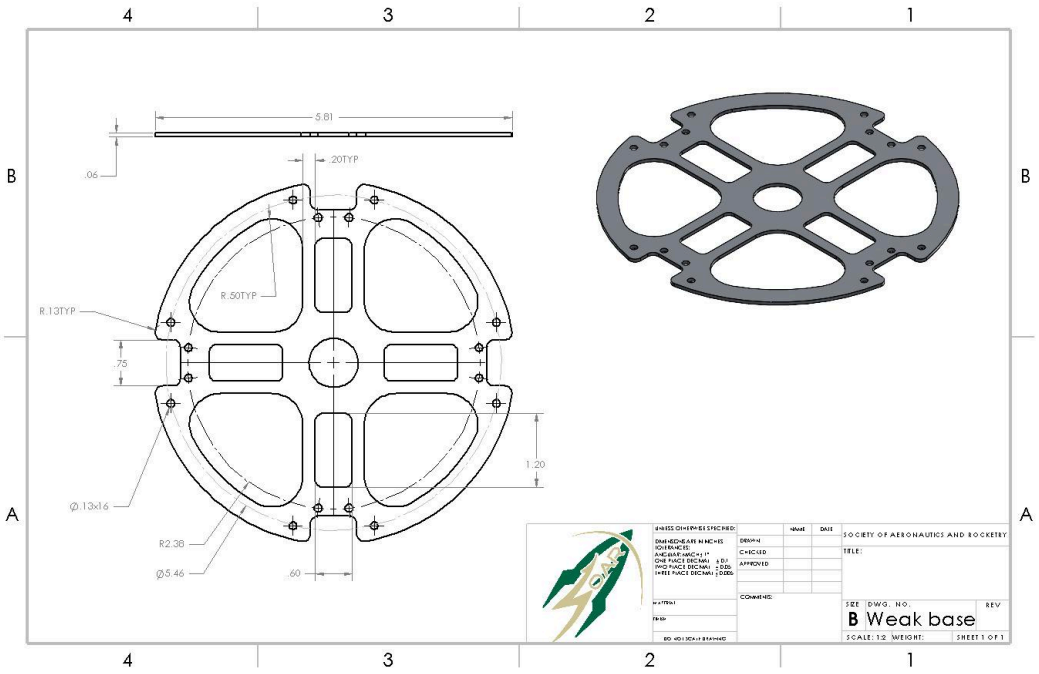


Figure 54. PCB Weak Support Base Engineering Drawing

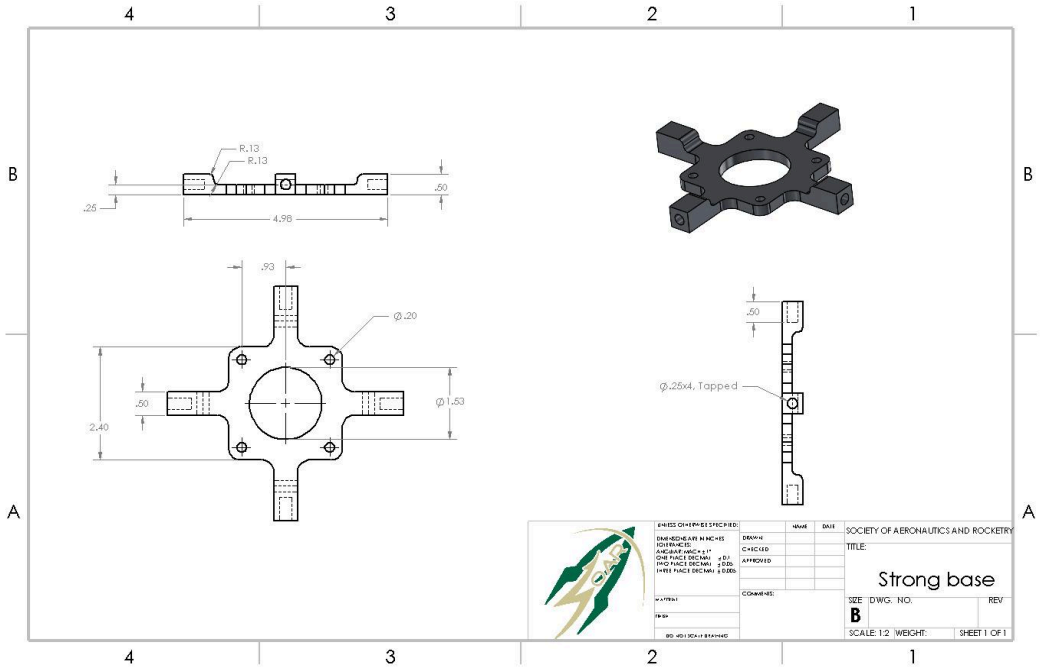


Figure 55. Motor Strong Support Base Engineering Drawing

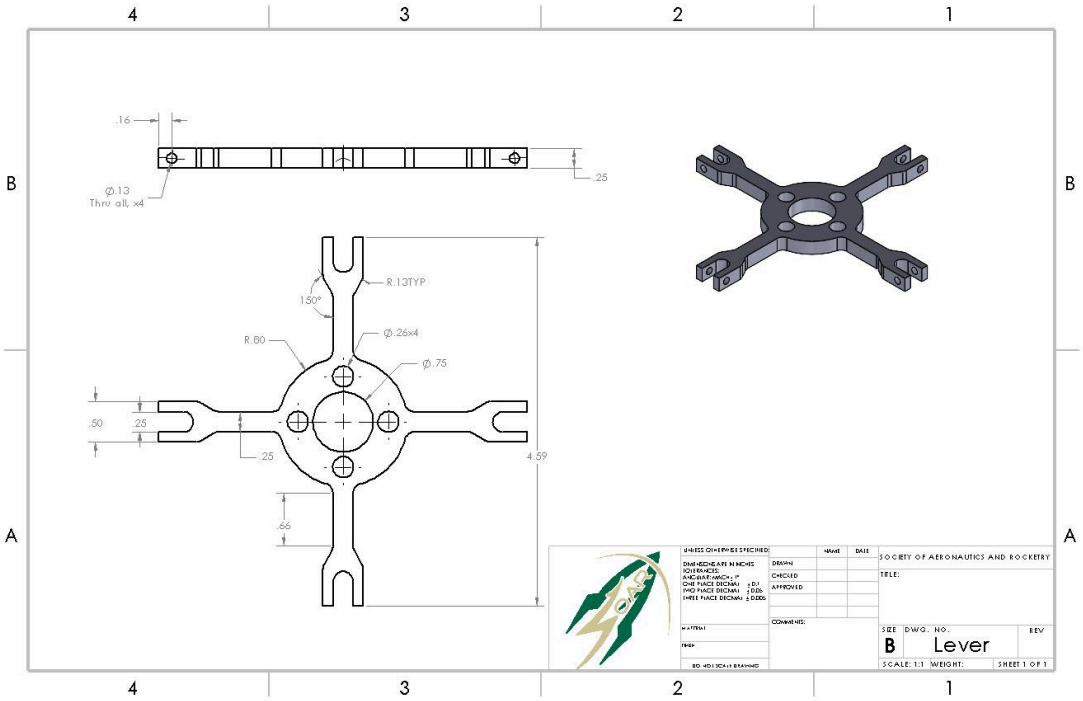


Figure 56. Lever Engineering Drawing

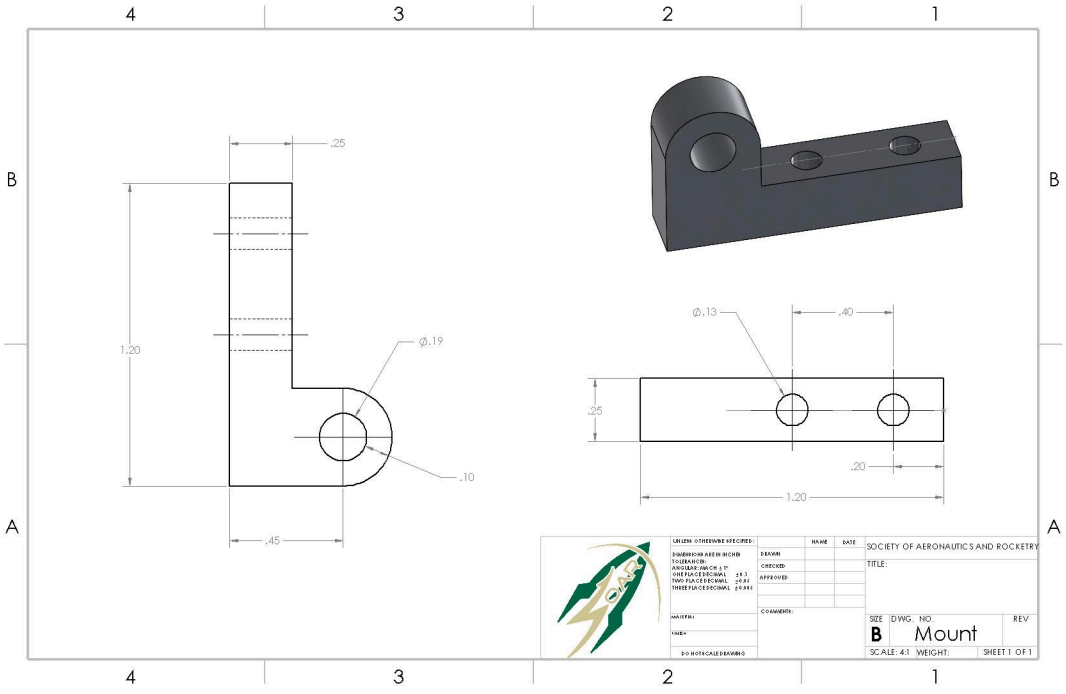


Figure 57. Mounts Engineering Drawing

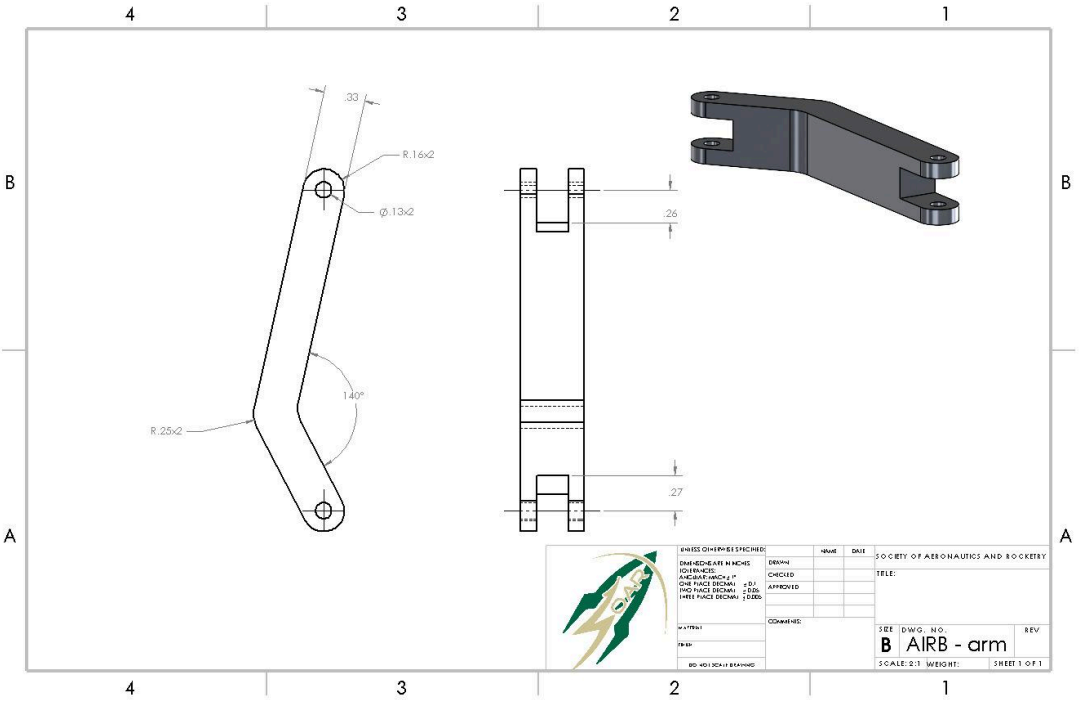


Figure 58. Arm Links Engineering Drawing

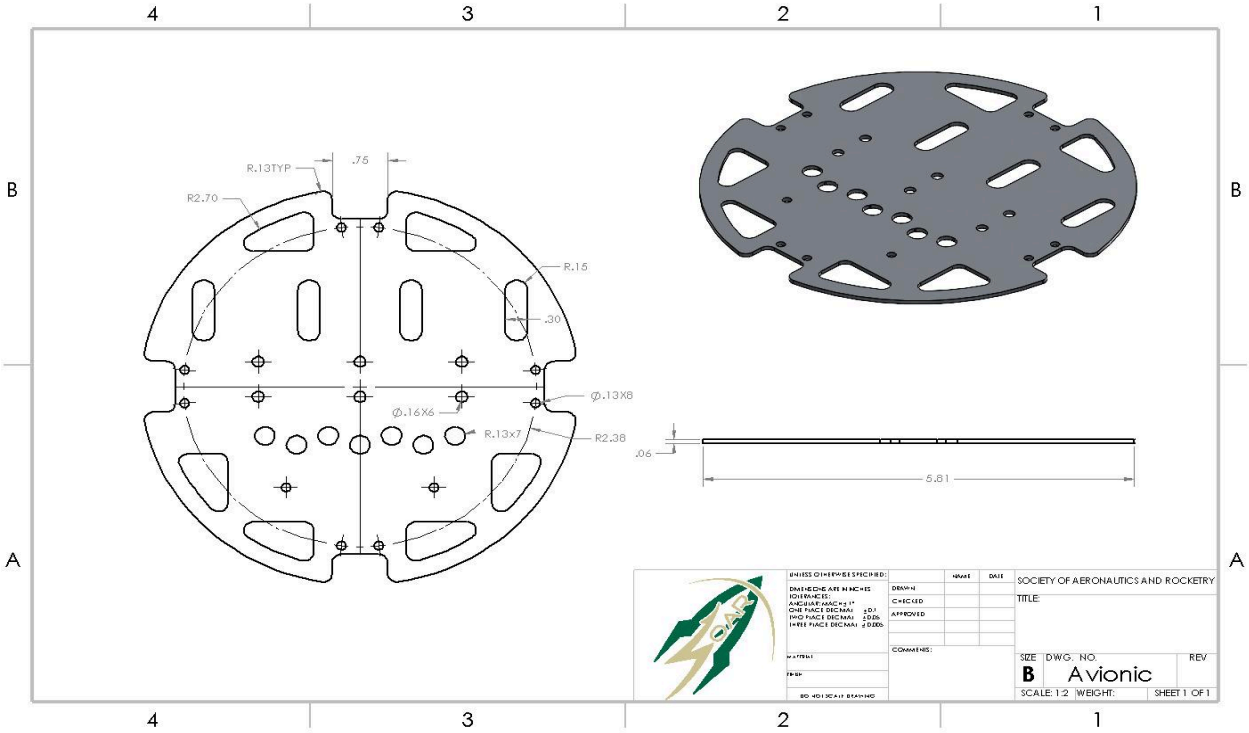


Figure 59. Avionics Weak Support Plate Engineering Drawing

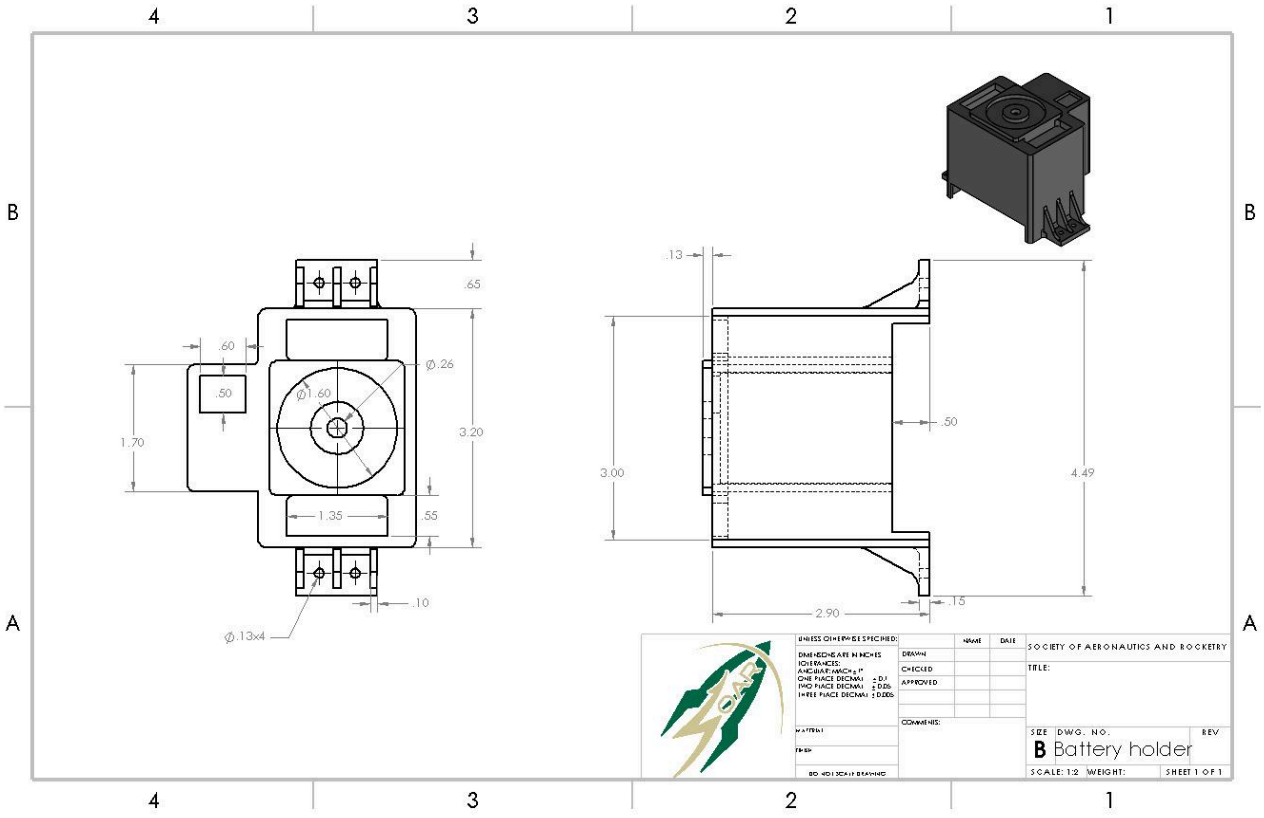


Figure 60. Battery Holder Engineering Drawing

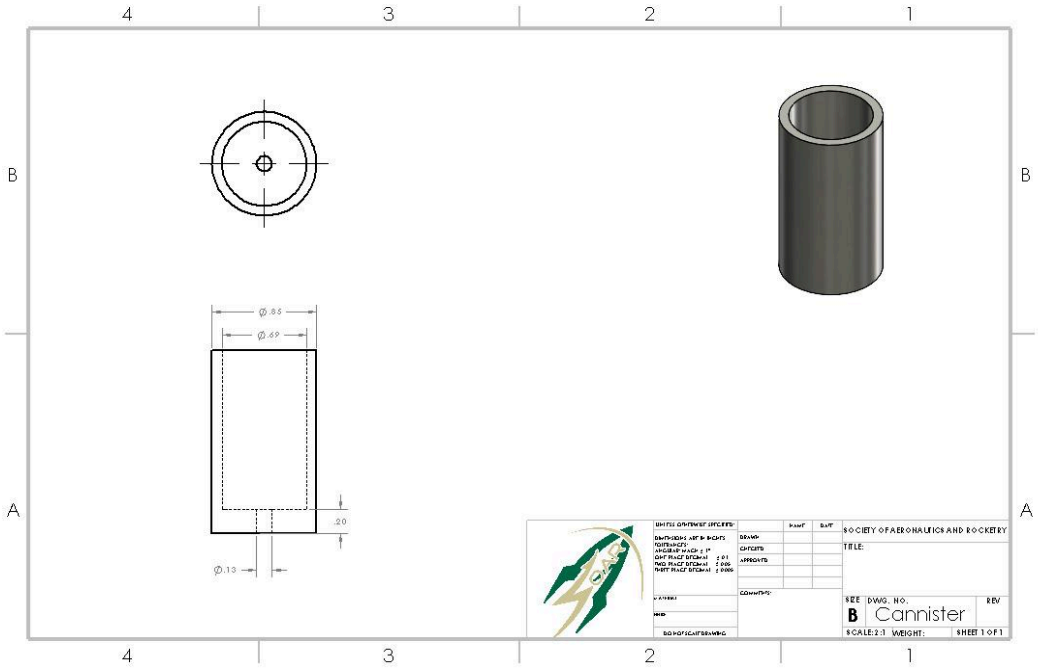


Figure 61. Ejection Canister Engineering Drawing

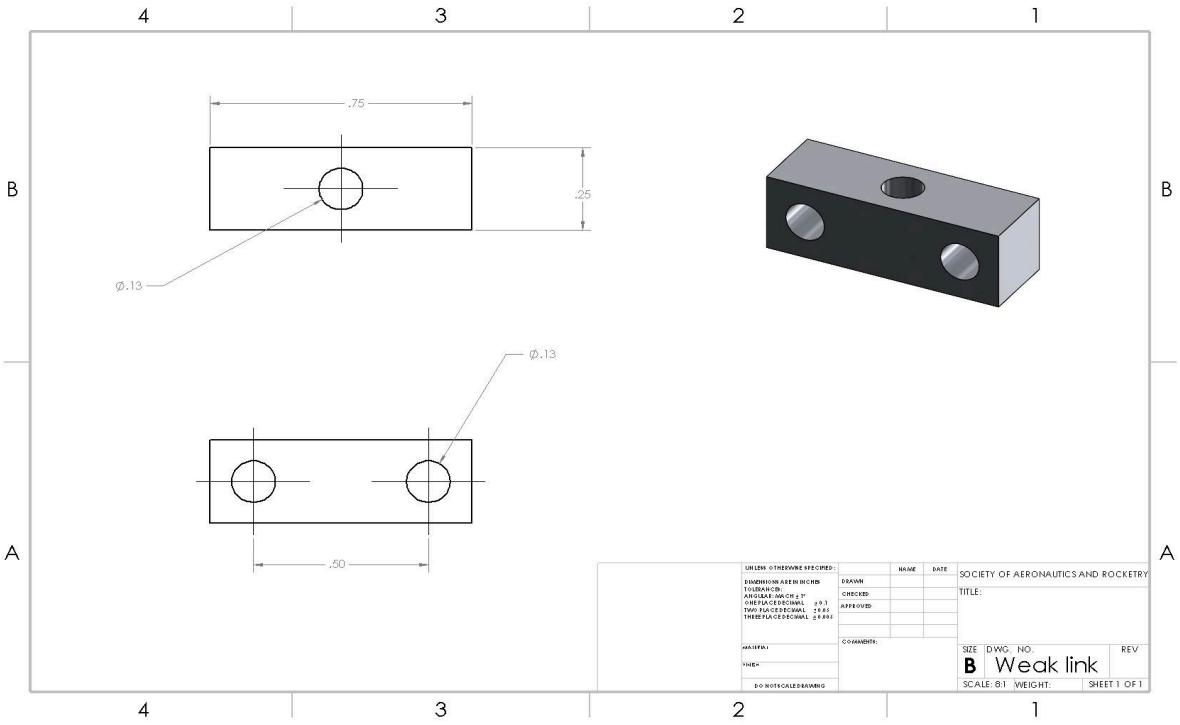


Figure 62. Weak Link Engineering Drawing

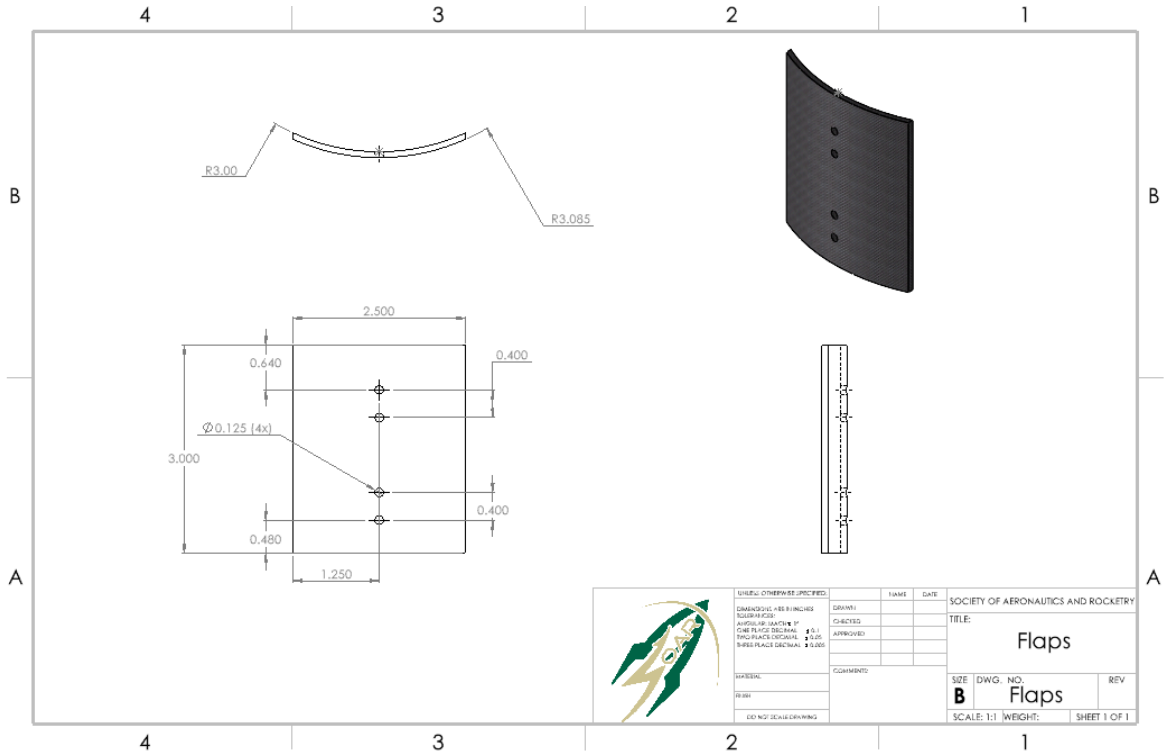


Figure 63. Flaps Engineering Drawing

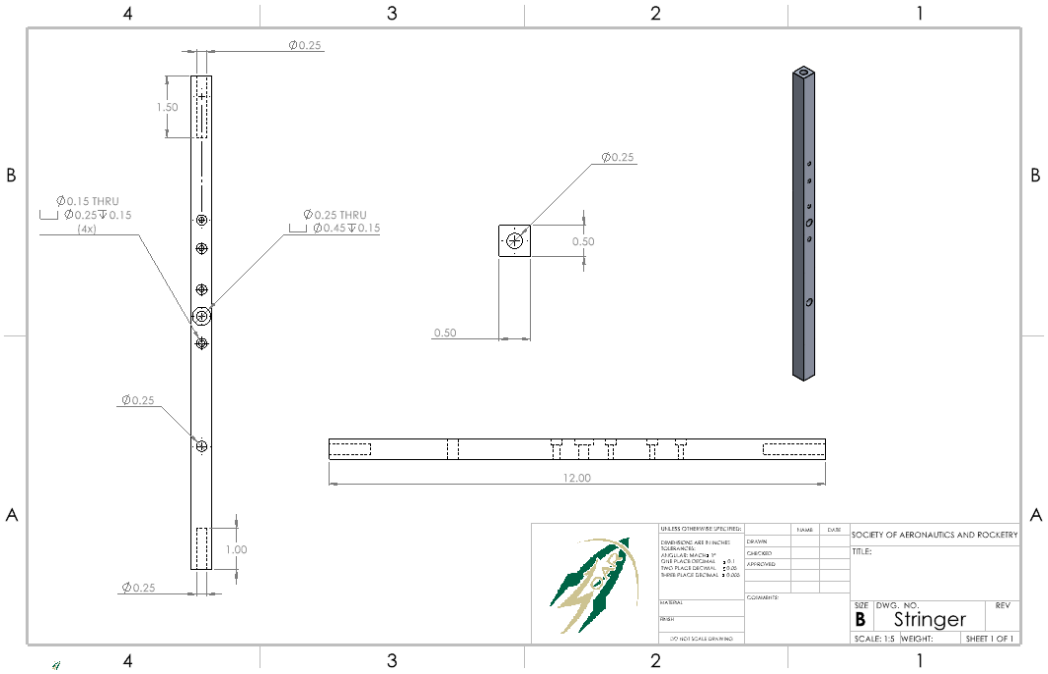


Figure 64. Stringers Engineering Drawing

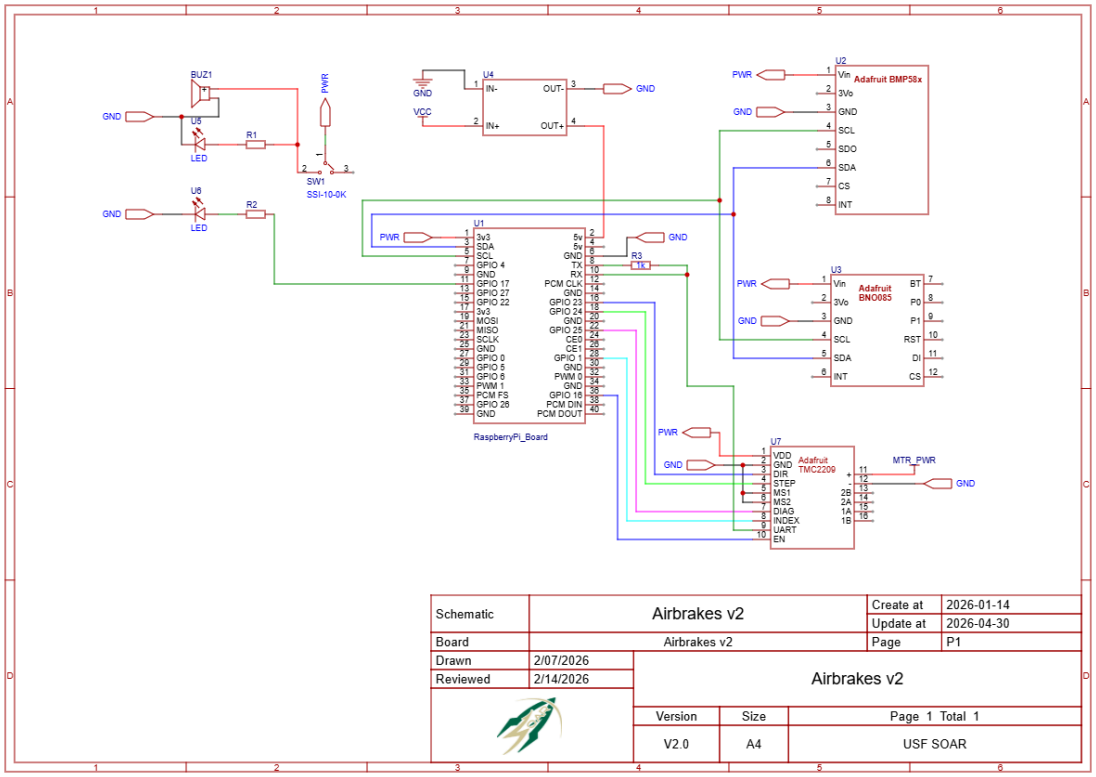


Figure 65. Airbrakes PCB Schematic

5. Recovery System

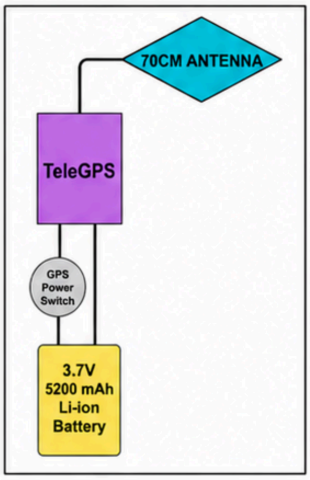


Figure 66. Nosecone Recovery System

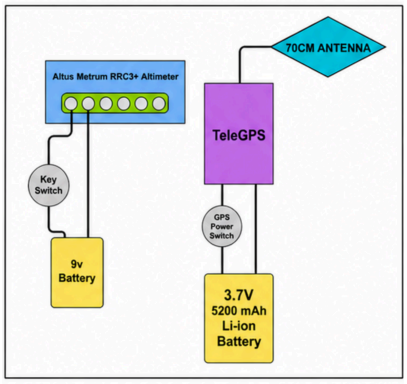


Figure 67. Payload Recovery System

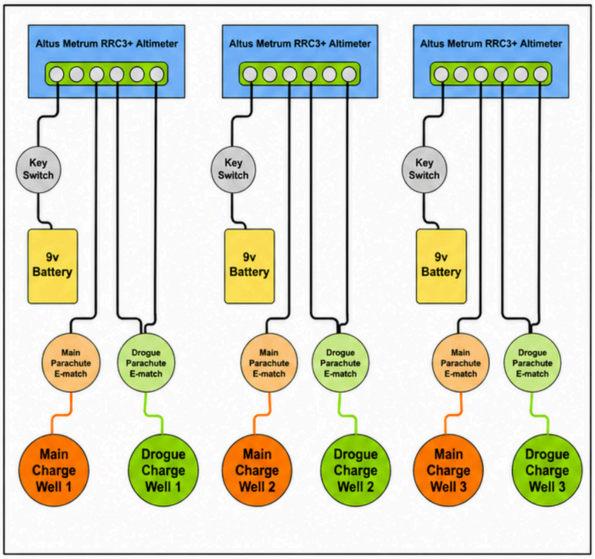


Figure 68. Avionics Bay Wiring Diagram

6. SRAD Telemetry System

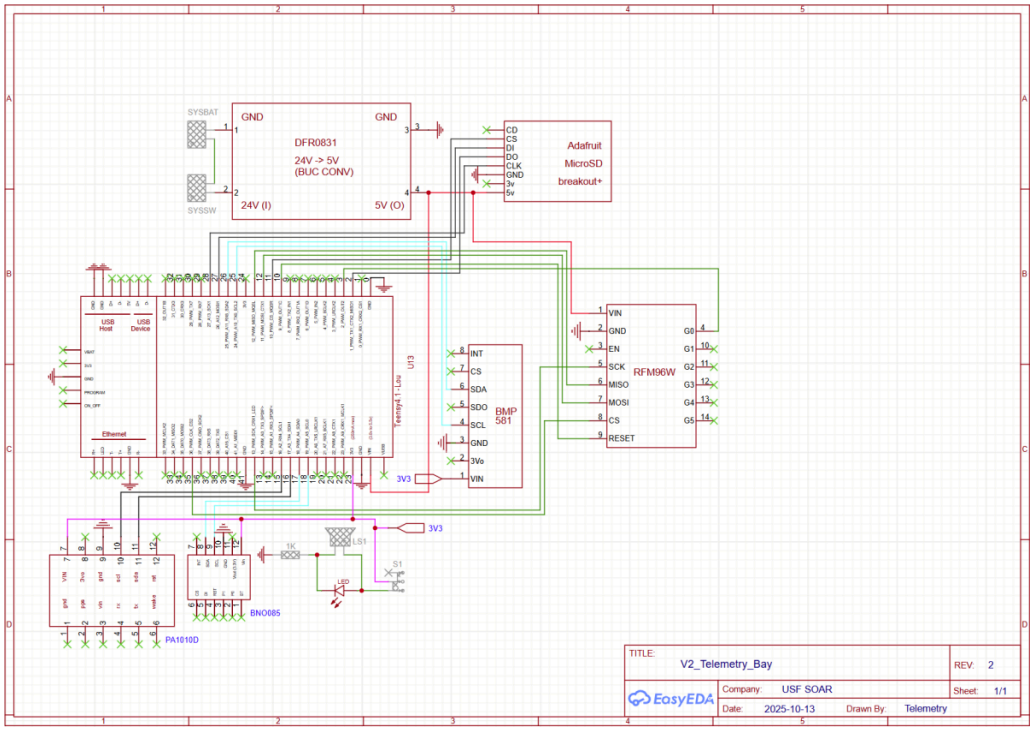


Figure 69. Telemetry Bay Schematic

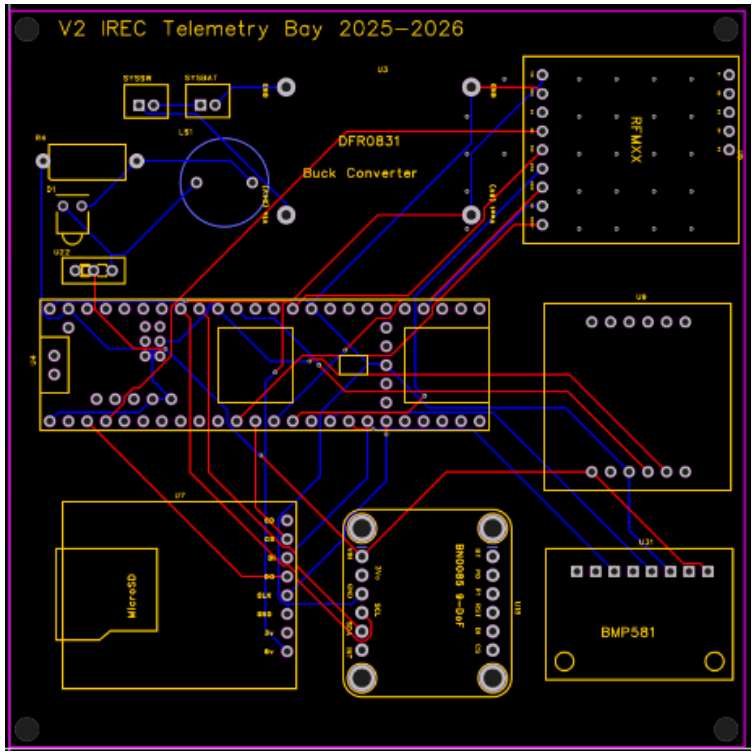


Figure 70. Telemetry Bay PCB

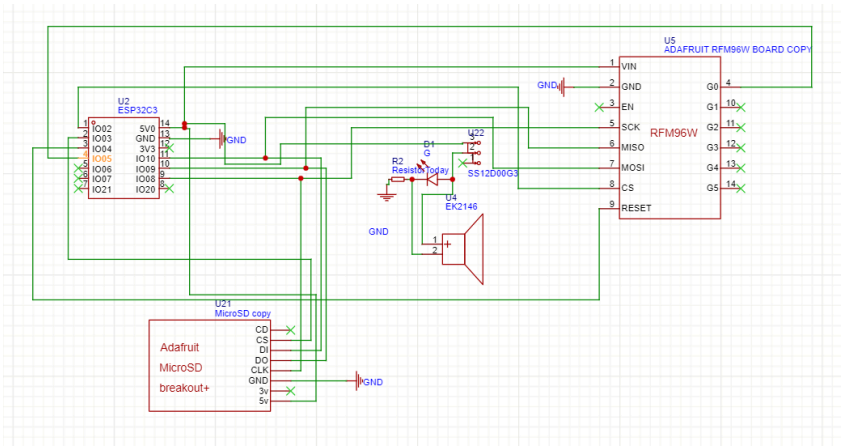


Figure 71. Ground Station Schematic

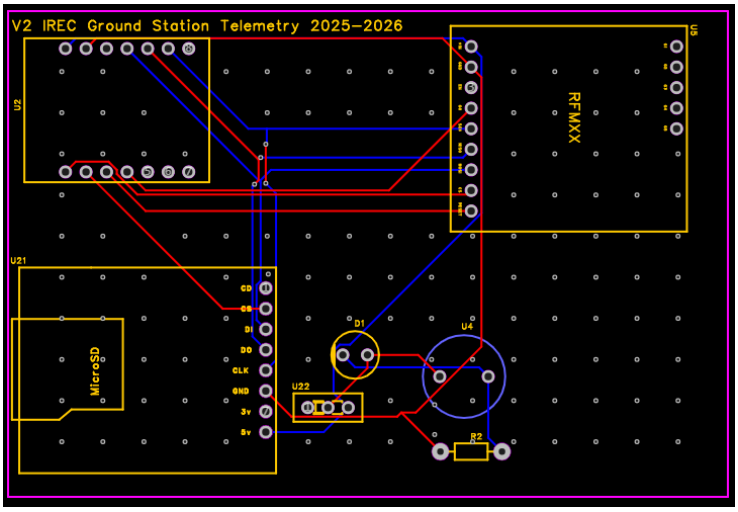


Figure 72. Ground Station PCB

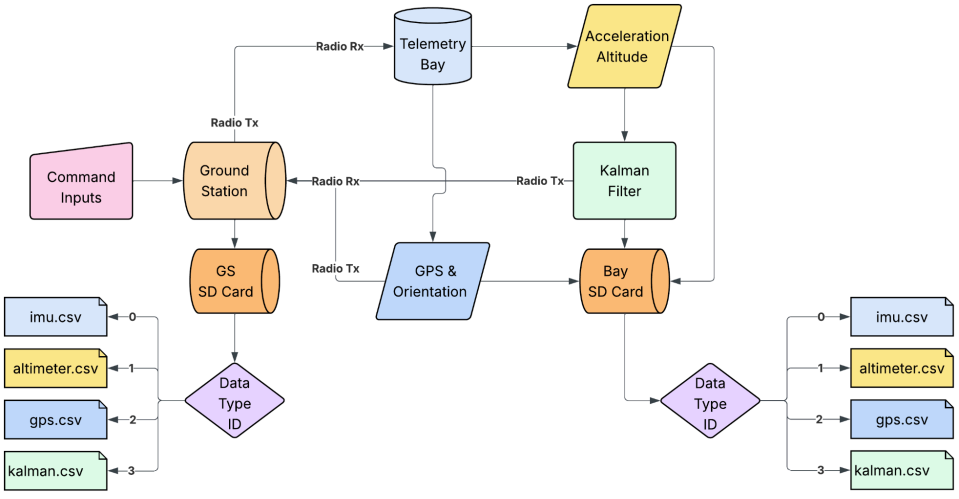


Figure 73. Telemetry Bay Ground Station and Telemetry Bay Interaction Diagram

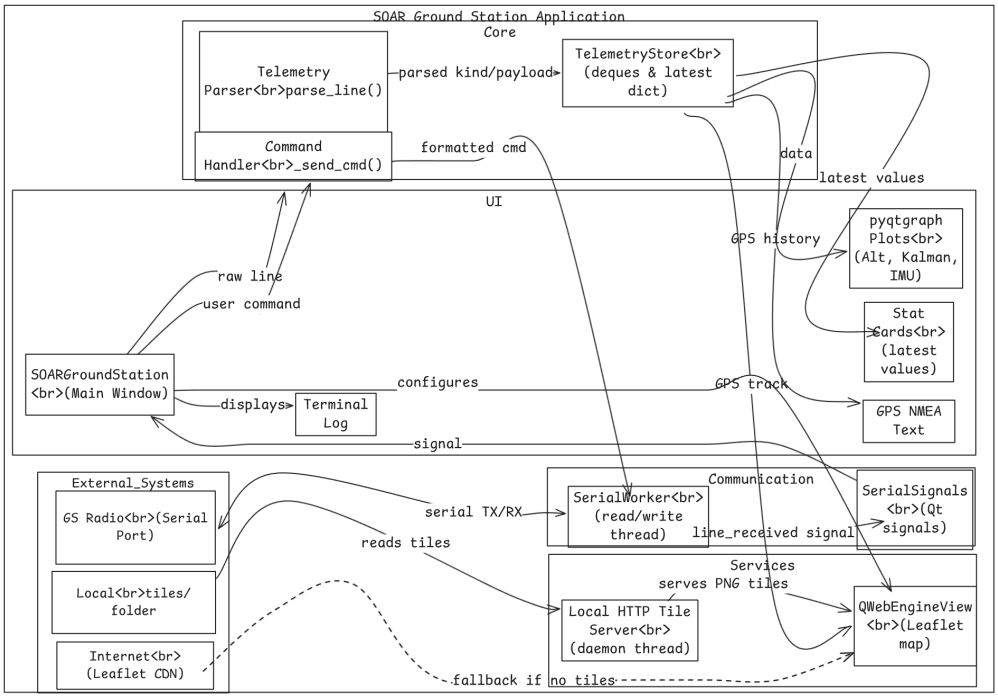


Figure 74. GUI Process Diagram and interaction with Ground Station Serial Output

Appendix G: Triangulation Methods

Triangulation, as defined in orienteering, is a method of identifying one's exact location using a compass, a map, and two or more distinct, identifiable landmarks. This process is particularly useful in situations where GPS may be unavailable, as it enables the determination of an exact position on a map. The method follows a defined sequence of steps, which are outlined below. Additionally, this approach can be extended through the use of trigonometry to estimate distances between points.

To perform triangulation, there are several key considerations that must be addressed. First, the proper equipment is required. At a minimum, this includes a compass, a map, and two or more identifiable landmarks. Landmark selection is critical to accuracy; poor choices can result in significant positional error. The procedure for triangulation is as follows:

1. Align the map with magnetic north using a compass, ensuring that the map's north corresponds to the true northward direction in the field.
2. Identify at least two landmarks from the observation point; three landmarks are preferred to improve accuracy.
3. Sight each landmark with the compass and record its bearing relative to north.
4. On the map, draw a line from each landmark using the measured bearing, extending the line in the reverse direction toward the observer's position.
5. Repeat steps 3 and 4 for all selected landmarks.
6. The intersection of the resulting lines indicates the estimated location.

The procedure described above is effective for determining one's position relative to known landmarks. In a rocketry application, however, the objective is reversed: the goal is to determine the landing location of the vehicle from known observation points, particularly in the absence of reliable GPS data. With appropriate modification, triangulation can be used to estimate both the landing location and its distance from a reference point. The following procedure outlines this adapted method:

1. Before launch, select at least two measurement points and mark their locations on a map.

2. At launch, station at least one observer at each point. Each observer is responsible for visually tracking the vehicle's trajectory; recording the descent using a camera is recommended, as it enables more accurate post-flight determination of the landing bearing.
3. From each observation point, draw a line on the map corresponding to the recorded bearing.
4. The intersection of these lines provides an estimate of the vehicle's landing location.
5. Establish a search radius around this intersection point to account for measurement uncertainty.
6. For improved accuracy, trigonometric methods may be used to estimate both the distance and direction from a given observation point to the landing location.

To illustrate this method, the following section examines the application during an actual launch. A satellite image of the launch site is shown below.

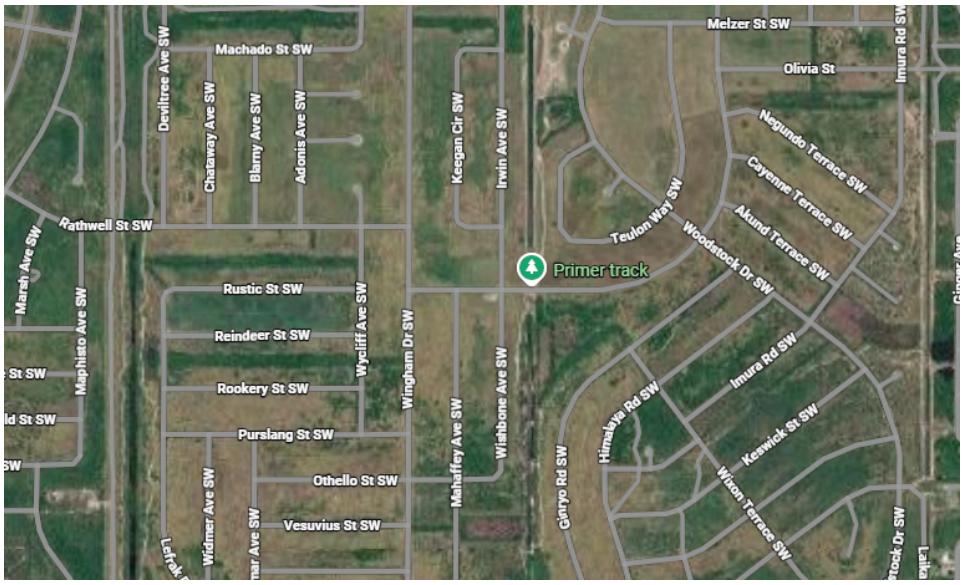


Figure 75. Primer Track Map

The locations of the launch site and selected measurement points are shown in the figure. The red "X" denotes the launch site, while each blue "X" represents a measurement location. Due to site constraints, the placement of measurement points required some adaptation. Points 1 and 2 were located along the same road, forming a nearly collinear arrangement. If the vehicle were to land along this same line, the resulting bearings from these two points would be nearly identical, thus reducing the effectiveness of triangulation and preventing an accurate prediction. To mitigate this limitation, a third measurement point was introduced to provide an additional independent bearing.



Figure 76. Markings on the Map

Following the launch, bearings were recorded from Points 2 and 3. This example demonstrates that measurements from two points can provide a reasonable estimate of the landing location; however, the inclusion of the third point would have most likely improved accuracy. The following measurements were obtained:

- From Point 2, a bearing of 103° relative to north was measured.
- From Point 3, a bearing of 110° relative to north was measured.

Using these bearings, lines were drawn from each measurement point on the map. The intersection of these lines, indicated by the magenta "X," represents the estimated landing location.

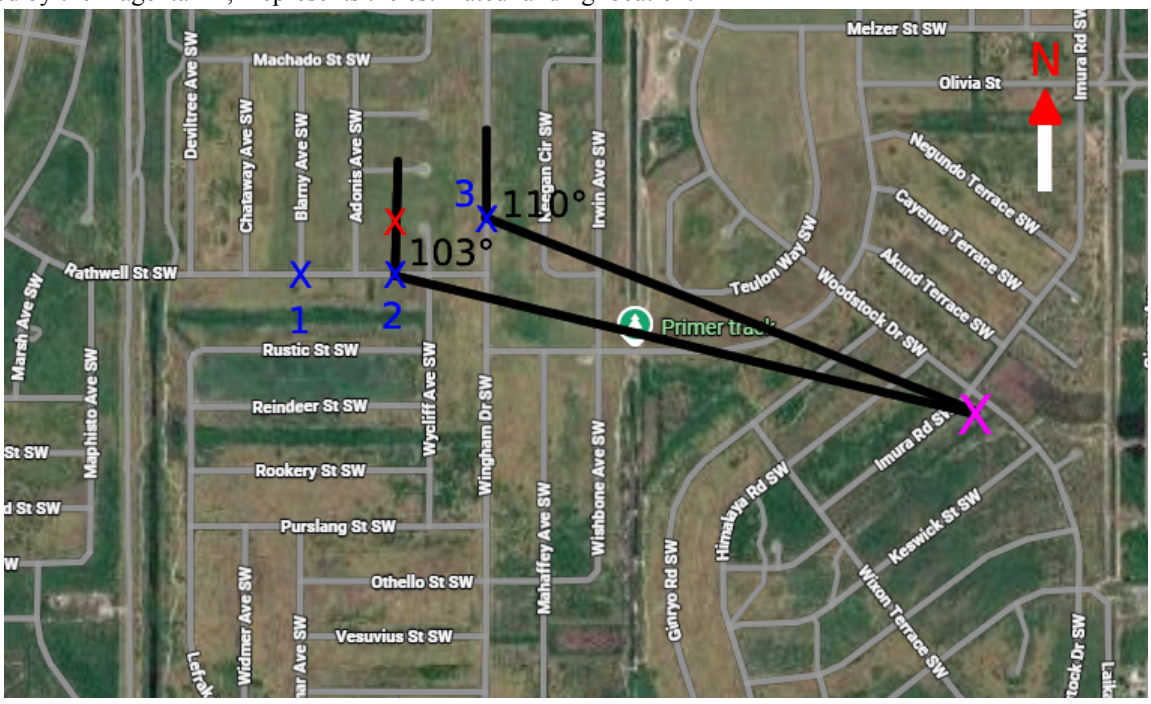


Figure 77. Triangulation on a Map

Comparison of the estimated intersection point with the actual landing location of *Aurora* indicates reasonable agreement, with *Aurora* recovered at the location marked by the yellow "X."

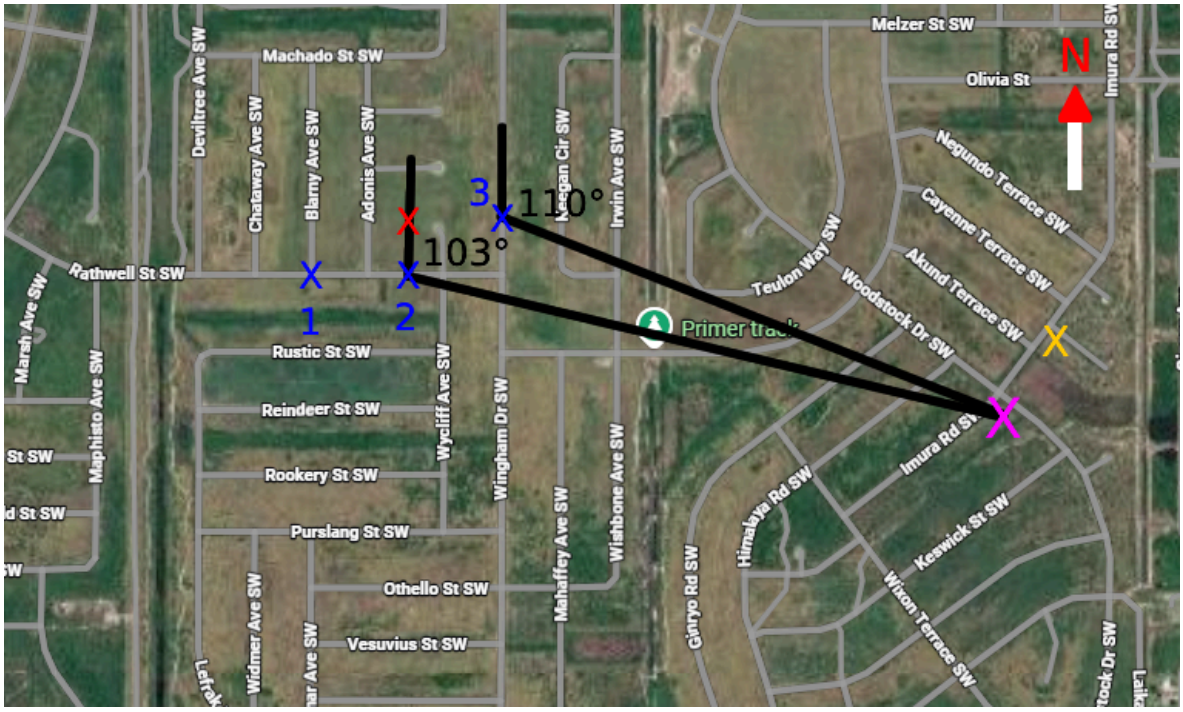


Figure 78. Triangulation on Map 2

If measurement had been taken from a third point, the estimated location of *Aurora* would likely have been more accurate. However, it is necessary to account for measurement uncertainty; accordingly, a search radius should be established around the predicted intersection. Based on the measurement tool in Google Maps, the triangulated estimate was approximately 500 feet from the actual landing location.

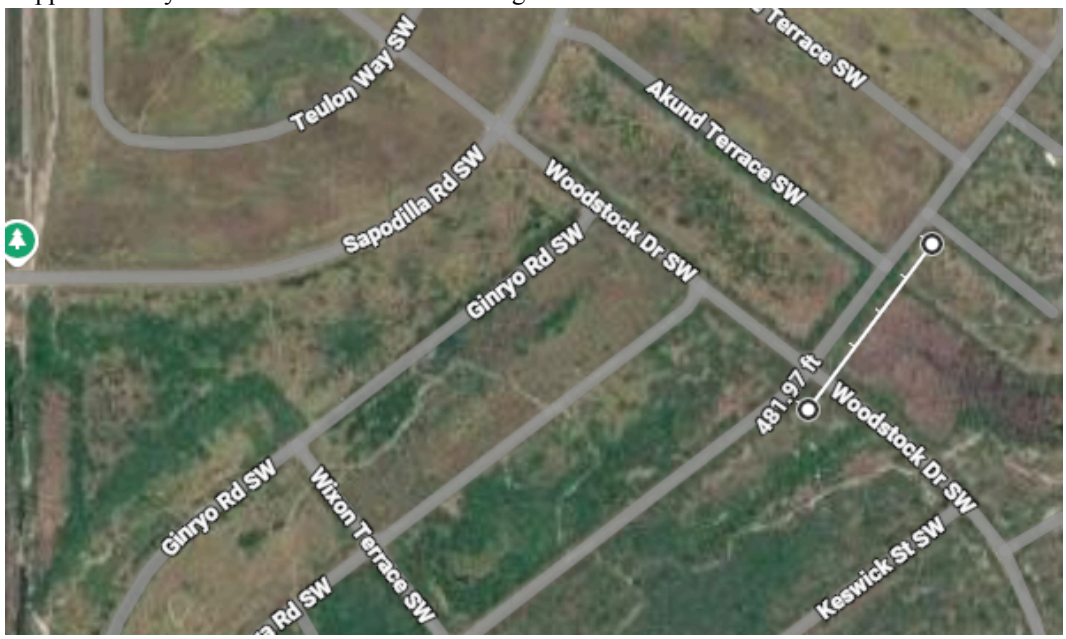


Figure 79. Distance from predicted to found location

To reduce this error, several improvements could be implemented to improve future results. First, the use of physical tools such as a printed map, protractor, and field notebook would improve reliability, as all measurements were recorded from memory using only mobile devices for reference. In addition, obtaining a bearing from the third measurement point would significantly improve accuracy by providing an additional independent constraint.

Furthermore, more strategic placement of observation points would improve geometric stability. In general, triangulation is most effective when observation points provide approximately 60° to 90° of angular separation. While this may be achievable in controlled settings or other scenarios, rocketry applications require observation points before launch without prior knowledge of the landing location. One potential improvement is the use of fixed, clearly defined landmarks such as street intersections rather than movable or ambiguous reference objects such as vehicles or tents, since intersections can be more precisely identified on a map.

Overall, the post-launch triangulation produced reasonable accuracy. By establishing a search radius around the estimated intersection point, similar performance could be replicated in future launches, and the improvements outlined above would further reduce positional error.

The estimated distance from Point 2 (near the launch site) to the predicted landing location was then computed using trigonometric methods. This calculation can be performed using either the Law of Sines or the Law of Cosines:

- Law of Sines:

$$\frac{a}{sin(A)} = \frac{b}{sin(B)} = \frac{c}{sin(C)}$$

- Law of Cosines:

$$c^2 = a^2 + b^2 - 2abcos(C)$$

- Where the lowercase letters represent triangle sides, lengths, and the uppercase letters represent the corresponding opposite interior angles.

Post-launch distance calculations:

1. To apply this method, determine the distance between Points 2 and 3 first. This distance is noted as “a.” From the measured horizontal and vertical offsets:
    - Horizontal Distance = 508.79ft
    - Vertical Distance = 295ft
    - Since this is a right triangle, the Pythagorean Theorem can be applied:

$$a^2 = 508.79^2 + 295^2$$

$$a = \sqrt{(508.79)^2 + (295)^2}$$

$$a = 588.13\ ft$$



Figure 80. Distance from point 3 to point 2

2. The interior angles at the observations were determined using trigonometric relationships. Given that the horizontal and vertical offsets are known with confidence, the tangent function was used. Note that "arctan()" denotes the inverse tangent function.
    - $\theta_2 = arctan(\frac{295}{508.78}) = 30.11°$
    - $\theta_3 = artan(\frac{508.78}{295}) = 59.89°$
    - As a verification step, the sum of the angles in the right triangle was confirmed:

$$90° + 59.89° + 30.11° = 180°$$

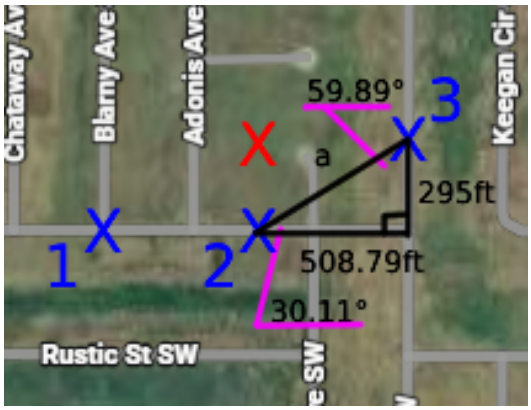


Figure 81. Angles on Map

3. The previously computed right-triangle angles must now be adjusted to account for the absolute bearings of each observation line. Specifically, the goal is to express all interior triangle angles in a consistent global reference frame.
    - First, the bearing adjustment for Point 3 is determined from the measured azimuth (the line drawn at Point 3). The complement to the north-south alignment is computed as:

$$180° - 110° = 70°.$$

    - This adjustment is added to the previously calculated internal angle at Point 3:

$$\theta_3 = 59.89° + 70° = 129.89°$$

    - A similar adjustment is applied at Point 2. Using the corresponding bearing offset, an additional 13° correction is obtained, yielding:

$$\theta_2 = 30.11° + 13° = 43.11°$$

    - Finally, the remaining interior angle ("A") at the point of interest is determined using the triangle angle sum constraint:

$$\theta_A = 180° - 129.89° - 43.11° = 7°$$

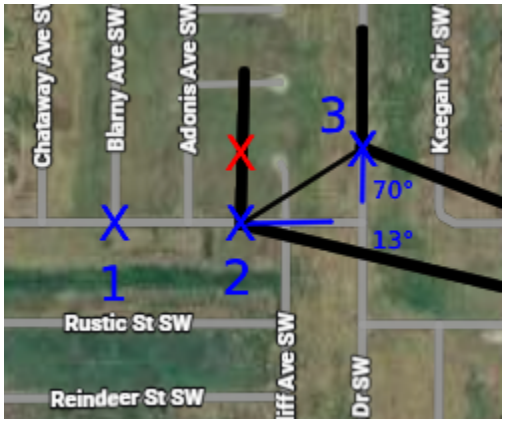


Figure 82. Triangulation points

4. With an angle-side-angle triangle defined, the Law of Sines can be used to estimate the distance from Point 2 to the point of interest, denoted as "b."

$$\frac{a}{\sin(A)} = \frac{b}{\sin(B)}$$

$$\frac{588.13\ ft}{sin(7°)} = \frac{b}{sin(129.89°)}$$

$$b = \frac{588.13 sin(129.89°)}{sin(7°)}$$

$$b = 3,702.81\ ft$$

A distance estimate was obtained using the measurement tool in Google Maps. The resulting distance between Point 2 and the actual landing location was 3,240.16ft. This indicates an error of approximately 460 feet relative to the calculated value.

This discrepancy is consistent with previously discussed sources of uncertainty, including limitations in bearing resolution, potential human error in field measurements, and the constraints of using non-fixed reference points. Given the scale of the launch area, an approximate 500-foot search radius is considered acceptable for operational recovery and would significantly reduce search time if this method were used in future flights.

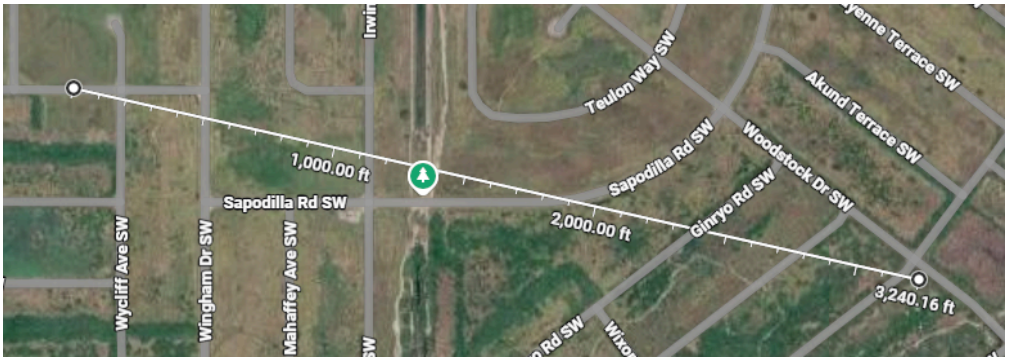


Figure 83. Total Drift

In some scenarios, angular measurements could be obtained directly using a protractor overlaid on the map, eliminating the need for trigonometric calculation. However, the accuracy of the final result is strongly dependent on the precision of both distance and angle measurements. Depending on the application, this trade-off may be acceptable.

For the present case, a trigonometric approach is recommended as the primary method, with protractor-based measurements used as a secondary verification tool. This approach improves consistency in cases where manual angle estimation becomes less reliable due to geometric complexity in a larger triangle.